Science
Stack

MONTHLY WEATHER REVIEW

VOLUME 81 NUMBER 8

AUGUST 1953

CONTENTS

	Page
A Suggested Technique for Quantitative Precipitation Forecasting — Jerome Spar	217
A Generalized Study of Precipitation Forecasting Part 2: A Graphical Computation of Precipitation . . . . P. M. Kuhn	222
An Aid for Forecasting the Minimum Temperature at Denver, Colo. — C. G. Gilbert	233
The Weather and Circulation of August 1953—Featuring an Analysis of Dynamic Anticyclogenesis Accompanying Record Heat and Drought . . . . . William H. Klein	246
Hurricane Barbara, 1953 . . . . . R. P. James and C. F. Thomas	255

Charts I–XV (Charts IV and V, Snowfall, omitted until November)

U. S. DEPARTMENT OF COMMERCE • WEATHER BUREAU

PUBLICATIONS OF THE U. S. WEATHER BUREAU

As the national meteorological service for the United States, the Weather Bureau issues several periodicals, serials, and miscellaneous publications on weather, climate, and meteorological science as required to carry out its public service functions. The principal periodicals and serials are described on this page and on the inside of the back cover. A more complete listing of Weather Bureau publications is available upon request to Chief, U. S. Weather Bureau, Washington 25, D. C.

Orders for publications should be addressed to the Superintendent of Documents, Government Printing Office, Washington 25, D. C.

MONTHLY WEATHER REVIEW

First published in 1872, the Monthly Weather Review serves as a medium of publication for technical contributions in the field of meteorology, principally in the branches of synoptic and applied meteorology. In addition each issue contains an article descriptive of the atmospheric circulation during the month over the Northern Hemisphere with particular reference to the effect on weather in the United States. A second article deals with some noteworthy feature of the month's weather. Illustrated. Annual subscription: Domestic, $3.50; Foreign, $4.50; 30 cents per copy. Subscription to the *Review* does not include the *Supplements* which have been issued irregularly and are for sale separately.

CLIMATOLOGICAL DATA—NATIONAL SUMMARY

This monthly publication contains climatological data such as pressure, temperature, winds, rainfall, snowfall, severe storms, floods, etc., for the United States as a whole. A short article describing the weather of the month over the United States, tables of the observational data, and a description of flood conditions are supplemented by 15 charts. An annual issue summarizes weather conditions in the United States for the year. More detailed local data are provided in the Climatological Data (by sections) for 45 sections representing each State or a group of States, and Hawaii, Alaska, and the West Indies. Subscription price for either the National Summary or for a Section: $1.50 per year (including annual issue), 15¢ per copy.

(Continued on inside back cover)

The Weather Bureau desires that the *Monthly Weather Review* serve as a medium of publication for original contributions within its field, but the publication of a contribution is not to be construed as official approval of the views expressed.

The issue for each month is published as promptly as monthly data can be assembled for preparation of the review of the weather of the month. In order to maintain the schedule with the Public Printer, no proofs will be sent to authors outside of Washington, D. C.

The printing of this publication has been approved by the Director of the Bureau of the Budget, February 11, 1952.

UNIVERSITY OF MICHIGAN LIBRARIES

DEPARTMENT OF COMMERCE
SINCLAIR WEEKS, Secretary

WEATHER BUREAU
F. W. REICHELDERFER, Chief

MONTHLY WEATHER REVIEW

Editor, JAMES E. CASKEY, JR.

Volume 81
Number 8

AUGUST 1953

Closed October 15, 1953
Issued November 15, 1953

A SUGGESTED TECHNIQUE FOR QUANTITATIVE PRECIPITATION FORECASTING

JEROME SPAR
Department of Meteorology and Oceanography, New York University

[Manuscript received August 31, 1953]

ABSTRACT

The theory and computation of integrated water vapor transport vectors are described and it is shown how the synoptic analysis of these vectors may be used for quantitative precipitation forecasting. An example of the vector field and the precipitation forecast is given. Although the prognostic formula does not give correct point values of the precipitation, reasonably good agreement is found between the distributions of forecast and observed precipitation. The technique is probably too laborious for daily forecasting routine but may be useful in the evaluation of rainmaking experiments.

INTRODUCTION

A variety of techniques for quantitative precipitation forecasting have been developed for use in hydrometeorology (see, for example, Fletcher [1]). The hydrometeorologist is primarily concerned with determining the maximum precipitation that can occur over a given area. The problem of predicting where, when, and how much precipitation will occur falls to the daily short-range weather forecaster who is generally both unfamiliar with and unable to apply the techniques of hydrometeorology. The inability of the daily weather forecaster to apply hydrometeorological techniques to precipitation forecasting is largely due to the fact that these techniques have not been adapted to his requirements.

This problem has been attacked recently by Thompson and Collins [2] who have developed a physical method of computing expected 12-hour rainfall from the fields of wind and humidity. In the method of Thompson and Collins the velocity divergence is computed for 50-mb. layers over a triangular area. The vertical velocity distribution is then computed from the divergence and the precipitation is computed by the method of Fulks [3].

A somewhat different technique is described in the present paper. By integrating in the vertical, water vapor transport vectors are computed from rawinsonde data over a large region of the United States. The continuity condition for water vapor is then employed to calculate the precipitation from the divergence of the integrated water vapor transport. The method has been put to a preliminary test by Locklear [4] who found it to be deficient in several respects. However, since the method is based on what appear to be reasonably sound physical considerations, it is felt that it deserves discussion and further testing. Probably the method will have to be supplemented and modified empirically.

THE CONTINUITY EQUATION FOR WATER VAPOR

Let ρ_s denote the density of water vapor, V the horizontal velocity vector, and w the vertical velocity. In the absence of evaporation and condensation, the continuity equation for water vapor may be written

$$\frac{\partial \rho_s}{\partial t}+\mathrm{div}_2 \rho_s V+\frac{\partial \rho_s w}{\partial z}=0 \qquad (1)$$

where z is the vertical coordinate and t denotes time.

Because of the practical difficulties involved in treating evaporation, it will be neglected. But let C denote the mass of water vapor condensed in the air per unit volume. The continuity equation then becomes

$$\frac{\partial \rho_s}{\partial t}+\frac{\partial C}{\partial t}+\mathrm{div}_2 \rho_s V+\frac{\partial \rho_s w}{\partial z}=0 \qquad (2)$$

Next, let us integrate (2) with respect to height between the limits 0 (representing the surface of the earth) and ∞ (representing the top of the atmosphere). In practice, the top of the atmosphere may be taken as some high level above which the water vapor density is inappreciable. Then

$$\frac{\partial}{\partial t}\int_0^\infty \rho_s dz+\frac{\partial}{\partial t}\int_0^\infty C\,dz+\mathrm{div}_2\int_0^\infty \rho_s \boldsymbol{V}\,dz=0 \qquad (3)$$

The vertical divergence term has been eliminated in (3) on the assumption that the vertical velocity vanishes at the surface of the earth and the water vapor density vanishes at "infinity".

The first integral in (3) is known as the precipitable water and is generally denoted by W_p. The second term in (3) represents the condensation rate in the column and will be denoted by I. On the assumption that all condensation products are precipitated, I may be identified with the precipitation intensity. This assumption is not as unreasonable as it may seem in view of the fact that even very deep clouds contain relatively little liquid water compared with the precipitation amounts that occur.

The last integral in (3) will be referred to as the vapor transport vector and will be denoted by $\boldsymbol{F}$. Then, (3) may be written as

$$I=-\frac{\partial W_p}{\partial t}-\mathrm{div}_2\boldsymbol{F} \qquad (4)$$

The forecaster is generally concerned with predictions of precipitation amounts in finite time intervals (although intensity forecasts may also be demanded). It is therefore necessary to integrate (4) with respect to time. Let the total precipitation in the time interval, $t-t_0$, be denoted by R, where t_0 represents the beginning of the period and t the end. Then,

$$R=-[W_p(t)-W_p(t_0)]-\int_{t_0}^{t}\mathrm{div}_2\boldsymbol{F}\,dt \qquad (5)$$

The initial precipitable water, $W_p(t_0)$, can be computed from the radiosonde data. However, the final precipitable water, $W_p(t)$, cannot be predicted and must be estimated by means of some assumption about the condensation-precipitation process. In tests of the method which have been conducted to date (e. g., by Locklear [4]) it has been assumed that $W_p(t)$ is the maximum (saturation) precipitable water corresponding to the initial temperature distribution. This is equivalent to the assumption that no precipitation can fall until the whole column of atmosphere has become saturated Furthermore, the vertical temperature distribution is assumed to be unchanged in the time interval, $t-t_0$. Neither assumption is really very satisfactory. The second assumption can probably be modified by introducing a temperature forecast into the method. But the first assumption leads to an underestimate of the precipitation since the atmosphere is obviously able to produce precipitation from clouds of finite depth. This is one phase of the method which will have to be modified empirically.

The second difficulty in the method is contained in the integral of the divergence of the vapor transport. In the absence of any rational basis for predicting $\mathrm{div}_2\boldsymbol{F}$, we are limited to the assumption that this quantity does not change in the interval, $t-t_0$. Whether or not this crude assumption is satisfactory can only be determined by experience.

If we introduce the assumption stated above into (5), we obtain the following formula for the estimation of the precipitation amounts:

$$R=-(W_{ps}-W_p)-(\mathrm{div}_2\boldsymbol{F})\,(t-t_0) \qquad (6)$$

where W_{ps} is the saturation value of the precipitable water corresponding to the initial vertical temperature distribution. The quantity $(W_{ps}-W_p)$ will be referred to as the water vapor deficit. Since the water vapor deficit may exceed the convergence of water vapor, R may be negative. A negative value of R is interpreted as zero precipitation for the present. However, when sufficient data have been collected on the method, it may be possible to assign to all values of R (positive and negative) a statement as to the probability of precipitation of any given amount.

PRECIPITABLE WATER

Methods of computing the precipitable water in a column of atmosphere have been described by Solot [5] and others, and the details need not be repeated here.

A simple formula for W_p, expressed in inches of liquid water, may be written to sufficient approximation as

$$W_p=\frac{1}{100}\,[q_1+2(q_2+\ldots+q_{n-1})+q_n] \qquad (7)$$

where q_i, the specific humidity in parts per thousand, is read at 50-mb. intervals beginning at the earth's surface. The corresponding formula for W_{ps} employs the saturation specific humidity.

THE VAPOR TRANSPORT VECTOR

The vapor transport vector, $\boldsymbol{F}$, has been defined above as

$$\boldsymbol{F}=\int_0^\infty \rho_s \boldsymbol{V}\,dz \qquad (8)$$

With the aid of the definition of specific humidity and the hydrostatic equation, (8) may be written

$$\boldsymbol{F}=\int_0^{p_0}\frac{1}{g}\boldsymbol{V}q\,dp \qquad (9)$$

where g is the acceleration of gravity and p is the air pressure.

$\boldsymbol{F}$ has the dimensions mass (length)$^{-1}$ (time)$^{-1}$ and the dimensions of $\mathrm{div}_2\boldsymbol{F}$ are mass (length)$^{-2}$ (time)$^{-1}$. However, since it is customary to express precipitation amounts in terms of depth rather than mass per unit area, $\boldsymbol{F}$ and $\mathrm{div}_2\boldsymbol{F}$ may be divided by the density of liquid water.

UNIVERSITY OF MICHIGAN LIBRARIES

The dimensions of these quantities are then (length)^2 (time)$^{-1}$ and length (time)$^{-1}$ respectively.

The calculation of F from rawinsonde data is most conveniently performed by dividing the atmosphere into layers 50-mb. thick, starting at the earth's surface, and integrating numerically. The practical formula for F then becomes

$$F=\frac{50 \text{ mb}}{g}\sum_i \overline{V_i q_i} \tag{10}$$

where the bar denotes the mean value of the product in the 50-mb. layer. Upon inserting the values of g and the conversion factor for centimeters to inches, and dividing by the density of liquid water (1 gm. cm.$^{-3}$), we obtain

$$F=\frac{1}{50}\sum_i \overline{V_i q_i} \tag{11}$$

where the units of F and V_i respectively, are (in. mi. hr.$^{-1}$) and (mi. hr.$^{-1}$), and q_i is expressed in parts per thousand. While the use of the mixed units, inches miles (hour)$^{-1}$, appears objectionable, it has the advantage that, when the divergence is computed by finite differences, div$_2$ F is easily obtained in the precipitation units, inches (hour)$^{-1}$.

F is computed by tabulating the wind velocities and specific humidities at 50-mb. intervals from the rawinsonde data. The products $V_i q_i$ are also tabulated and the mean values of the products for each 50-mb. layer are obtained. The vectors $\overline{V_i q_i}$ are then added vectorially on a polar diagram to obtain F. The decrease of specific humidity with height makes it practicable in most cases to terminate the numerical integration at the 400-mb. level.

The specific humidity distribution can easily be obtained from the dew point curve and the values of V_i can be interpolated with the aid of the pressure-height curve. It would be convenient both for accuracy and efficiency of computation if each rawinsonde station were to compute its own F vector and transmit it with the rawinsonde data. However, this recommendation cannot be considered seriously until the technique has been tested further.

APPLICATION

The calculation of the estimated precipitation, R, from equation (6) can be done on two maps. On the first map is plotted the water vapor deficit, in inches, for each rawinsonde station. Isopleths of $(W_{ps}-W_p)$ are then drawn.

On the second map the values of F_x and F_y, the west-east and south-north components of F in inches miles (hour)$^{-1}$, are plotted for each rawinsonde station. Isopleths of F_x and F_y are drawn using different colors to distinguish the components. A finite difference grid is placed on the map and the divergence of F, in inches (hour)$^{-1}$, is computed for each grid point. The values of div$_2$ F multiplied by the forecast interval, $t-t_0$, (usually 24 hours) are then plotted at the corresponding grid points on the first map and equation (6) is used to compute R. Isopleths of R may then be constructed on a separate map or overlay to obtain the distribution of the estimated precipitation.

It has been pointed out above that the water vapor deficit factor in (6) may lead to an underestimate of the precipitation. In fact, negative values of R will often be found in regions where measurable amounts of precipitation occur. It is not expected that the values of R will correspond to the precipitation amounts observed in the forecast period. But, if the distribution of R is similar to that of the precipitation, R may be considered a good estimator of the precipitation and empirical relation between R and the precipitation amount may be found.

A sample computation is shown in the figures. The F vectors and the water vapor deficit were computed for 28 radiosonde stations in the eastern half of the United States at 0300 GMT, March 11, 1953. The distribution of F is shown in figure 1. The divergence of F was then calculated by the component method using a grid length of 200 miles. The divergence field is shown in figure 2 where positive values denote divergence of the water vapor flux and negative values denote convergence. Figure 3 shows the distribution of the water vapor deficit.

From figures 2 and 3 the 24-hour rainfall distribution was calculated for the period 0300 GMT, March 11 to 0300 GMT, March 12, 1953. The calculated rainfall distribution is shown in figure 4. The isopleths of expected rainfall have been drawn for a geometric progression of rainfall values beginning with 0.2 inches. The zero line is also shown. But negative values of expected rainfall have been eliminated in the figure. The observed 24-hour rainfall distribution for the period 0630 GMT, March 11, to 0630 GMT, March 12, 1953 (fig. 5) shows that the method did succeed in predicting the major centers of precipitation but failed to give the correct distribution of amounts. Thus, where the method predicted 3.2 inches of rain (in Louisiana and Mississippi) only 0.7 inch was observed, while where the method predicted 0.7 inch (in South

FIGURE 1.—Distribution of water vapor transport vector (F), 0300 GMT, March 11, 1953. A full barb represents 2 inch mile (hour)$^{-1}$ and a flag represents 10 in. mi. hr.$^{-1}$.

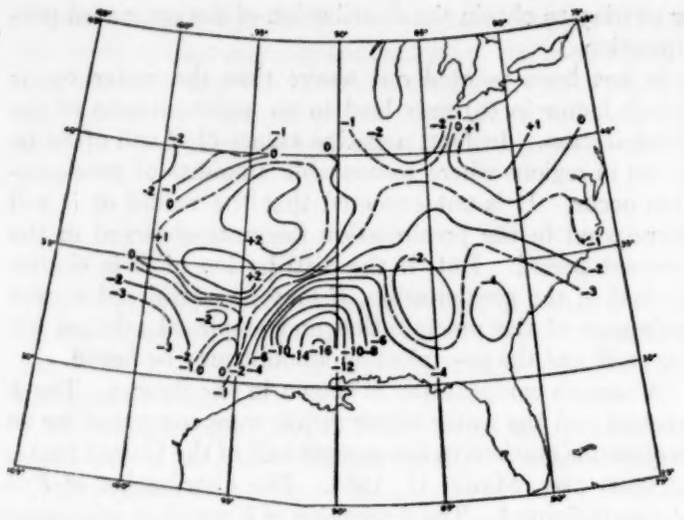

FIGURE 2.—Divergence of water vapor transport ($\text{div}_3 F$) 0300 GMT, March 11, 1953 Units are 10^{-5} in. hr.$^{-1}$.

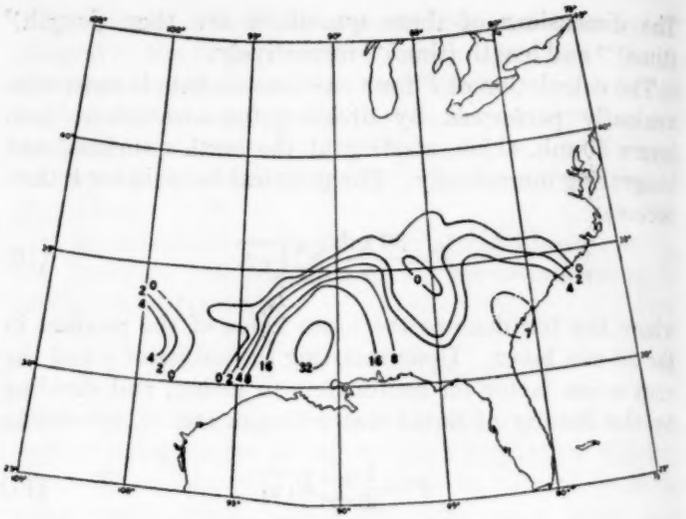

FIGURE 4.—Predicted 24-hour precipitation in tenths of inches, 0300 GMT, March 11, to 0300 GMT March 12, 1953.

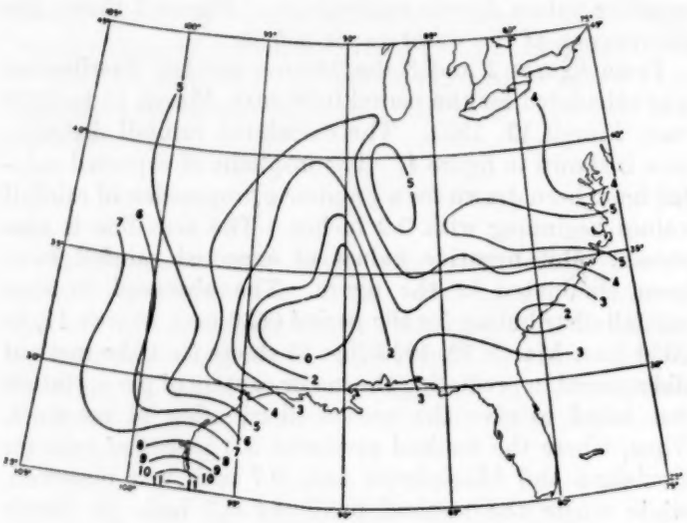

FIGURE 3.—Water vapor deficit ($W_{ps} - W_p$) in tenths of inches.

FIGURE 5.—Observed 24-hour precipitation in tenths of inches, 0630 GMT, March 11, to 0630 GMT, March 12, 1953.

Carolina) more than 1.6 inches were reported. (Savannah recorded 1.95 inches in this period.)

The failures of the method could be due to any of the factors previously mentioned. It appears likely, however, that the major deficiencies of the method are its inability to consider the variations of the divergence of the water vapor transport during the forecast period and the neglect of small scale convergence and convection (i. e., instability). At the present time there appears to be no method of eliminating these difficulties.

RECOMMENDATIONS

The method described above is extremely laborious and time-consuming in its present form and is not practical for use by local forecasting offices. However, it would be possible for a central forecasting office, if sufficient personnel are available, to construct one such prognostic map each day for the entire United States. These prognostic maps could then be distributed by facsimile methods for use by the local forecasting agencies.

The time required for the calculations severely restricts the length of the period for which the forecast is useful. This time could be reduced materially if each rawinsonde station were to compute and transmit with the RAOB report the deficit of precipitable water and the water vapor transport vector. The remaining calculations could then be done in about one hour by an adequate staff.

The method offers some promise as an aid in the evalua-

UNIVERSITY OF MICHIGAN LIBRARIES

tion of artificial rain-making experiments. One of the major difficulties of this type of evaluation is the lack of a satisfactory estimate of the natural precipitation to be expected. Although the method presented here may not provide a completely satisfactory forecast, it does give an estimate, based on reasonable physical principles and arrived at objectively, of the expected rainfall. Since the method is not based on average or climatological relationships, it might be useful in the evaluation of rain-making experiments which have been conducted in unusual weather situations, e. g., extremely heavy natural rain storms.

REFERENCES

1. R. D. Fletcher, "Hydrometeorology in the United States", *Compendium of Meteorology*, American Meteorological Society, Boston 1951, pp. 1033–1047.
2. J. C. Thompson and G. O. Collins, "A Generalized Study of Precipitation Forecasting. Part 1: Computation of Precipitation from the Fields of Moisture and Wind", *Monthly Weather Review*, vol. 81, No. 4, Apr. 1953, pp. 91–100.
3. J. R. Fulks, "Rates of Precipitation from Adiabatically Ascending Air", *Monthly Weather Review*, vol. 63, No. 10, Oct. 1935, pp. 291–294.
4. J. Q. Locklear, The Divergence of Moisture Transport, M. S. thesis, New York University, 1952 (unpublished).
5. S. B. Solot, "Computation of Depth of Precipitable Water in a Column of Air", *Monthly Weather Review*, vol. 67, No. 4, Apr. 1939, pp. 100–103.

A GENERALIZED STUDY OF PRECIPITATION FORECASTING

PART 2: A GRAPHICAL COMPUTATION OF PRECIPITATION

P. M. KUHN

Short Range Forecast Development Section, U. S. Weather Bureau, Washington, D. C.

[Manuscript received August 27, 1953; revised September 23, 1953]

ABSTRACT

A graphical technique for estimating areal precipitation patterns associated with given contemporary charts of streamlines and isotachs and of moisture at four selected levels is developed from the basic physical considerations presented by Thompson and Collins [1]. Procedures are described for calculating the vertical velocity at four selected levels by a kinematic method. The vertical velocities obtained are combined with a graphical solution of Fulks' formula for the rate of precipitation from pseudo-adiabatically ascending air and a method is derived for calculating the 12-hour rate of precipitation. An areal comparison is made of computed and observed precipitation.

INTRODUCTION

As part of continuing research instituted by Thompson and Collins [1] for the general purpose of studying precipitation forecasting, attempts are being made to extend and to modify their technique in such a way as to enable the areal distribution of precipitation to be computed graphically. This paper is a description of the development and testing of one solution to the problem.

Proceeding on a purely physical basis, Thompson and Collins employed in their pilot study observed winds to compute divergence over a triangular area in the Midwest. From this divergence vertical motion was then derived using continuity considerations and, with observed moisture, was used to compute the average rate of precipitation over the area. Their procedure was completely numerical and designed for either hand or machine computation, requiring only the wind and RAOB data obtained from soundings at the vertices of the triangle. Effects of subjective analysis of the data were thus purposely eliminated.

On the other hand, in the present investigation, computations were made using carefully analyzed standard-level maps, combining the parameters derived from the wind and moisture fields by graphical addition, subtraction, and multiplication. Since one of the purposes of this study was the further testing of the usefulness of observed winds in estimating precipitation over large area, the physical model used by Thompson and Collins was retained with only a few necessary changes in the computational constants.

THE BASIC PHYSICAL MODEL

In the basic model it was assumed that the rate of precipitation depended only on the vertical motion of the air column and the moisture contained therein. Non-adiabatic effects of radiation, evaporation, and cloud storage were neglected, as were orographic and frictional influences on the vertical motion. An expression derived by Fulks [2] was used to compute the rate of precipitation. The rate of precipitation, r, from a shallow layer of saturated air ascending pseudo-adiabatically is given by:

$$r=\left[\frac{\epsilon}{RT}\left(\frac{de}{dz}+\frac{eg}{RT}\right)\right]V_s\Delta z=I\,V_s\Delta z \tag{1}$$

where

ϵ is the ratio of the density of water vapor to that of dry air at constant pressure and temperature
R is the gas constant for dry air
T is the mean absolute temperature of the layer
e is the saturation vapor pressure of the layer
z is the height
g is the acceleration due to gravity
V_s is the vertical velocity in the layer, positive upward
Δz is the thickness of the layer

Fulks' expression assumes that the air is saturated throughout the period in which it is being lifted. In order to take into account the frequent case in which the atmosphere is not initially saturated, Thompson and Collins defined an "effective" vertical velocity which would produce the same amount of precipitation in a given time if the air were initially saturated as would the actual vertical velocity with the air initially not saturated. This effective vertical velocity is given by:

$$V_s'=V_s+\frac{T_0-T_{d0}}{\Delta t\left(\frac{dT}{dz}-\frac{dT_d}{dz}\right)} \tag{2}$$

where V_s is the mean vertical velocity of the layer, T_0 and T_{d0} are the temperature and dew point within the layer,

UNIVERSITY OF MICHIGAN LIBRARIES

respectively, with the subscript "0" denoting the value at the beginning of the time interval Δt. Making approximations for the lapse rates and performing the computations for a 12-hour period, the effective vertical velocity is given by:

$$V'_z = V_z - 0.28(T_0 - T_{d0}) \tag{3}$$

where vertical velocities are expressed in centimeters per second and temperatures in degrees Celsius.

The actual vertical velocity can be obtained by numerical integration of the equation of continuity, assuming that density varies only in the vertical and that the vertical velocity at the surface is zero. Then the vertical velocity, V_{z2}, at the top of a layer is given by:

$$V_{z2} = -\frac{1}{2}\left[\frac{\rho_1}{\rho_2} D_1 + D_2\right]\Delta z + \frac{\rho_1}{\rho_2} V_{z1} \tag{4}$$

where D is the horizontal velocity divergence, ρ is the density, and the subscripts 1 and 2 refer to the bottom and top of the layer, respectively.

The horizontal divergence is computed by a graphical method which will be described in a later section. Then from equations (1) through (4) the contribution, r_i, by each of several layers is computed. The total rate of precipitation, P, over the area is then found by summing over the layers.

$$P = \sum_i r_i$$

where the index i ranges over all layers from the surface to the top of the atmosphere. In practice, the summation can usually be terminated at 500 mb. since the layers above have too little moisture to contribute significant amounts.

ADAPTATION OF BASIC MODEL FOR GRAPHICAL ANALYSIS

In the present study, two major modifications of the basic model were made. Instead of computing precipitation for a single triangle, computations were made for a net of triangles covering the eastern half of the United States (east of 100° W.), and a streamline-isotach analysis was used to provide wind data instead of relying on the winds reported at certain sounding stations. Since preliminary tests indicated that computations for only four levels, 950, 850, 700 and 500 mb. gave essentially the same precipitation values as computations for a stratification into more layers, only these four were used.

Horizontal velocity divergence was obtained by an extension of the method suggested by Bennett [3] and Bellamy [4]. Instead of using observed winds at only those vertices coinciding with winds-aloft stations, a streamline-isotach analysis was made. This permitted a grid, consisting of many adjacent equilateral triangles to be used. A transparent overlay, hereafter called Divergence Grid, was designed for a map with scale factor of

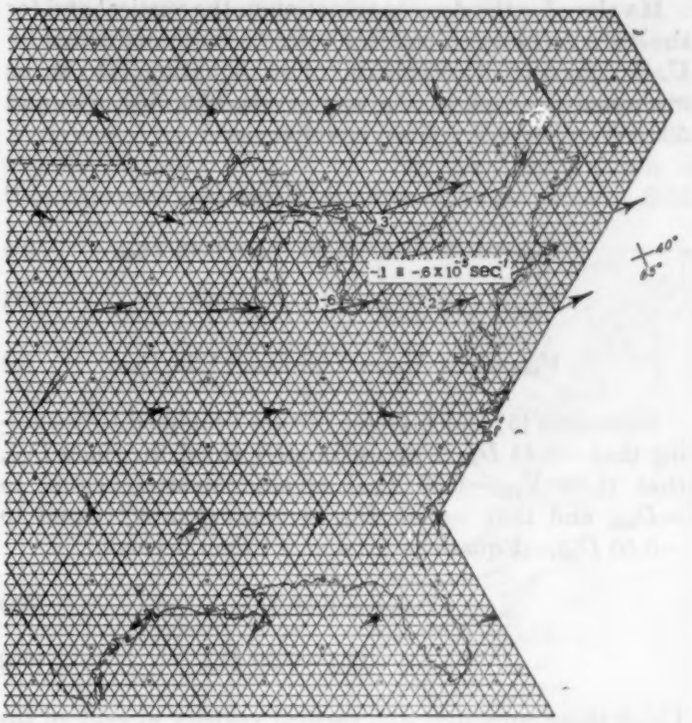

FIGURE 1.—Portion of divergence grid used in computing horizontal velocity divergence. Vectors at 950 mb. for 0300 GMT, December 28, 1949, have been constructed at the vertices of each equilateral triangle in the grid. Numbers show the values of the partial divergence in units per 5 hours, for one triangle. Their sum is the total divergence, converted here to units per second and plotted at the center of the triangle.

1:12,500,000. This Divergence Grid, containing 109 triangles, is reproduced on smaller scale in figure 1. It was not considered necessary to modify the grid to correct for divergence of the meridians or for slight map distortion.

Several advantages can be claimed for the use of a streamline-isotach analysis. In the first place, calculations are not dependent on data from a given station, and no days or areas need be lost because of missing soundings. Further, the smoothing involved in the analysis may tend to eliminate errors and winds of a scale so small as not to be commensurate with the grid size. This procedure differs from that of Graham [5] in that a large grid of symmetrical triangles is employed rather than a single, movable triangle. Also streamlines are drawn instead of isogons.

Since all the grid triangles are identical, a series of thin lines, parallel to the sides of the triangles, can be constructed so that each of the three equal altitudes of every triangle is divided into ten equal intervals. These divisions, in the form of parallel lines, facilitate the computation of the partial divergences. With their aid the partial divergences can easily and quickly be read to increments of 5 percent.

The choice of 280 nautical miles as the optimum dimension for the sides of the triangles was based on the mean distance between adjacent reporting RAOB-RAWIN stations in the United States, about 230 miles, and the size of the smallest disturbance which it was felt could be treated by large-scale methods, about 300 miles.

If values for the density variation in the vertical and for the distance between pressure surfaces is approximated by U. S. Standard Atmosphere values, equation (4) can be evaluated for each of the four levels, 950, 850, 700 and 500 mb. These simplified equations are:

$$V_{z950}=-0.44\ D_{950} \tag{5}$$

$$V_{z850}=1.09\ V_{z950}-0.50\ D_{950}-0.46\ D_{850} \tag{6}$$

$$V_{z700}=1.17\ V_{z850}-0.91\ D_{850}-0.77\ D_{700} \tag{7}$$

$$V_{z500}=1.31\ V_{z700}-1.68\ D_{700}-1.28\ D_{500} \tag{8}$$

Equations (5) and (6) were further simplified by assuming that $-0.44\ D_{950}$ is approximately equal to $-0.50\ D_{950}$, that $(1.09\ V_{z950}-0.50\ D_{950})$ is approximately equal to $-D_{950}$, and that $-0.46\ D_{850}$ is approximately equal to $-0.50\ D_{850}$. Equations (5) and (6) then become:

$$V_{z950}=-0.50\ D_{950} \tag{5a}$$

$$V_{z850}=-D_{950}-0.50\ D_{850} \tag{6a}$$

Using these equations, the vertical velocity at each of the four levels can be computed by graphical means.

Similarly equation (1) can be modified and condensed for graphical computation. If the modification for non-saturation is made, the contribution of a given layer to the total rate of precipitation is

$$r=V'_z Ik \tag{9}$$

where r is the rate in inches per 12 hours contributed by the layer, V'_z is the effective vertical velocity in centimeters per second, I, the expression in the brackets in equation (1), is determined from a diagram developed by Fulks [2], and k is a factor (constant for a given level) which includes the Standard Atmosphere thickness and conversion constants for changing units. For convenience in computation, table 1 of values of Ik was prepared for the various temperatures encountered at the four levels. Thus to obtain the contribution of a given level, we simply multiply graphically V'_z by Ik. Total precipitation, P, for the 12-hour period is then given by

$$P=r_{950}+r_{850}+r_{700}+r_{500} \tag{10}$$

where again the addition is carried out graphically.

GRAPHICAL PROCEDURES

The preceding description of the basic physical model and its adaptation for graphical analysis indicates a requirement for three basic sets of isopleth fields in the computation of a quantitative precipitation pattern: (1) the field of divergence of horizontal velocity at the 950-, 850-, 700- and 500-mb. levels; (2) the field of vertical velocity (isanabats) at these levels; and (3) the field of moisture,

TABLE 1—*Tabular values of the factor Ik for given temperatures and selected pressure surfaces*

Temp. °C	950 mb.	850 mb.	700 mb.	500 mb.
20	.04	.05	.06	.08
19				
18				
17				
16	.04			
15	.03			
14				
13				.08
12				.07
11				
10			.06	
9		.05	.05	
8		.04		
7				
6				
5				.07
4				.06
3				
2				
+1	.03			
0	.02		.05	
−1		.04	.04	
−2		.03		
−3				.06
−4				.05
−5				
−6				
−7			.04	
−8			.03	
−9		.03		.05
−10		.02		.04
−11				
−12	.02			
−13	.01			
−14			.03	
−15			.02	.04
−16				.03
−17				
−18		.02		
−19		.01		
−20				
−21				.03
−22			.02	.02
−23			.01	
−24				
−25	.01			
−26				
−27				
−28				
−29				
−30		.01	.01	.02

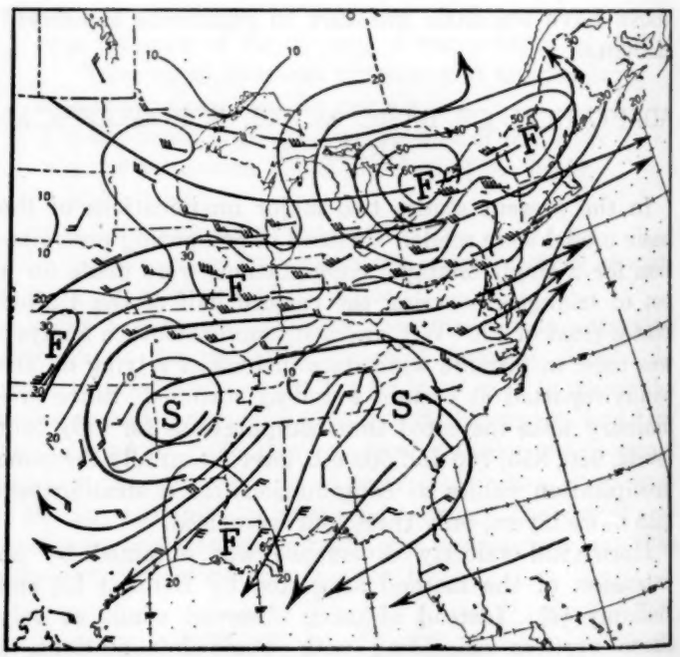

FIGURE 2.—Streamline-isotach field at 950 mb. for 0300 GMT, December 28, 1949. Arrowed lines are streamlines everywhere tangent to the observed winds (full barb equals 10 knots). Thin solid lines are isotachs in increments of 10 knots.

UNIVERSITY OF MICHIGAN LIBRARIES

expressed by isopleths of 0.28 $(T_0 - T_{d0})$, at these levels. These three fields are all obtained and combined graphically to provide the final isohyetal field. The Appendix contains a detailed description of the individual operations that will enable others to perform the computations, but the following brief summary is provided for the reader interested in only the broad outline of the procedures.

Initially, the divergence is computed, with the aid of the Divergence Grid (fig. 1), from a streamline-isotach analysis (fig. 2) for each level. The resulting fields of divergence are graphically combined in accordance with equations (5a), (6a), (7), and (8) to obtain the fields of vertical velocity (figs. 3–6). Graphical subtraction of the moisture field (fig. 7) from the vertical velocity field,

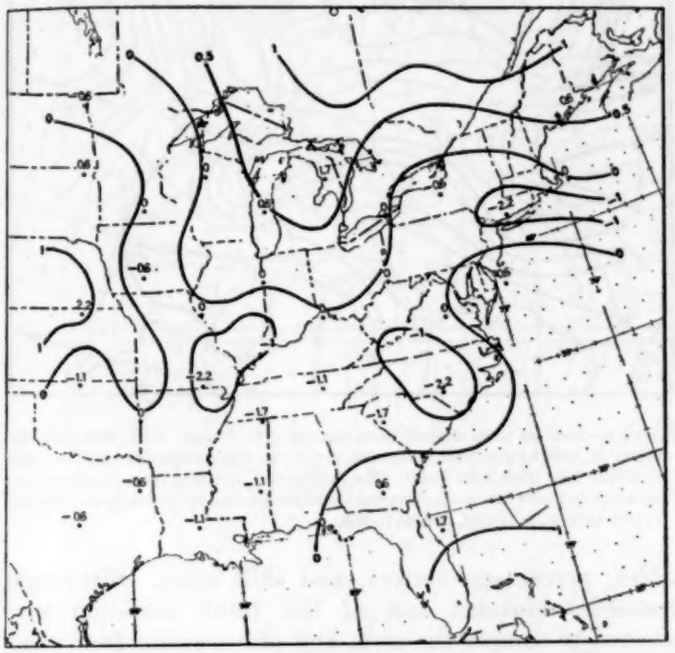

FIGURE 3.—Isanabats in cm.sec^{-1} at 950 mb., 0300 GMT, December 28, 1949. Positive values indicate ascent and negative values descent. Plotted values are divergences in units of 10^{-5} sec^{-1} computed from the field of figure 2 by use of the grid of figure 1. Positive signs indicate convergence and negative, divergence. The 950-mb. vertical velocity is equal to $-0.50D_{950}$ from equation (5a).

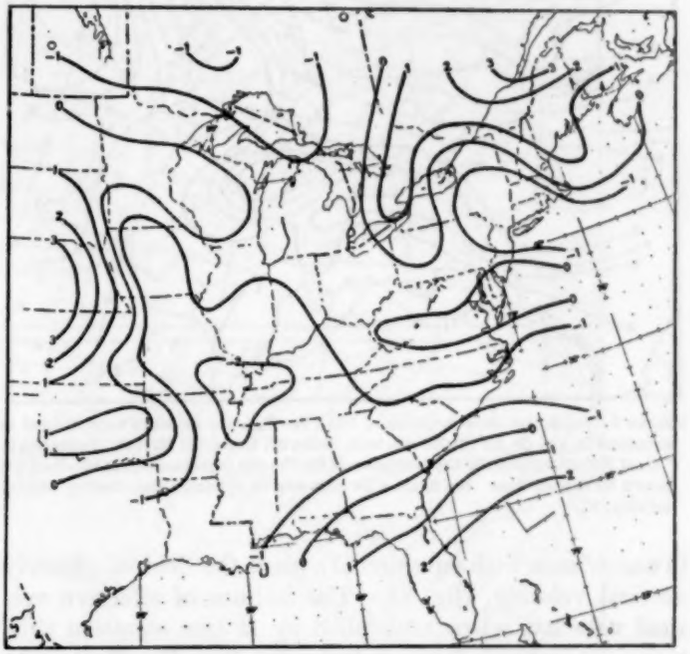

FIGURE 5.—Isanabats in cm.sec^{-1} at 850 mb. for 0300 GMT, December 28, 1949 (dashed lines of fig. 4). Positive values indicate ascent and negative, descent. This chart represents the graphical solution of equation (6a).

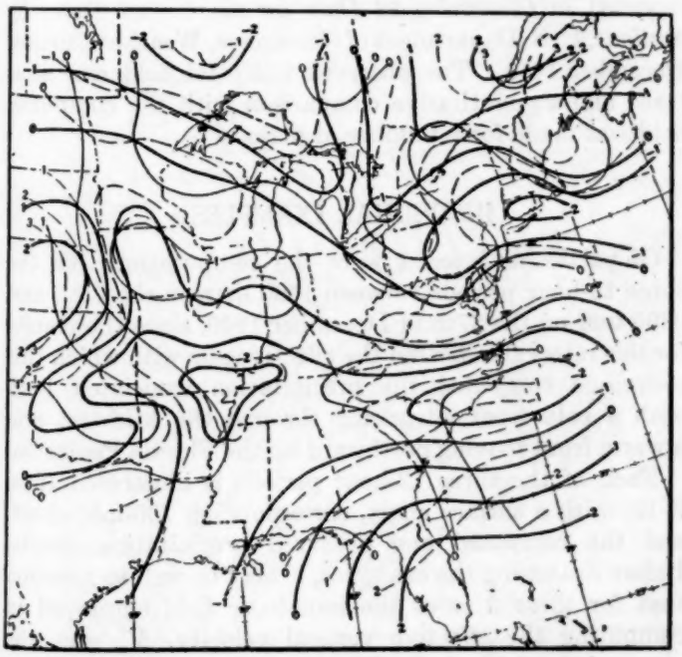

FIGURE 4.—Graphical summation following equation (6a) of $-D_{850}$ (heavy solid lines) and $-0.50D_{950}$ (thin solid lines) to produce the isanabats in cm.sec^{-1} at 850 mb. (dashed lines) for 0300 GMT, December 28, 1949. Positive values indicate ascent and negative, descent. The vertical velocity analysis is shown separately in figure 5.

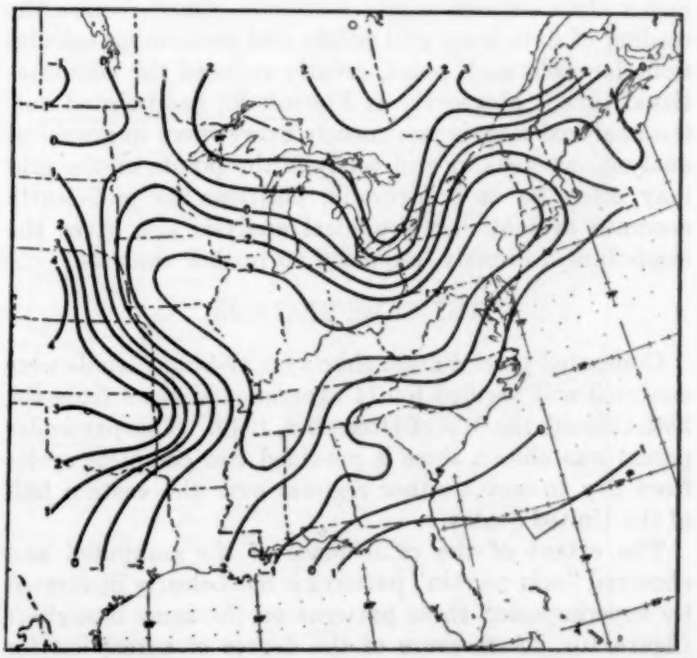

FIGURE 6.—Isanabats in cm.sec^{-1} at 700 mb. for 0300 GMT, December 28, 1949. This field represents the graphical solution of equation (7). Positive values indicate ascent and negative, descent.

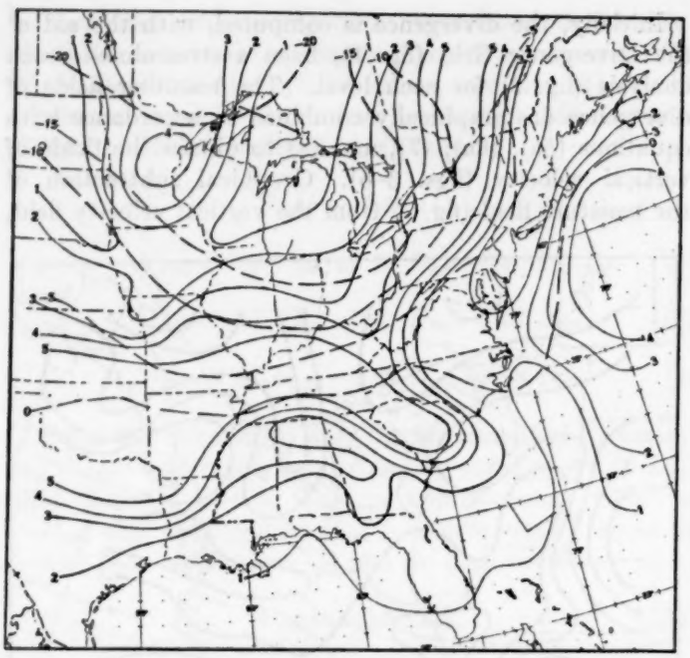

FIGURE 7.—Solid lines show isopleths of 0.28 ($T_s - T_{sa}$), the moisture term defined in equations (2) and (3), for the 700-mb. level, 0300 GMT. December 28, 1949. Isotherms in ° C. at 700 mb. required in the evaluation of the Ik term (equation (9)) at this level are shown by dashed lines. See figure 8 for next step in obtaining the effective vertical velocity, V'_s.

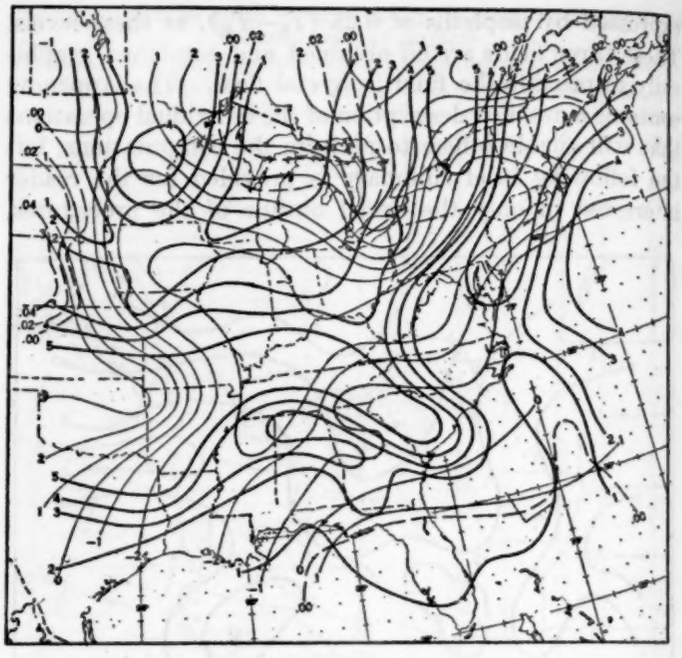

FIGURE 8.—Isohyets (thin dashed lines) computed for 700-mb. level, 0300 GMT, December 28, 1949, by graphical subtraction of 0.28 ($T_s - T_{sa}$) field (heavy solid lines) from isanabatic field (thin solid lines). The isolines of V'_s resulting from this subtraction (equation (3)) have here been converted by multiplication by the Ik factor (equation (9) and table 1), to precipitation in inches.

in accordance with equation (3), gives the field of effective vertical velocity, (fig. 8). The isolines of effective vertical velocity, when multiplied by Ik (see equation (9)), represent isohyets for each layer (fig. 8). Finally, graphical summation of the isohyets for the 950-, 850-, 700-, and 500-mb. levels gives the total isohyetal pattern in accordance with equation (10).

The extensive use of graphical addition and subtraction, rather than successive grid additions, which require the reading of data from grid points and performing calculations for each such point, greatly reduced the computational time. Moreover, as Fjørtoft [6] has pointed out, the analyzed map is used nearly everywhere in graphical analysis, whereas in grid analysis the points of the grid may often be in unfavorable positions for sufficiently accurate evaluation. Graphical analysis also gives the isopleth field directly, requiring no further analysis.

TEST COMPUTATIONS

Computed precipitation charts for 12-hour periods were analyzed and verified for 14 experimental cases from the 25th through the 31st of December, 1949. This particular period was chosen since it provided two complete cycles from dry to wet weather regimes over the eastern half of the United States.

The extent of the coincidence of the computed and observed "rain-no rain" patterns is most clearly illustrated by superimposing these patterns on the same base chart (figure 10). A measure of the degree of agreement for all cases studied was obtained by use of contingency tables, percentage correct, and skill score. Sixty-eight first-order stations east of the 100th meridian were selected to sample the area, and observations from these stations were used in this part of the verification.

To examine the quantitative precipitation computations, observed precipitation maps were plotted from the hourly precipitation data for all recording gages as reported in *Climatological Data for the United States by Sections*, U. S. Department of Commerce, Weather Bureau, December 1949. The observed isohyetal field was analyzed and a quantitative comparison with the computed field was made for a number of periods.

INDIVIDUAL EXAMPLES

Of particular interest were the computations for the three 12-hour periods between 1500 GMT on the 25th and 0300 GMT on the 27th of December 1949, since the results for this interval indicated the effectiveness with which this technique computed the precipitation associated both with a cold front advancing through the Midwest and a warm front moving northward up the Florida Peninsula.

Each of the three 12-hour periods is illustrated (figs. 9–12) with a surface chart, corresponding 700-mb. chart, and the computed and observed precipitation charts. Before discussing the examples, it may be well to mention that for these 3 cases the isanabatic field employed in computing the effective vertical velocity, V'_s was the mean of the fields derived for the beginning and the end of the 12-hour interval.

UNIVERSITY OF MICHIGAN LIBRARIES

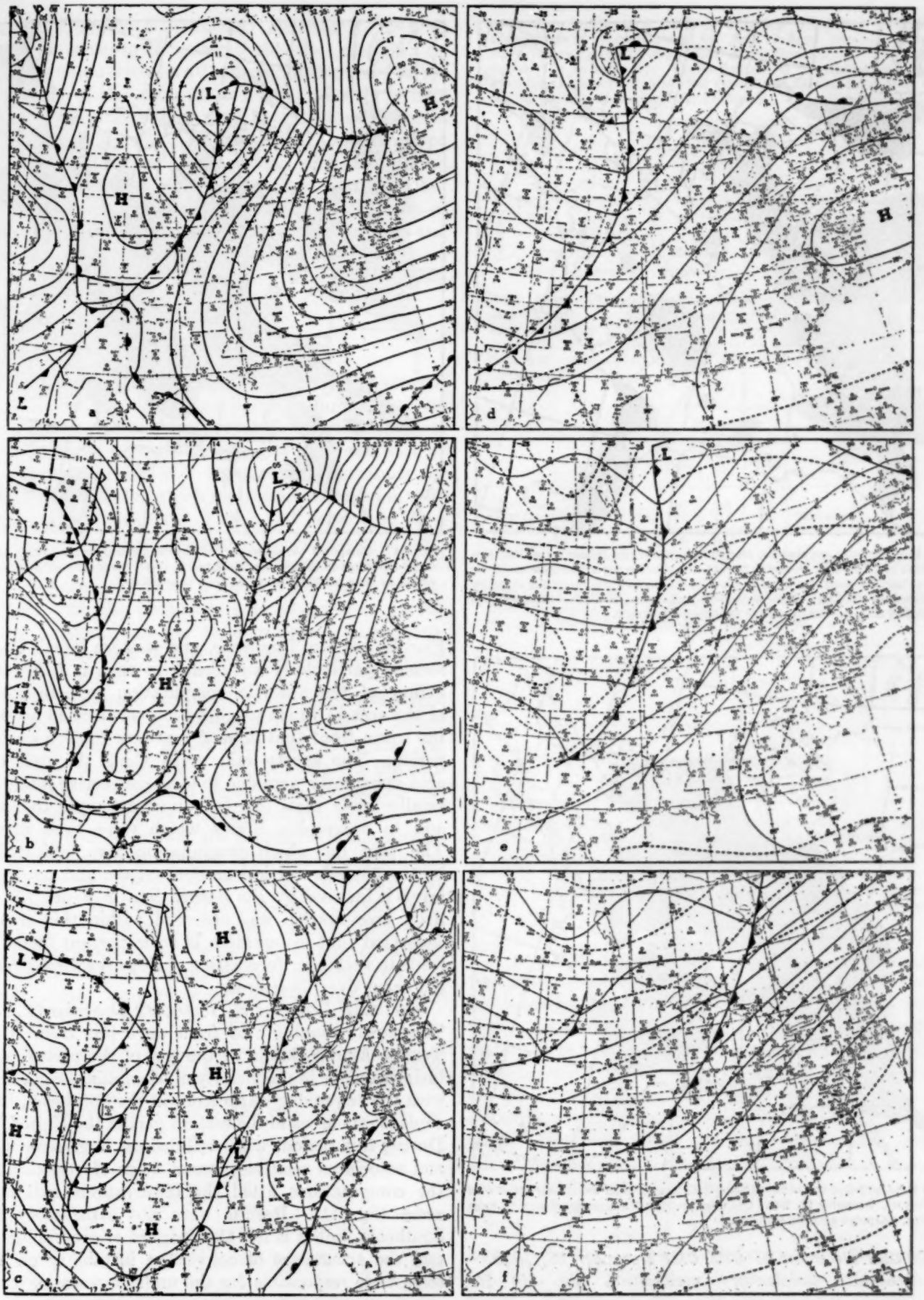

FIGURE 9.—Series of charts illustrating the surface and 700-mb. conditions at the times of the three examples of computed and observed precipitation shown in figures 10–14. Parts a, b, and c are surface charts for 1830 GMT, December 25, 1949; 0630 GMT, December 26, 1949; and 1830 GMT, December 26, 1949, respectively. Parts d, e, and f are the 700-mb. charts for the 1500 GMT and 0300 GMT observation times, corresponding to the surface charts, in the same order.

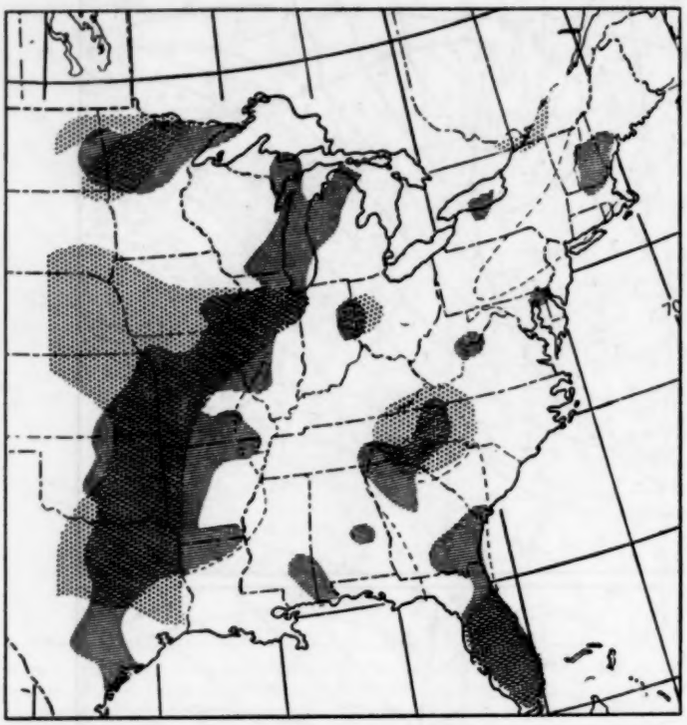

FIGURE 10.—Computed and observed precipitation patterns for 12-hour period 1500 GMT, December 25 to 0300 GMT, December 26, 1949. Observed precipitation areas are shown by cross hatching, computed areas by stippling. Amount of overlapping is an indication of accuracy of method. Thin dashed lines enclose areas for which precipitation was indicated by the computations for the 700–500-mb. layer only.

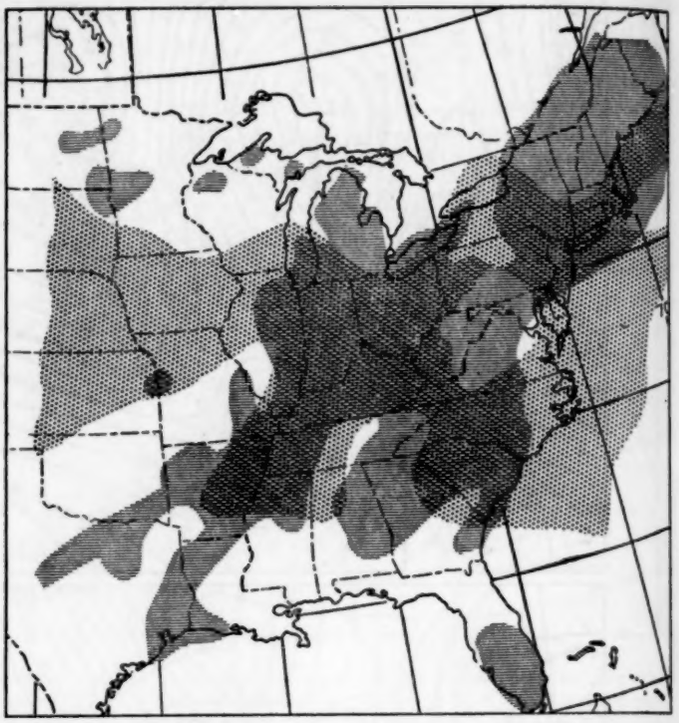

FIGURE 12.—Computed and observed precipitation patterns for the 12-hour period 1500 GMT, December 26 to 0300 GMT December 27, 1949. Observed precipitation areas are shown by cross hatching, computed areas by stippling.

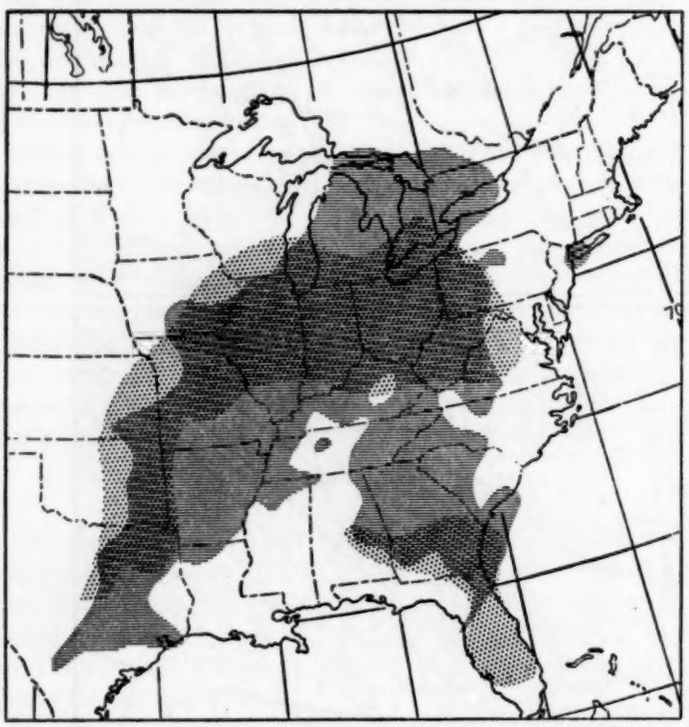

FIGURE 11.—Computed and observed precipitation patterns for the 12-hour period 0300 to 1500 GMT, December 26, 1949. Observed precipitation areas are shown by cross hatching, computed areas by stippling.

1500 GMT December 25–0300 GMT December 26, 1949.—The generally satisfactory verification (fig. 10) for Florida, eastern Tennessee, and western North Carolina, seemed particularly significant in that it indicated the ability of the analytic computation to compute most of the area in which precipitation occurred in advance of the warm front that crossed southern Florida during the period. The spotty rain areas along the east coastal area apparently were due to local convective features of a smaller scale than this technique attempts to measure, and to orographic effects which have been neglected. The area for which precipitation was indicated only by the 500-mb. vertical motion pattern and not by lower levels is inclosed by the dashed line in figure 10. Since little precipitation was observed within this area, it is suspected that evaporation is an important factor which leads to such over-forecasting. However, high cloudiness did occur over these areas.

0300 GMT December 26–1500 GMT December 27, 1949.—The slowly moving cold front on a line from Houston, Tex. to Alpena, Mich. at the end of the period, and the incipient wave in the vicinity of Memphis, Tenn., together with the advancing warm front in the Southeast, brought copious rain areas to the eastern part of the United States. During this period, with well-defined large-scale systems and associated relatively broad fields of vertical motion, the computations fitted the observations well in most areas (fig. 11). Results were not satisfactory in the Southeast, but it is felt that neglect of orographic effects and the occurrence of convective instability on a local scale were responsible for the under-forecasting noted.

UNIVERSITY OF MICHIGAN LIBRARIES

1500 GMT December 26–0300 GMT December 27, 1949.—This example seems to demonstrate the effect of neglecting downslope motion with its attendant "drying out" in the western zone of the computation area. For it is here that the computations show their most serious defect in over-forecasting (fig. 12). In this region the downslope motion due to the slope of the ground surface appeared to be effectively cancelling the upward motion indicated by the horizontal divergence pattern. The inclusion of an orographic correction term for the vertical motion and an evaporation correction term for higher level precipitation contributions should reduce the tendency to over-forecasting in certain regions.

VERIFICATION

In evaluating the significance of the results of computations demonstrated in the preceding examples, composite contingency tables were prepared. Verification was obtained by using a representative grid of 68 stations, as previously stated. Table 2 summarizes the results for five 12-hour periods for which mean isanabatic fields were used in the computations. The 3 test cases just illustrated were included in this period which ran from 0300 GMT, December 25, to 1500 GMT, December 27, 1949. Table 3 presents the same 5 cases when computations were made with the isanabatic field assumed to persist from the beginning of the 12-hour period throughout. It seems evident that the use of mean vertical velocities improves the results.

In all, 14 cases were computed on the assumption that the isanabatic field at the beginning of a 12-hour period persisted, covering the period 0300 GMT, December 25, 1949, to 0300 GMT, January 1, 1950. Table 4 is the contingency table for these 14 cases and summarizes the overall results for computations made in this manner.

Figures 13 and 14 exhibit the computed and observed isohyetal pattern for the period 1500 GMT, December 25, through 0300 GMT, December 26, 1949. In general, the results were not as satisfactory as the areal "rain-no rain" verifications. In this, as in four other cases studied, there was a general tendency for the heaviest computed rainfall to be somewhat less than the corresponding heaviest observed rainfall. (See table 5.) Also evident was some displacement of the centers of intensity.

TABLE 2.—*Contingency table comparing computed and observed occurrence of precipitation for five 12-hour periods from 0300 GMT, December 25 through 0300 GMT, December 27, 1949. Computations of precipitation occurrence were based on isanabats obtained by averaging the isanabatic fields at the beginning and end of each 12-hour period*

		Computed: Rain	Computed: No rain	Computed: Total	
Observed	Rain	98	37	135	Skill score .44
	No rain	52	153	205	Percent 74
	Total	150	190	340	

TABLE 3.—*Contingency table comparing computed and observed occurrence of precipitation for five 12-hour periods from 0300 GMT, December 25 through 0300 GMT, December 27, 1949 (same 5 periods as in table 2). Computations of precipitation occurrence were based on assumption that isanabatic field at beginning of each period persists throughout the 12 hours*

		Computed: Rain	Computed: No rain	Computed: Total	
Observed	Rain	95	40	135	Skill score .40
	No rain	60	145	205	Percent 71
	Total	155	185	340	

TABLE 4.—*Contingency table comparing computed and observed occurrence of precipitation for fourteen 12-hour periods from 0300 GMT, December 25 through 0300 GMT, December 31, 1949. Computations of precipitation occurrence based on assumption that isanabatic field at beginning of each period persists throughout the 12 hours.*

		Computed: Rain	Computed: No rain	Computed: Total	
Observed	Rain	266	112	378	Skill score .40
	No rain	157	417	574	Percent 72
	Total	423	529	952	

TABLE 5.—*Contingency table for quantitative precipitation estimates and observations (in.) for five 12-hour periods from 0300 GMT, December 25 through 0300 GMT, December 27, 1949*

		Computed: 0	.01–.10	.11–.20	.21–.50	>.50	Total
Observed	0	153	41	6	5	0	205
	.01–.10	17	15	5	0	0	37
	.11–.20	15	34	5	1	0	55
	.21–.50	5	3	25	2	3	38
	>.50	0	0	0	0	5	5
	Total	190	93	41	8	8	340
Skill score							.24
Percent							53

CONCLUSIONS

A graphical technique for estimating areal precipitation patterns associated with given flow patterns at standard levels has been derived from basic physical considerations. In a test of the model it was found that approximately 75 percent of the area was correctly estimated on a "rain-no rain" basis. This technique is not presented for use in current forecasting, since prognostic charts of streamlines and isotachs are not available for test purposes. However, some tentative conclusions can be drawn as to factors which must be included in any such generalized forecasting technique, and some hint is available as to their relative importance.

In all cases computed, the greatest precipitation contribution occurred in the layers between 950 mb. and 700 mb., although vertical velocities were greater in the higher layers. This points out that the moisture content is as

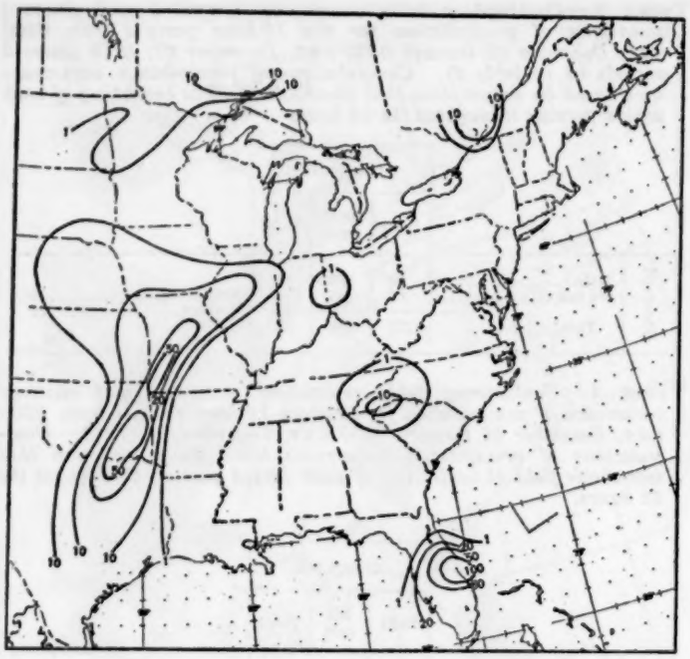

FIGURE 13.—Isohyets of computed precipitation in hundredths of an inch for the 12-hour period 1500 GMT, December 25 to 0300 GMT December 26, 1949. Compare with figure 14.

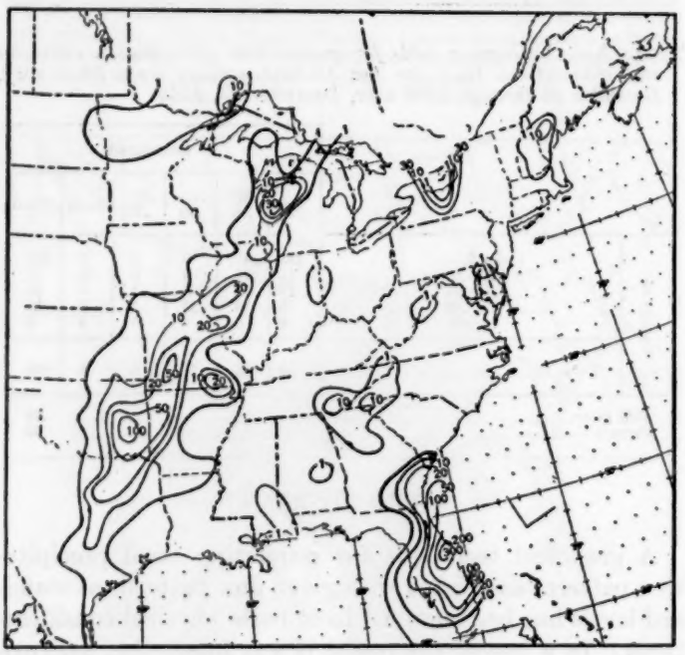

FIGURE 14.—Isohyets of observed precipitation in hundredths of an inch for the 12-hour period 1500 GMT, December 25 to 0300 GMT, December 26, 1949.

important as vertical motion in quantitative precipitation forecasting.

The tendency of the layer from 700 mb. to 500 mb. to over-compute precipitation suggests that cloud storage and evaporation of precipitation falling from high levels may produce large percentage errors when small amounts of precipitation are forecast.

Results also indicate that it will be necessary to consider the effects of topography and skin friction on vertical velocity near the ground. Preliminary studies on these two factors are in progress with encouraging results.

ACKNOWLEDGMENTS

Mr. George O. Collins, Short Range Forecast Development Section, and Mr. Jack C. Thompson, Weather Bureau Airport Station, Los Angeles, Calif., advised the author in all phases of this study. Mr. Roger A. Allen, Chief, Short Range Forecast Development Section gave valuable assistance in the final revision of the manuscript. Credit is due Mr. John L. Strong for drafting most of the figures.

Dr. Joseph A. Smagorinsky, Scientific Services Division and Mr. Rodney D. Graham, Weather Bureau Airport Station, Los Angeles, Calif. offered helpful suggestions on the manuscript.

REFERENCES

1. J. C. Thompson and G. O. Collins, "A Generalized Study of Precipitation Forecasting, Part 1: Computation of Precipitation from the Fields of Moisture and Wind", *Monthly Weather Review*, vol. 81, No. 4, Apr. 1953, pp. 91–100.
2. J. R. Fulks, "Rate of Precipitation from Adiabatically Ascending Air", *Monthly Weather Review*, vol. 63, No. 10, Oct. 1935, pp. 291–294.
3. G. T. Bennett, "Calculation of the Dilatation of Area from Simultaneous Wind Records at Three Neighboring Stations". Note on p. 102 from *The Life History of Surface Air Currents. A Study of the Surface Trajectories of Moving Air*, W. N. Shaw and R. G. K. Lempfert, Great Britain Meteorological Office (M. O. 174) London, 1906.
4. J. C. Bellamy, "Objective Calculations of Divergence, Vertical Velocity, and Vorticity", *Bulletin American Meteorological Society*, vol. 30, No. 2, Feb. 1949, pp. 45–49.
5. R. D. Graham, "A New Method of Computing Vorticity and Divergence", *Bulletin American Meteorological Society*, vol. 34, No. 2, Feb. 1953, pp. 68–74.
6. R. Fjørtoft, "On a Numerical Method of Integrating the Barotropic Vorticity Equation", *Tellus*, vol. 4, No. 3, Aug. 1952, pp. 179–194.

APPENDIX—GRAPHICAL PROCEDURES

DIVERGENCE

The steps required for the graphical computation of divergence may be summarized as follows:

1. Analysis of streamlines and isotachs to provide the necessary wind data over the chosen area for the selected levels.

2. Plotting at each vertex of each triangle in the divergence grid (fig. 1), which is printed on a transparent overlay, a wind vector corresponding to 5-hour displace-

UNIVERSITY OF MICHIGAN LIBRARIES

ment of the air as indicated by the streamline direction and the isotach field at that point. A 5-hour displacement was chosen because it gave vectors of convenient length for the divergence grid.

3. Reading the partial divergence for each vertex of the triangles along an imaginary line perpendicular to the triangle base opposite each vertex. These imaginary lines are divided, by lines parallel to each of the bases of the triangles, into tenths of each of the altitudes of the triangles. The sample triangle in figure 1 illustrates the partial divergences of .3, −.6, and .2 per 5 hours for each of the vertex vectors readily read off the overlay. It is evident that the geometrical arrangement of the divergence grid in figure 1 effectively cuts the number of partial divergence calculations in half as the absolute values of the partial divergence at any two opposite vertex angles are equal but their signs are opposite.

4. Summing the partial divergence for each triangle, and converting to units of 10^{-5} sec^{-1} (fig. 1).

These steps result in a map overlay for each level on which the divergence is plotted at the centroid of each triangle. These overlays are retained for later use. Figure 2 illustrates the streamline-isotach analysis at 950 mb. for 0300 GMT, December 28, 1949, the period used to cover the details of the computations, and figure 1 shows the corresponding plotted divergence overlay.

Several preliminary tests were made to determine the best orientation of the Divergence Grid, for it is fixed by a set of reference coordinates when used over the streamline-isotach charts. In some instances, however, where a narrow, low level "jet" appeared, it was necessary to move the Divergence Grid so that the base line of a group of grid triangles lay along the axis of the "jet". This technique tended to eliminate the extreme non-linearity in the wind field when the core of the "jet" was narrower than the distance between triangles.

VERTICAL VELOCITY

As the next step in the computation of a quantatitive precipitation pattern, isanabatic charts at the chosen levels are obtained by graphical addition of vertical velocity at the bottom of a layer and divergence within the layer. Equations (5a), (6a), (7) and (8) give the constant multipliers for the various levels, and the following paragraphs give level-by-level procedures.

Vertical velocity at 950 mb.—Each of the divergence values on the 950-mb. divergence grid chart is relabeled after multiplicaton by the factor 0.50, obtained from equation (5a). Working directly from the relabeled divergence grid, the 950-mb. isanabats are analyzed at intervals of one centimeter per second on an acetate overlay, and retained for later use. Figure 3 depicts this field of isanabats, which, together with the 950-mb. divergence analysis is retained for use in the 850-mb. computations.

Vertical velocity at 850 mb.—In this step, following equation (6a), graphical addition appears for the first time. Using the divergence isopleths for 950 mb. previously prepared on acetate, and the analysis of a $0.50D_{850}$ field on the previously plotted D_{850} overlay, the two fields are graphically summed. Figure 4 illustrates the technique which results in the isopleths of vertical velocity at 850 mb. illustrated in figure 5.

Vertical velocity at 700 mb.—By reference to equation (7), it is apparent that two steps of graphical addition are necessary in the computation of 700-mb. isanabats, since no justifiable approximations could be made in the formula. However, relabeling the $0.50D_{850}$ isolines by merely doubling their values provides a fair approximation to the $0.91D_{850}$ isolines. For more precise calculations it would obviously be necessary to analyze $0.91D_{850}$ isolines. Following the analysis of a $0.77D_{700}$ chart, the graphical addition of $-D_{850}$ and $-0.77D_{700}$ is carried out on acetates. A reanalysis of the V_{s850} field, as required in equation (7), furnishes the isolines of $1.17V_{s850}$. A second graphical addition, involving the sum of $1.17V_{s850}$ and $-(D_{850}+.77D_{700})$ then gives the isanabatic field at 700 mb. which is kept for use in the 500-mb. computations. Figure 6 gives the resulting 700-mb. isanabatic field.

Vertical velocity at 500 mb.—An inspection of equation (8) indicates that it is necessary to analyze the field of $1.31V_{700}$ and $1.28D_{500}$ before performing the two steps of graphical addition that provide the isanabatic field at 500 mb. The $1.68D_{700}$ field is relabeled by doubling the $0.77D_{700}$ field and, hence, is an approximation. Performing the required graphical summations provides the field of vertical motion at 500 mb.

Mean vertical velocity.—One of the basic assumptions in the original study [1] was that the field of vertical motion remained unchanged throughout the 12-hour period subsequent to the computations. In an attempt to improve upon this assumption, "mean" isanabatic fields may be analyzed by graphically averaging the vertical velocities at the beginning and end of a particular 12-hour period.

RATE OF PRECIPITATION

In the moisture computations, the same method is followed for each of the levels for which vertical motion is computed. Consequently it is possible to illustrate this analysis by reference to the 700-mb. level, only, for a typical calculation.

Equation (3) shows that the addition of a moisture term to the vertical motion term gives the effective vertical velocity. The field of $0.28(T_0-T_{d0})$ is obtained by plotting the values of this quantity from all available soundings and analyzing the map. T_0 and T_{d0} are the temperature and dew point at the top of the chosen layers at the beginning of the period. This analysis, together with the entry of the isotherms at 5°C. intervals required in the evaluation of Ik is made on acetate over the appropriate upper level charts. Figure 7 illustrates the field of $0.28(T_0-T_{d0})$ at 700 mb.

To obtain the effective vertical velocity, V_z', isopleths

of 0.28 ($T_0 - T_{40}$) are subtracted graphically from the isanabatic field for 700 mb. This analysis is carried out on acetate by superimposing the chart represented in figure 7 over the corresponding V_s chart as shown in figure 6. As computations of precipitation are made only where $V_s > 0$, the $V_s = 0$ isanabat is first traced in color to outline such areas. In these areas, the graphical subtraction is performed to obtain the effective vertical velocity, V_z'. Colored isopleths are very effective in reducing the possible confusion that may arise due to the many lines appearing on this analysis. Figure 8 illustrates the graphical subtraction required to obtain the V_z' isopleth field at 700 mb.

The conversion from isopleths of effective vertical velocity to isohyets is made according to equation (9). The term Ik is evaluated for the areas where $V_s > 0$ by noting the mean temperature range over those areas and noting the corresponding value of this constant from the values given in table 1. The isolines of V_z' are multiplied by Ik and relabeled as isohyets for each of the four levels (See fig. 8).

It is evident from table 1 that the term Ik is fairly uniform over a wide range of values of T_0, especially at the lower levels. Thus as this study progressed, it became clear that this method of evaluating the isohyets produced results closely approximating those values of the isohyets obtained from a logarithmic graphical multiplication of Ik by V_z'. The latter method, when required by strong areal variation of Ik, necessitates graphical addition of the logarithms of the V_z' field and the logarithms of Ik. The antilogs of the sum, which are products of the two variables, will give the isohyetal field at each level. However tests indicated, that the logarithmic, graphical technique could give significantly better results only in areas of a large temperature gradient. The analysis of the precipitation contribution from each layer, described above, which assumes no areal variation of Ik, does not involve any graphical computations, merely necessitating the re-labeling of the V_z' isolines as isohyets. To obtain the categorical answer, "rain" or "no rain", areas inclosed by the .01-inch isohyet at each level are combined on acetate into a composite precipitation chart for the surface.

The quantitative isohyetal pattern for the surface is made up of the sum of the precipitation contributions from each of the four levels and is readily acquired by four relatively simple, graphical addition steps as indicated by equation (10).

UNIVERSITY OF MICHIGAN LIBRARIES

AN AID FOR FORECASTING THE MINIMUM TEMPERATURE AT DENVER, COLO.

C. G. GILBERT

Weather Bureau Airport Station, Denver, Colo.

[Manuscript received July 14, 1952; revised manuscript received August 10, 1953]

ABSTRACT

Research on objective forecasting of minimum temperatures is reviewed and the general approach to the problem at Denver is discussed. The variables selected and the graphical combination of these variables are described in detail. Results of forecasts made by exclusive use of the aid are presented and a comparison is made between these forecasts and the official minimum temperature forecasts issued to the public. It is found that the "system" forecasts compare very favorably with the official forecasts and the conclusion is drawn that with continued use of the aid and greater familiarity with its shortcomings the forecasters will be able to consistently improve upon the forecasts produced by the aid and in the long run improve the overall skill in forecasting the minimum temperature for Denver.

INTRODUCTION

A number of articles have appeared in the meteorological literature in recent years on objective methods of forecasting various weather elements. Few of these studies have shown any significant improvement over official forecasts made from the same data. This is not surprising since most of these studies have been based on the experience of forecasters at a particular location with the particular weather element, and no new concept or better understanding of the atmospheric processes has been introduced. (The present study is no exception in this respect.) On the other hand, most of these studies have shown that *equal* results or skills are attainable through relatively simple, objective, *quantitative* procedures. It appears that most of our knowledge of forecasting of a particular weather element for a certain place can be boiled down to a few variables and put on a quantitative basis. It is in the word "most" that the forecaster still has the edge on an objective system. Since equal or almost equal skill is incorporated in the objective system it behooves the forecaster to know what answer it gives, know what has gone into it, and then consider the current synoptic situation from the standpoint of the unusual in the situation that the objective method has not considered, and possibly could not consider. This would relegate the objective "system" or "method" to the position of an "aid" to the forecaster where it belongs. In using such an aid it is important that the forecaster record all occasions on which he differs with the aid appreciably so that over a period of time he can determine whether, on the average, he is improving the forecasts by changing them.

In this study an attempt was made to systematize and put on a quantitative basis the main factors used by experienced forecasters for forecasting the daily minimum temperature at Denver, Colo. The minimum temperature forecast chosen was the one made in the morning at around 0800 MST at Denver based on the 1230 GMT (0530 MST) surface and related charts. This forecast is for the following night and constitutes a 12—24-hour forecast depending upon the time of occurrence of the minimum temperature. Normally it amounts to a 24-hour forecast since the minimum temperature usually occurs around 0530 MST.

ANTECEDENTS

Surprisingly few articles have been written on what would seem to be one of the important subjects in day-to-day forecasting. A minimum temperature forecast appears in almost every general forecast written today whether it is for a specific locality or for a large area such as a State. Those text books on meteorology and forecasting which even mention minimum temperature confine the discussion to those factors which affect the minimum temperature at a point and introduce such wide variability in minimum temperatures within the same air mass. These factors will be discussed in a section below under Sources of Error.

Rules for use of the 12-hour sea level pressure change chart in forecasting temperature trends 24 to 48 hours in advance have been formulated or compiled by several experienced forecasters such as Cook [1], Lloyd [2] and others. But the determining of the estimate of the actual minimum temperature for a given locality is left to the experience of the forecaster for that locality.

Objective methods of temperature forecasting have been used for many years in the "fruit-frost" protection service in California and other States. In this type of work forecasts are for a short period, the forecast being made in the late afternoon or evening for the minimum temperature

278278—53——2

occurring the same night or following morning. The time lag is at most 12 hours. The forecast is based chiefly on the effect that moisture in the lowest layers of air has on nighttime radiation. When the time lag of the forecast is extended to 24 hours or longer the effect of air movement becomes much more important. The forecast problem then becomes primarily that of locating on this morning's weather map the source of air which will be over the station tomorrow morning.

One of the first attempts to put 24-hour minimum temperature forecasting for a locality on an objective basis was by Wilson [3] for Washington, D. C. His technique required the selection each day of an index station located upwind from Washington at a distance equivalent to 24 hours of air flow on the 10,000-foot chart. The surface temperature at this station was then used in a simple linear regression formula to obtain the forecast minimum temperature for Washington. Later Brier [4] showed that comparable results could be obtained from a least-squares equation relating the 0130 EST temperature at Columbus, Ohio, to the temperature at Washington 30 hours later.

Further research in developing objective methods of forecasting the minimum temperature was done in 1945 at New York University sponsored by the Weather Bureau. The first report on this research made by Miller and Burgtorf [5] described a method of estimating the mean seasonal origin of air coming into New York City. For each season of the year a fixed station upstream was selected as the mean seasonal origin and a relationship was shown to exist between the minimum temperature at this fixed station and the subsequent minimum temperature at New York City the following morning. This research was later supported by the U. S. Army Air Forces and in a second report issued by the Air Forces Weather Station at New York University (Mantis and Dickey [6]), a method was outlined for forecasting the daily 24-hour surface air trajectory into New York, thus varying the index station from day to day. In 1947 Mook and Price [7] of the Weather Bureau applied the Trajectory Method to Washington, D. C., and conducted additional studies directed toward refinements of these methods.

In 1949 Dickey [8] developed an objective system for estimating the probability of a large fall in temperature 30 hours in advance for Washington, D. C., and in another report [9] applied similar criteria to Philadelphia to forecast the daily minimum temperature. Hardy [10] in 1951 applied the Philadelphia method with certain refinements to New York City.

GENERAL APPROACH TO THE DENVER PROBLEM

The basic approach underlying all of the above-mentioned studies is the attempt to determine the source of air expected over the station at verification time and establish relationships between temperatures in this air at forecast time with the subsequent minimum temperature at the station. This, of course, is the basic and logical approach to all longer range temperature forecasting, subjective or objective, for locations in relatively flat country. A barrier such as the Rocky Mountains with elevations 5,000 to 9,000 feet higher than the station, immediately to the west and extending for several hundred miles north and south introduces complications to such an approach. Any attempt to construct surface air trajectories from pressure patterns would be useless. Such trajectories, if constructed, would be extremely fictitious. Representative temperatures in the air mass expected to be over Denver do show a good relationship with the Denver minimum temperature, however, when the air mass is a cold outbreak from the north or northwest and on a few occasions from the northeast. In such cases there is a definite progression, or advection, of cold air over the entire region and temperatures behind the cold front show a definite relationship to Denver's minimum temperature. As the cold air pushes southward, however, and engulfs New Mexico, Kansas, and Texas, the reaction to warmer temperatures takes place to the north of Denver first and progresses southward. This warming is accompanied, or caused, by the development of a "lee trough" east of the mountains. The warmer temperatures then cannot be attributed to advection of warmer air from the south but must be accounted for by insolation and dynamic heating and warm air advection aloft from the northwest. For this reason temperatures to the north were found to be more highly correlated with the subsequent minimum temperature at Denver than those to the south or southeast when the surface pressure pattern at forecast time might indicate that the air flow into Denver was from the southeast.

Similarly when a trough or low pressure system moves in off the Pacific to the west or southwest of Denver the southwest flow normally expected ahead of such a trough is blocked in the lower levels by the mountain ranges, and as a consequence surface temperatures "upstream" to the southwest of Denver show very little relationship to the Denver minimum temperature. In such cases, also, temperatures to the north and northwest of Denver were found to be related to the minimum temperature at Denver.

The sea level pressure distribution, the changes in pressure as reflected on the 12-hour pressure change chart, and the movement of the pressure change centers are used extensively at Denver to forecast temperature trend. The general approach to the minimum temperature forecast problem for Denver, then, was to establish a trend forecast from sea level pressure and pressure change variables and then investigate temperature variables both at the surface and at 700 mb. for estimating the actual minimum temperature. The search for temperature variables related to Denver's minimum was guided by the considerations discussed above.

UNIVERSITY OF MICHIGAN LIBRARIES

VARIABLES INVESTIGATED

TREND FORECAST

Experience in forecasting temperatures and temperature changes at Denver has established association of certain pressure distributions or patterns with subsequent temperature trends. One such pattern which indicates a trend toward warmer temperatures is the existence and intensification of a "plateau" or "Great Basin" High centered over the plateau region west of the Continental Divide. A measure of the existence of such a High cell is the current sea level pressure at Grand Junction, Colo. (Any other station west of the Divide would probably work almost as well.) Grand Junction was chosen as a result of preparing two composite 0530 MST sea level pressure charts for cases in which the minimum temperature at Denver 24 hours later was 10° F. or more below normal and 10° or more above normal. The greatest pressure difference between these two charts was located at Grand Junction. The intensification, or dissipation, of the High is reflected in the 12-hour pressure change at Grand Junction. The intensification of the High is usually accompanied by the development of a trough to the east of the Divide creating a strong west-to-east pressure gradient which results in down-slope winds in the Denver area and dynamic warming. The development of this trough is preceded by 12-hour pressure falls to the north of Denver, east of the Divide.

The pattern most generally associated with a trend toward colder temperatures 24-hours in advance is the existence of low pressure over the plateau region, somewhat to the south of Denver, and high pressure with cold temperatures to the north. Rising pressure to the north and falling pressure to the west or southwest of Denver are indicative that the cold air will push southward east of the Divide and engulf Denver. The current (0530 MST) pressure at Grand Junction again indicates the existence of low pressure west of Denver and the 12-hour pressure change at the same station accompanied by a pressure rise to the north indicates the movement of colder air southward. The station to the north selected for measuring the 12-hour pressure change was Sheridan, Wyo. This station was selected again on the experience of forecasters for this region as being a somewhat greater distance from Denver than the average 24-hour movement of cold air from the north, and thus is in general behind the cold front advancing southward in such situations.

Temperatures have a decided tendency to regress toward the normal when extreme values are reached. Or in other words, if the temperature one morning is considerably below normal, the probability that the temperature the following morning will be higher is greater than that it will be lower. This concept in itself would suggest that the daily departure from normal be used as a variable in predicting trend. If the normal minimum temperature varied greatly during the season being investigated, or if the study were made on a yearly basis, the departure would be the logical variable to use. The normal minimum temperature at Denver during winter varies from 15° to 28° F., but since the tendency for regression toward normal is most pronounced when the departures from normal are most extreme, the observed minimum itself was considered a sufficient measure of its abnormality. However, before making the final decision on this variable, the departure from normal was tried instead of the temperature itself. Little difference was shown so the current minimum was used.

To summarize the above discussion, the following variables were used to determine a trend forecast:

1. Current minimum temperature. This is the minimum temperature that has occurred during the night up to 0530 MST.
2. The 0530 MST sea level pressure at Grand Junction, Colo.
3. The 12-hour pressure change at Grand Junction, Colo. (1730 to 0530 MST) corrected for diurnal tendency.
4. The 12-hour pressure change at Sheridan, Wyo., also corrected for diurnal tendency.

These four variables were combined graphically to arrive

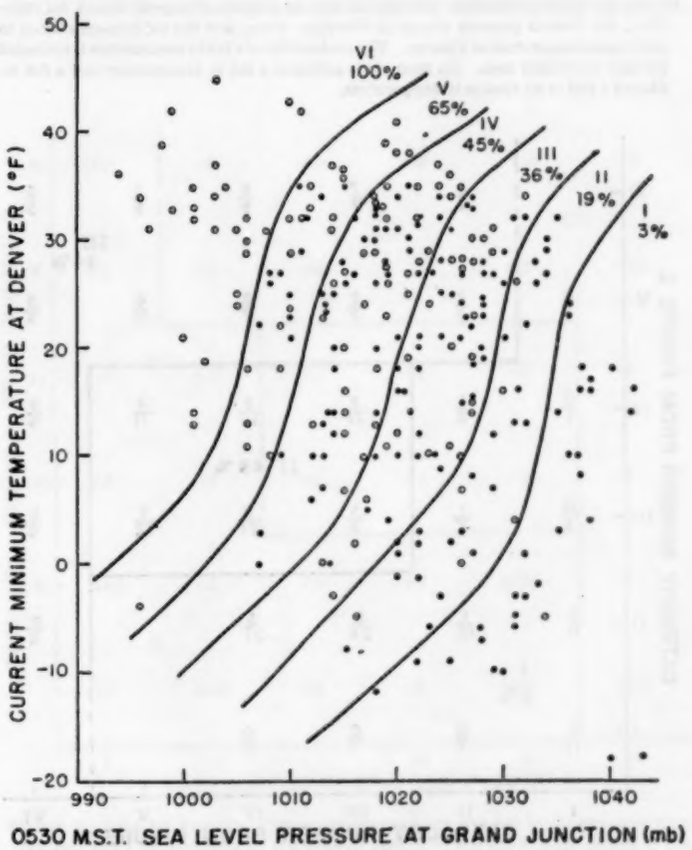

FIGURE 1.—Joint relationship between the current minimum temperature at Denver, the 0530 MST sea level pressure at Grand Junction, and the subsequent change in the Denver minimum temperature. The probability of a *fall* in temperature is indicated for each numbered area. An open circle indicates a fall in temperature and a dot indicates a rise or no change in temperature.

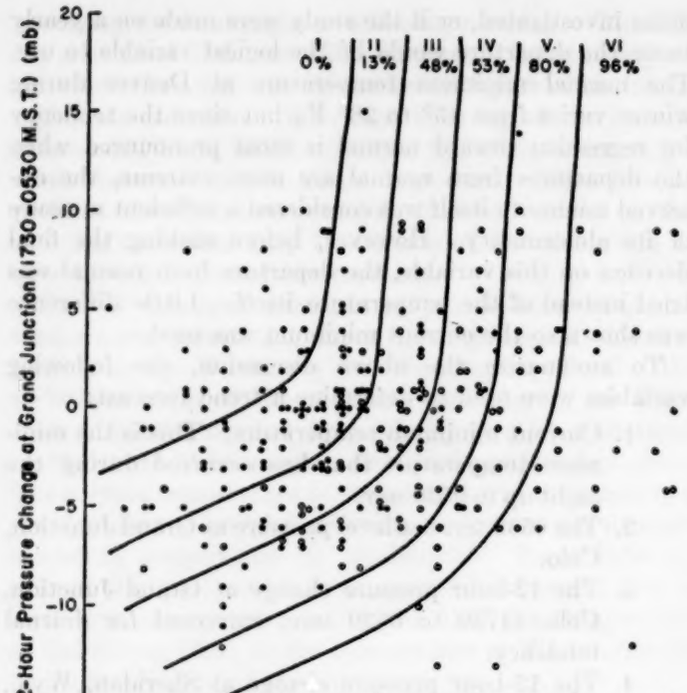

FIGURE 2.—Joint relationship between the 12-hour pressure change at Grand Junction, Colo., the 12-hour pressure change at Sheridan, Wyo., and the subsequent change in minimum temperature at Denver. The probability of a *fall* in temperature is indicated for each numbered area. An open circle indicates a fall in temperature and a dot indicates a rise or no change in temperature.

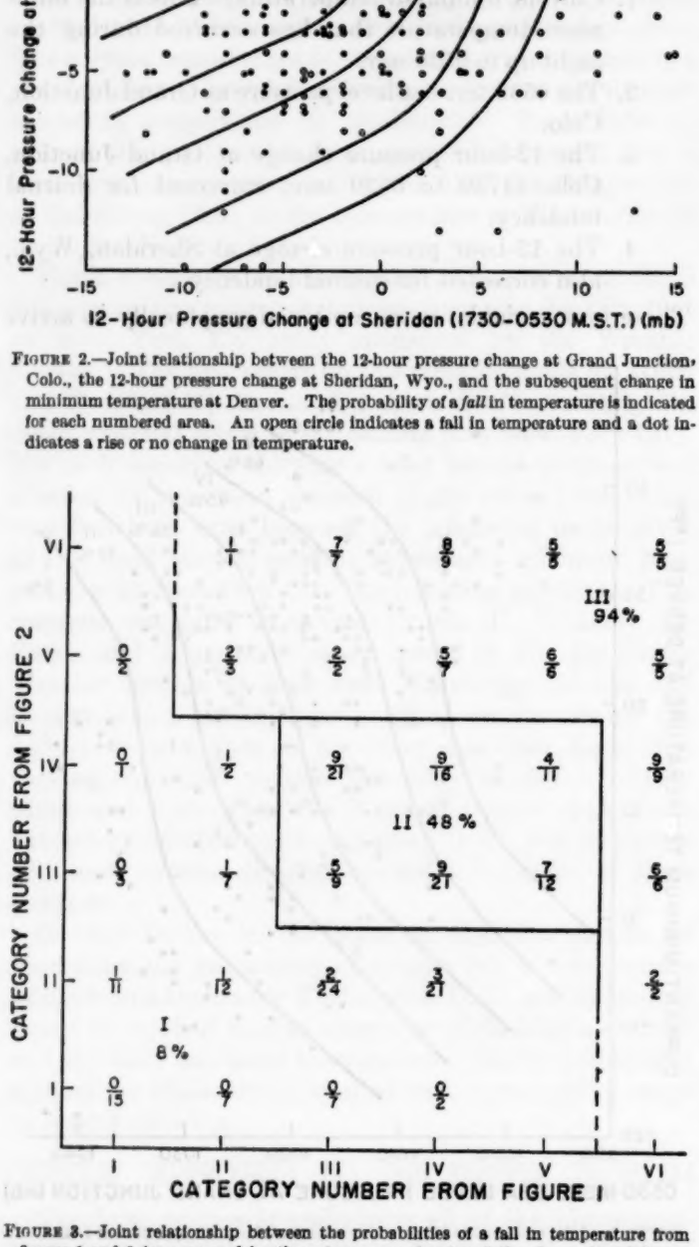

FIGURE 3.—Joint relationship between the probabilities of a fall in temperature from figures 1 and 2 (as expressed by the category numbers) and the change in minimum temperature. The denominator of the fraction at each point is the total number of cases and the numerator is the number of cases with falls in temperature.

at a trend forecast. The analysis used actually gives the probability of the trend rather than a yes or no answer that warmer or colder will result. It was found later, however, as might be expected, that the probability of trend was related strongly to the average change in minimum temperature.

The current minimum temperature at Denver and the 0530 MST sea level pressure at Grand Junction were paired and used as coordinates of a scatter diagram on which was plotted the subsequent change in the minimum temperature, a positive value indicating warming and a negative value cooling. The temperature change was plotted on the chart as a circle or a dot, the circle indicating a temperature fall and the dot a temperature rise or no change. Areas containing approximately equal numbers of cases were delineated on this chart and then the ratio of the number of temperature falls to the total number of cases in each area was determined. This ratio was expressed as a percentage and entered on the chart at the center of the area. On the basis of these percentages, the chart was then divided into six elongated areas or channels in which the percentage of occurrence (or probability of occurrence) of a fall in temperature progressively increases across the chart (fig. 1). The areas of probability were labeled with category numbers from I to VI, the area of lowest probability being designated category I.

The 12-hour pressure changes at Grand Junction and Sheridan were used as coordinates of a second scatter diagram with the change in minimum temperature again plotted on the chart as a circle or a dot (fig. 2). The same type of analysis was made on this chart as described above.

For each case category numbers were determined from figures 1 and 2. These category numbers were then used as coordinates of a third chart. For each combination of category numbers the total number of cases and the number of temperature falls were tabulated. These numbers were entered at the point determined by each combination of category numbers, the denominator being the total cases and the numerator the number of temperature falls (fig. 3). The chart was then divided into three areas, one in which falls in temperature predominate, one in which rises in temperature predominate, and the third in which an approximately equal number of rises and falls occur. In area I of figure 3 the probability of a fall in temperature is only 8 percent, or the probability of a rise or no change is 92 percent. In area II the probability of a rise or fall is approximately 50 percent, and in area III the probability of a fall in temperature is 94 percent.

ESTIMATING THE ACTUAL MINIMUM TEMPERATURE

The first approach to estimating the actual minimum temperature was to treat the three groups delineated on figure 3 separately and a complete system was developed

on that basis. However, it turned out that the same variables gave best results in all three groups and the analyzed charts showed so much similarity that the three groups were combined into the same charts, thus requiring only three charts for the forecast instead of nine (three for each group). The trend indication from figure 3 was retained, however, to evaluate some of the variables.

There are two main factors which determine the magnitude of the minimum temperature at a station. These are the temperature "this morning" of the air mass expected over the station "tomorrow morning," and the modification this air mass will undergo in reaching the station. There are other factors, such as snow cover, wind, and the presence or absence of clouds, which affect the final temperature reading and which will be discussed more fully under Sources of Error, but the major portion of temperature change is accounted for by the two factors mentioned. The following variables were used to measure the effects of these two factors:

1. The Maximum Temperature at Denver "Today." This variable is an indirect measure of the temperature of the surface of the ground over which the new air mass will pass and thus is a measure of the modification the air mass will undergo in reaching the station. Cook [11] has shown there is a very high degree of correlation between the afternoon maximum and the succeeding night time minimum on clear, relatively calm nights. While the variance is no doubt considerably larger when all days are considered, the correlation is still sufficiently strong to make the maximum temperature a very good forecasting variable for the minimum temperature. In order to use this variable in an early morning forecast a forecast of the maximum temperature for "today" obviously has to be made. The average error of the official forecasts of "today's" maximum temperature is relatively small, sufficiently small in fact, that there is very little difference between the correlation of the observed maximum and subsequent observed minimum and the correlation of the forecast maximum with the subsequent observed minimum. (These correlations are: observed maximum *vs.* observed minimum .87; and forecast maximum *vs.* observed minimum .85.) Furthermore, the technique of forecasting the maximum temperature "today" is fairly uniform among forecasters. The observed maximum was therefore used in constructing the charts. This variable was used in all three trend groups from figure 3.

2. Temperature at Surface Index Station. As stated above under General Approach, in only one group of cases, where a cold air mass is moving down from Canada, does the surface temperature at the index station chosen represent the temperature of the *air mass* which will be over Denver at verification time. This is essentially Group III and part of Group II from the trend chart, figure 3. In the rising temperature cases, Group I and part of Group II of figure 3, the temperature at the index

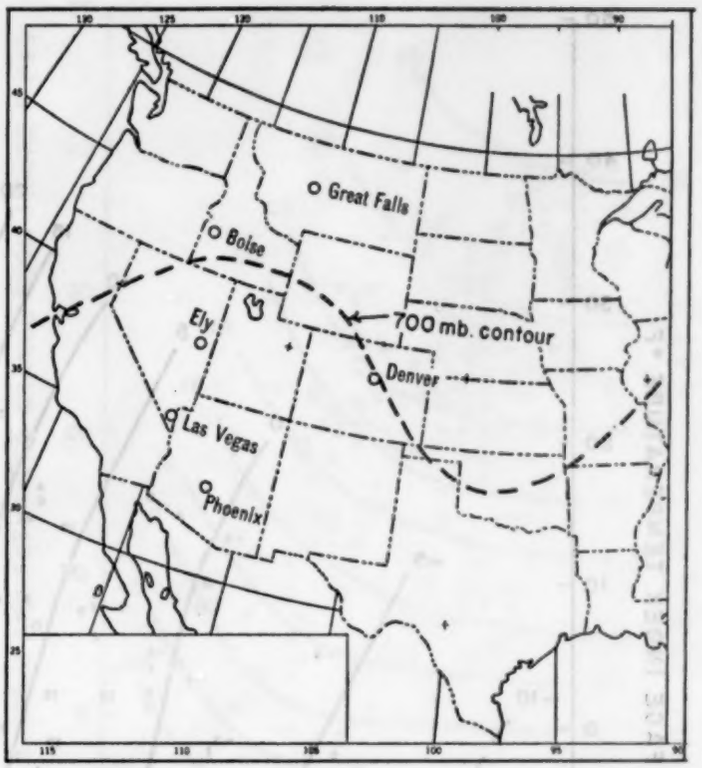

FIGURE 4.—Location of raob stations used in selecting the 700-mb. index temperature.

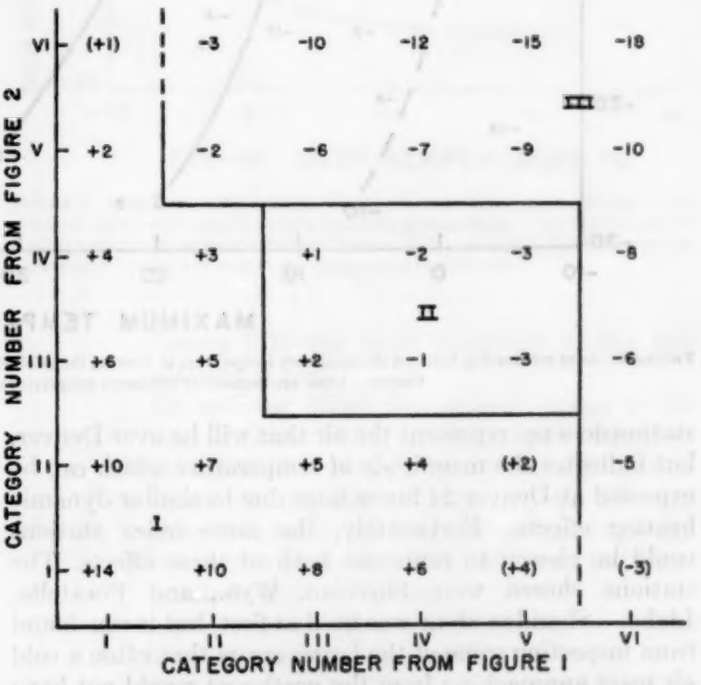
CATEGORY NUMBER FROM FIGURE 2
CATEGORY NUMBER FROM FIGURE 1
VI (+1) -3 -10 -12 -15 -18
V +2 -2 -6 -7 -9 -10
IV +4 +3 +1 -2 -3 -8
III +6 +5 +2 -1 -3 -6
II +10 +7 +5 +4 (+2) -5
I +14 +10 +8 +6 (+4) (-3)
I II III IV V VI
III
II
I

FIGURE 5.—Joint relationship between the probabilities of a fall in temperature from figures 1 and 2 (as expressed by the category numbers) and the average change in the minimum temperature. The number plotted at each point is the average change (° F.) for all cases falling at that point. A positive value indicates a rise in temperature, a negative value a fall in temperature. Numbers in parentheses were entered arbitrarily to fill out the chart and are not based on data.

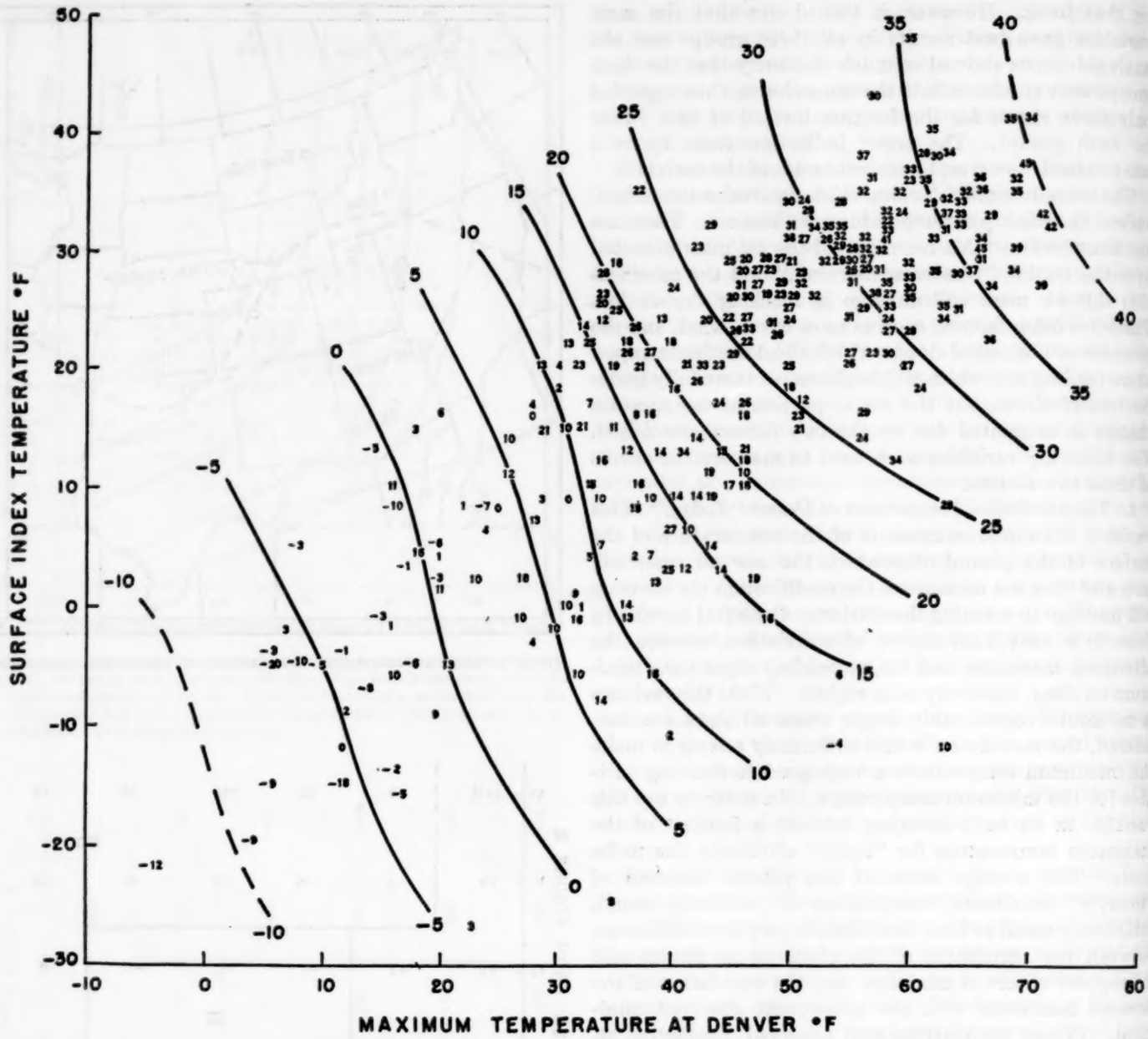

FIGURE 6.—Joint relationship between the maximum temperature at Denver, the minimum temperature at the surface index station, and the subsequent minimum temperature at Denver. Lines are isograms of minimum temperature (° F.) fitted to computed average values over the chart.

station does not represent the air that will be over Denver, but indicates the magnitude of temperature which can be expected at Denver 24 hours later due to similar dynamic heating effects. Fortunately, the same index stations could be chosen to represent both of these effects. The stations chosen were Sheridan, Wyo., and Pocatello, Idaho. Sheridan alone was used at first, but it was found from inspecting some of the larger errors that often a cold air mass approaching from the northwest would not have reached Sheridan by 0530 MST and thus a station west of the Divide would be more representative of the air. Similarly when a warming trend was indicated, the reaction to warmer often had not taken place at Sheridan yet but had west of the Divide. The following scheme was evolved, therefore, for choosing the index station: If the case fell in Group I (warmer) of figure 3, the warmer of Sheridan or Pocatello was used; if the case fell in Group III (colder), the colder of Sheridan or Pocatello was used; and if the case fell in Group II the average of the two stations was used.

3. The 700-mb. Index Temperature. For a further indication of the temperature of the air mass expected over Denver at verification time, a simple measure of advection at 700 mb. was employed. This measure of advection is illustrated in figure 4. The contour line through Denver on the 2000 MST 700-mb. chart was traced upstream until it passed between two of the radiosonde stations indicated in figure 4. The 700-mb. temperature employed

was then again based upon the trend indications of figure 3. If the case fell in Group I, the temperature at the more southerly of the two stations between which the contour line passed was used; if the case fell in Group III, the temperature at the more northerly station was used; and if the case fell in Group II, the average of the two stations was used. If the contour passed east of Great Falls, the temperature at Great Falls was used in all cases, or if it passed east of Phoenix in a southerly flow, the temperature at Phoenix was used. When the contour through Denver was closed, Boise, Idaho was arbitrarily chosen as the index station. This assumes eastward movement of the closed system and subsequent advection of air from the northwest.

4. Average Change as Indicated by the Trend Forecast Variables. A fourth variable makes use of the pressure variables used in the trend forecast to arrive at an estimate of the actual minimum temperature. Figure 3 was reanalyzed and the average change in the minimum temperature was computed for each point determined by the category numbers from figures 1 and 2 instead of the probability of a fall in temperature. The resulting chart is shown in figure 5. The changes progress rather uniformly from large positive values (warmer) in the lower left section of the chart to large negative values (colder) in the upper right section of the chart. (The four numbers in parenthesis on this chart were entered arbitrarily to fill out the chart and are not based on data.) Comparison of figure 5 with figure 3 shows a high degree of association between the probability of change in temperature and the average change. The average change determined from figure 5 for any particular day was added to the current minimum temperature to obtain an estimate of the minimum which would occur the following morning. This estimate was used as an additional variable to combine with the others discussed above to arrive at the final forecast of the minimum temperature.

To summarize, the following variables were utilized to forecast the actual minimum temperature:

1. "Today's" maximum temperature.
2. Minimum temperature at Sheridan or Pocatello, depending upon the trend indication of figure 3:
   Group I—the warmer of Sheridan or Pocatello
   Group II—the average of Sheridan and Pocatello
   Group III—the colder of Sheridan or Pocatello
3. The 700-mb. Index Temperature: This temperature is obtained by tracing the 700-mb. contour through Denver upstream until it passes between two of the stations indicated in figure 4. The index station chosen depends on the trend indication of figure 3, as follows:
   Group I—the more southerly of the two stations is used.
   Group II—the average of the two stations is used.
   Group III—the more northerly of the two stations is used.
   Exceptions: When the contour passes to the east of Great Falls, the Great Falls temperature is used in all groups. When the contour passes to the east of Phoenix, the Phoenix temperature is used in all groups. If the contour is closed, in a closed Low, the temperature at Boise is used.
4. Average change as determined from figure 5 plus the current minimum temperature.

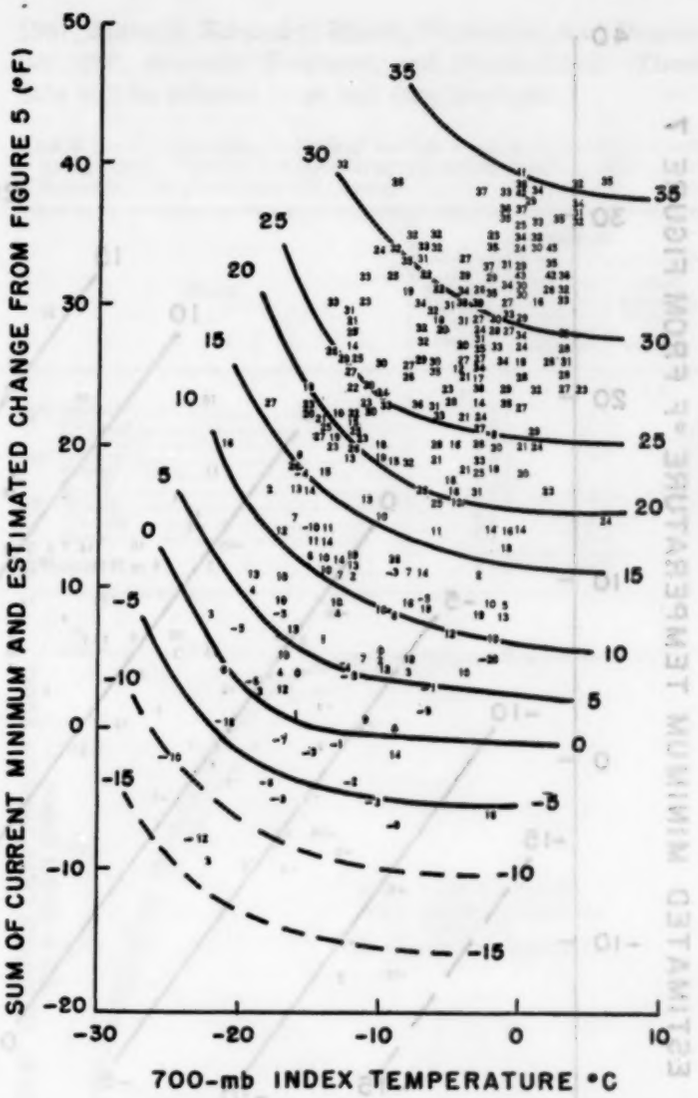

FIGURE 7.—Joint relationship between the 700-mb. index temperature, the sum of the current Denver minimum temperature and the average change from figure 5, and the subsequent minimum temperature at Denver. Lines are isograms of minimum temperature (° F.) fitted to computed average values over the chart.

COMBINING THE TEMPERATURE VARIABLES

The four temperature variables were combined and related to the subsequent minimum temperature by graphical techniques. The surface index temperature and

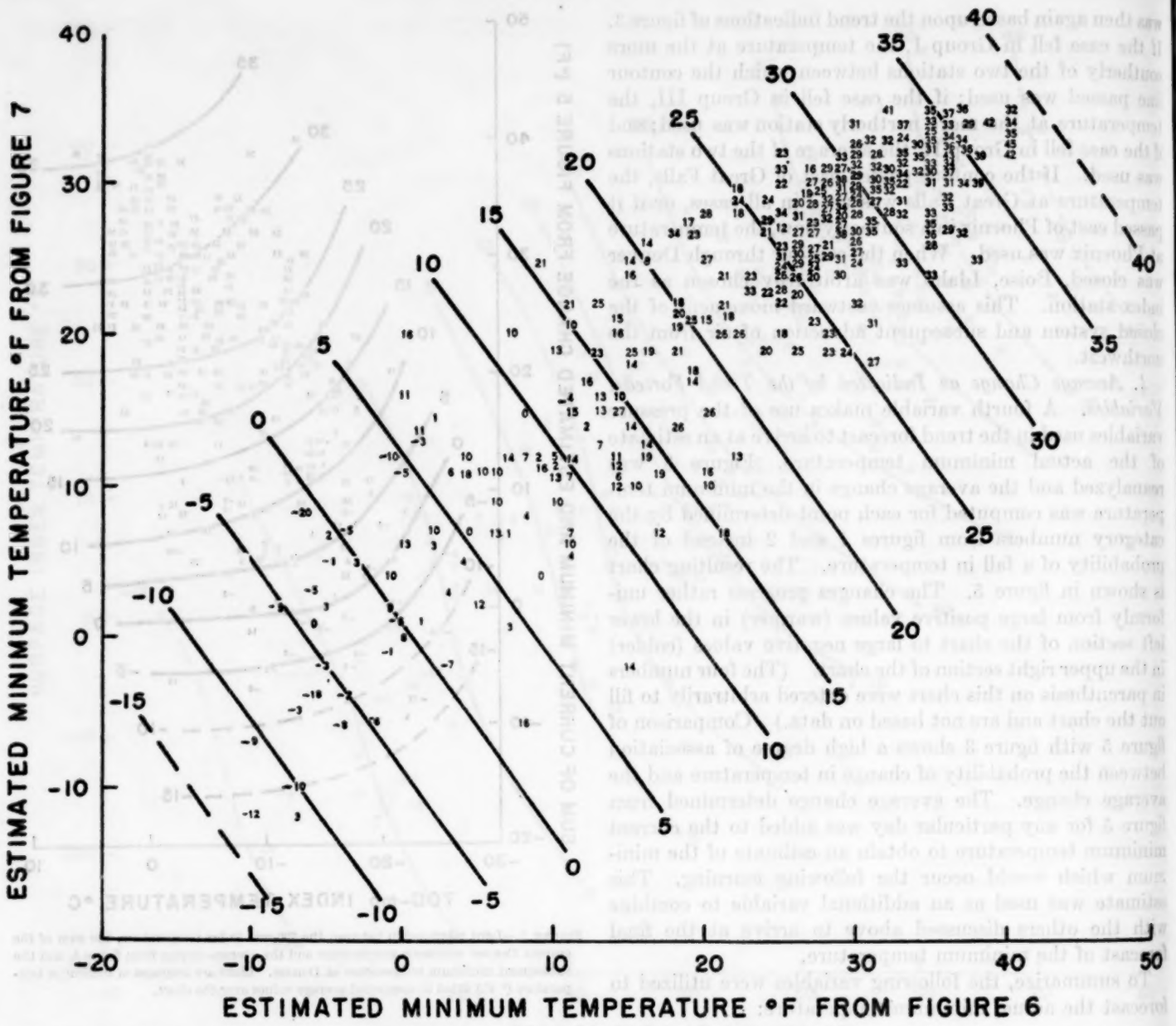

FIGURE 8.—Joint relationship between minimum temperature estimates from figures 6 and 7 and the subsequent minimum temperature at Denver. Lines are isograms of minimum temperature (° F.) fitted to computed average values over the chart.

the maximum temperature were paired and used as coordinates of a scatter diagram with the observed minimum temperature plotted at the point determined by the two coordinates. Areas with approximate equal numbers of cases were outlined on the chart and the average values of the minimum temperatures within these areas computed. Isolines of minimum temperature were then fitted to these average values for 5° intervals (see fig. 6).

The 700-mb. index temperature and the sum of the current minimum and the average change from figure 5 were then used as coordinates of a second scatter diagram with the observed minimum again plotted in the body of the chart. A similar analysis was made of this chart as shown in figure 7.

For each case estimates of the minimum temperature were obtained from the isolines of figures 6 and 7. These two estimates were then used as coordinates of a third scatter diagram and the observed minimum temperature again plotted. The same analysis was made on this chart and isolines of minimum temperatures drawn (fig. 8). An estimate from figure 8 gives the final forecast of the minimum temperature.

While sets of curved lines were drawn on figures 6 and 7, the more or less even spacing of the lines and the relatively slight curvature suggest that perhaps the true relationships are linear. A least-squares regression equation of the following form was therefore computed:

UNIVERSITY OF MICHIGAN LIBRARIES

$$Y=aX_1+bX_2+cX_3+dX_4+e$$

where Y=the verification minimum temperature

X_1=the maximum temperature

X_2=the surface index temperature

X_3=the current minimum plus the estimated change from figure 5.

X_4=the 700-mb. index temperature

The constants a, b, c, d, and e were evaluated, which resulted in the following equation for forecasting the minimum temperature, Y:

$$Y=.35X_1+.19X_2+.24X_3+.37X_4-.75$$

The multiple correlation of the four variables with the verification minimum temperature was .92. The results obtained by using the equation to forecast the minimum temperature were very similar to those obtained from the charts, but the chart results seem to have a very slight advantage both in the average error and the extreme errors made, both in the original data and the test data (historical). (See below.)

The graphical technique has the advantage that no assumptions whatever need be made about the relationships between the independent variables and the dependent variable. In this particular case the assumption of linearity will probably prove to be true in the long run, but in other forecast problems such an assumption might well lead to very erroneous results. In general in using the graphical technique of combining variables it is better to draw the isopleths most consistent with the data on the chart, and make no assumptions whatever. Another advantage of the graphical technique over regression equations that should be considered is that the analysis can be made without recourse to a calculating machine, while the computation of a five variable regression equation without a modern calculator would be laborious indeed.

RESULTS

Three years of winter months were used for developmental or original data upon which the charts were based. These data included January, February and March of 1948-49-50 (271 cases). For test purposes the months of January, February, March, and December of 1947, December 1950, January, and February of 1951 were utilized (209 cases). (Charts for February 28 and March 1, 1947 were missing.) These data will be referred to as test data (historical). The system has been in use in day-to-day forecasting beginning in March 1951, so a very practical day-to-day test on ten additional months has been possible. The months are March and December 1951, January, February, March, November, and December 1952, January, February, and March 1953. These data will be referred to as test data (current).

TABLE 1.—*Comparison, on basis of average error, of Objective forecasts using charts, Objective forecasts using regression equation, and Official forecasts. Original data (271 cases)*

Month	Average error		
	Objective forecasts using charts	Objective forecasts using regression equation	Official minimum temperature forecasts
	°F.	°F.	°F.
1948: January	4.3	4.5	4.8
February	4.2	4.3	5.2
March	3.9	4.5	5.4
1949: January	5.3	4.9	5.7
February	3.1	3.7	5.0
March	3.3	3.5	3.5
1950: January	4.3	7.6	7.0
February	2.9	3.2	3.8
March	3.2	4.0	4.3
All months	3.8	4.5	5.0

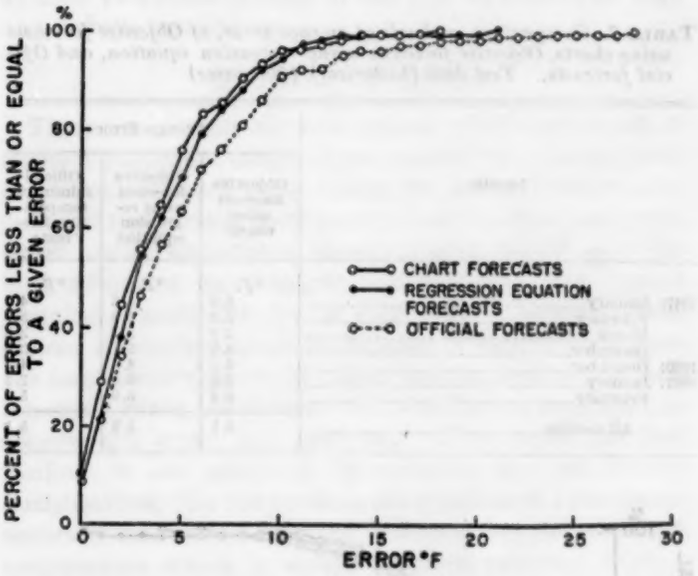

FIGURE 9.—Cumulative frequency distributions of errors for Objective system forecasts using charts, Objective system forecasts using the regression equation, and Official forecasts. Original data (271 cases).

Original Data. A comparison was made on the original data between the results obtained when the charts were used and the results when the regression equation was used to make the forecast. This comparison is presented in table 1 on the basis of average error by months. In this table the average errors of the official minimum temperature forecasts are also listed. The official forecast is the one issued at approximately 0800 MST for the following night. This forecast is generally presented as a 6° range of temperature and for comparison purposes, the forecast temperature was taken as the middle of the range. For example, a forecast of 20°–25° F. was considered a forecast of 23°.

Figure 9 shows cumulative distribution curves of the errors for the three sets of forecasts. The chart fore-

casts show a consistently higher percent of errors less than or equal to any given error that the official forecasts show.

Test Data (historical). All forecasts from test data were made using the official maximum temperature forecasts. The same analysis of errors was made for these seven months of test data as described above for the original data. Table 2 shows the average errors for the three sets of forecasts. The average errors for all seven months are practically identical and in only two individual months is there an appreciable difference between the chart forecasts and the official forecasts, one in which the objective system was better and one in which the official forecasts were better. The cumulative frequency curves of errors in figure 10 are also very similar and show no significant differences, except that the regression equation forecasts have the largest extreme error.

Test Data (current). The objective forecasts were computed only from the charts when the system was put into daily use since the chart forecasts consistently showed a slight advantage over the regression equation forecasts in both the original and test data (historical). A similar summarization of results as described above was made of the day-to-day test data. The summarization has been made by seasons, however, to try to discover if there has been any apparent increase in accuracy, on the average, since the aid has been in use. Tables 3 and 4 show the average errors for the two seasons and figures 11 and 12 the cumulative frequency curves of errors.

In the first season the forecasts are practically identical, with the objective forecasts perhaps having a slight edge, whereas in the second season the official forecasts consistently have the better forecasts, on the average. This might well be attributed to the forecasters being more familiar with the objective system, especially with its shortcomings and where it is likely to "bust," and thus, on the average, are able to improve upon the objective indication of the forecast. If this were true, the official forecasts should show progressive improvement from the period

TABLE 2. *Comparison, on basis of average error, of Objective forecasts using charts, Objective forecasts using regression equation, and Official forecasts. Test data (historical) (209 cases)*

Month	Average Error		
	Objective forecasts using charts	Objective forecasts using regression equation	Official minimum temperature forecasts
	°F.	°F.	°F.
1947: January	5.0	5.2	4.7
February	5.5	6.0	5.7
March	3.8	3.7	3.8
December	4.9	5.1	3.9
1950: December	4.8	4.8	4.5
1951: January	5.8	6.6	7.4
February	5.8	6.0	5.5
All months	5.1	5.3	5.1

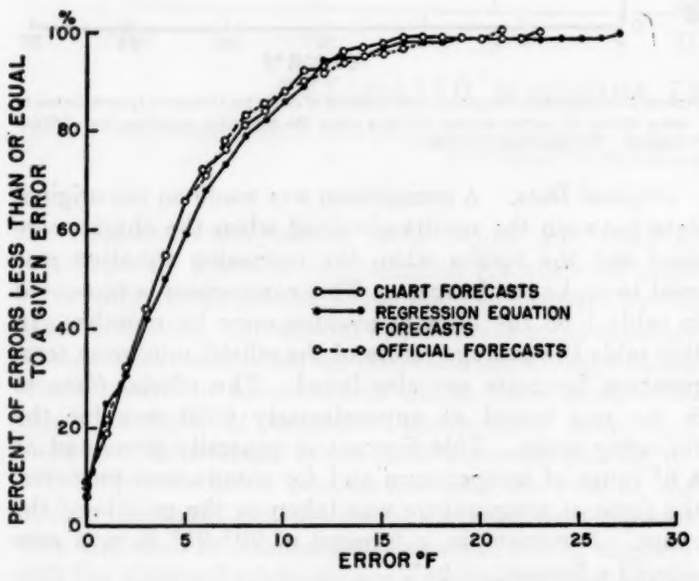

FIGURE 10.—Cumulative frequency distributions of errors for Objective forecasts using charts, Objective forecasts using the regression equation, and Official forecasts. Test data (historical) (209 cases).

TABLE 3.—*Comparison, on basis of average errors, of Objective forecasts (charts) and Official forecasts. Test data (current) first season objective aid was used. (153 cases)*

Month	Average error	
	Objective forecasts	Official forecasts
	°F	°F
Mar. 1951	4.6	5.5
Dec.	5.5	6.0
Jan. 1952	4.1	4.0
Feb.	3.2	3.2
Mar.	3.6	3.6
All months	4.2	4.4

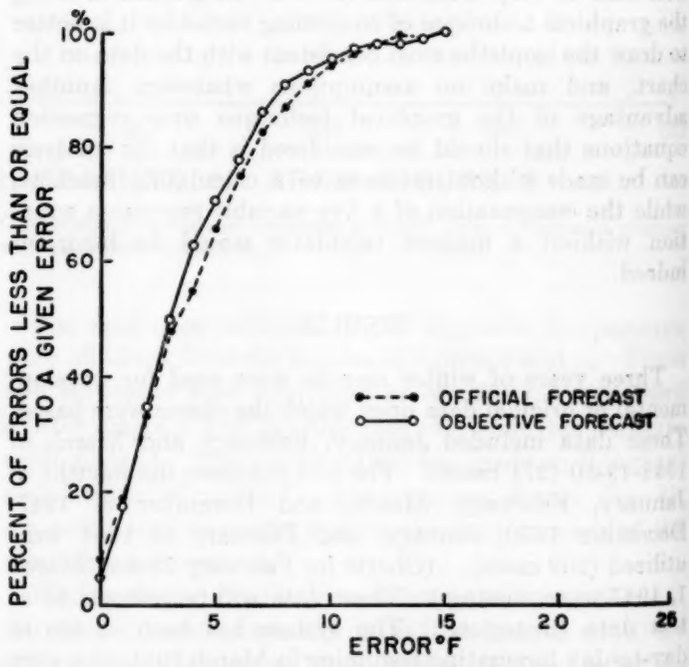

FIGURE 11.—Cumulative frequency distributions of errors for Objective forecasts (charts) and Official forecasts. Test data (current) first season objective aid was used (153 cases).

UNIVERSITY OF MICHIGAN LIBRARIES

TABLE 4.—*Comparison, on basis of average errors, of Objective forecasts (charts) and Official forecasts. Test data (current) second season objective aid was used. (151 cases)*

Month	Average error	
	Objective forecasts	Official forecasts
	°F	°F
Nov. 1952	4.8	3.9
Dec.	3.8	3.8
Jan. 1953	6.2	6.0
Feb.	4.4	3.4
Mar.	3.4	3.0
All months	4.5	4.0

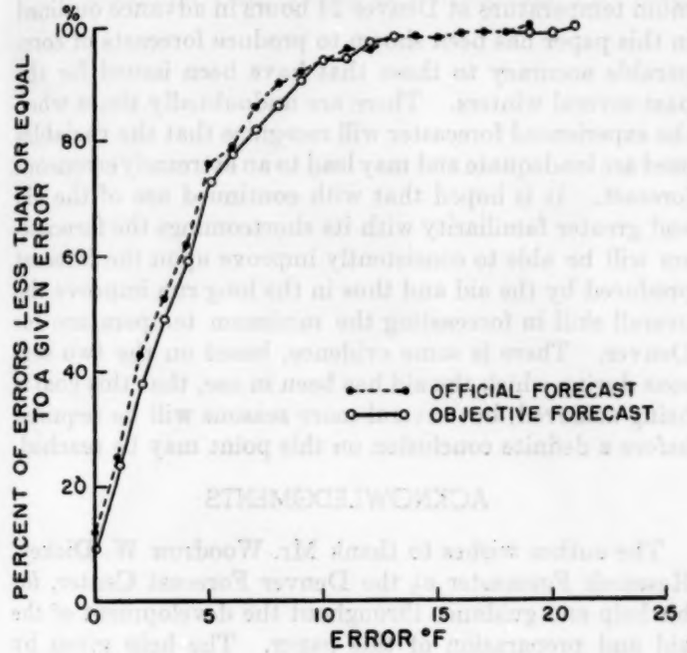

FIGURE 12.—Cumulative frequency distributions of errors for Objective forecasts (charts) and Official forecasts. Test data (current) second season objective aid was used (151 cases).

the aid was put in use through the two seasons when the aid was used. This does show up in the average error, as shown below, but more strikingly in the cumulative frequency distributions of errors as shown in figure 13.

	Average error	*Average change in minimum temperature*
Period before aid was available (original data and test data, historical, 18 months)	5.0	7.5
1st season aid was available	4.4	6.2
2nd season aid was available	4.0	6.4

To offset this evidence of improved accuracy is the fact that the average change in minimum temperature (and presumably the average difficulty of the forecast) was greater during the period before the aid was available, as shown above. Another weakness of the analysis is the fact that the period before the aid was available includes almost four times as many months as either of the seasons when the aid was available. While there is some evidence

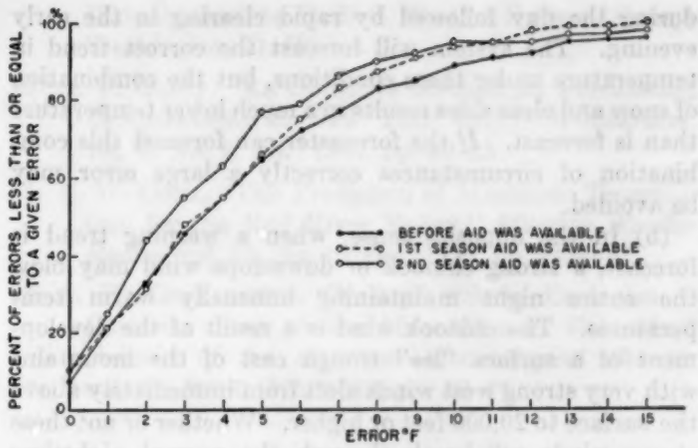

FIGURE 13.—Cumulative frequency distributions of errors for Official forecasts for three periods of time: (1) Before objective aid was available, 18 months; (2) first season aid was available, 5 months; and (3) second season aid was available, 5 months.

that the aid has contributed to an increase in accuracy, at least two more seasons of use will be needed to draw any definite conclusions.

SOURCES OF ERROR

There are certain obvious sources which contribute to errors in minimum temperature forecasting. Factors such as amount of cloud cover during the day and night, condition of the ground, snow cover, wind direction, and wind speed are of undisputed importance in determining the final minimum temperature which occurs, but from a practical standpoint for a long period forecast these factors themselves must be forecast if their effects upon the temperature are to be taken into account in the final forecast. Since the forecast of these factors is subject to considerable error, and since their effects upon the final reading of the minimum temperature are not known quantitatively the net result is the creation of a maximum accuracy that can be expected in forecasting the minimum temperature which is several degrees removed from a zero error.

There are several sources of possible failure of the system due to assumptions made in developing the system and due to the fact that a method of this kind tends to forecast "average" situations and the unusual situation is only partially accounted for, and sometimes entirely unaccounted for. Several situations which have been noted in the use of the system that apparently account for some of the larger errors are described below. These are separated into two groups, (1) Correct Trend, but forecast change too small, and (2) Incorrect Trend, with resulting large error.

(1) Correct Trend.

(a) On rare occasions the temperature "tomorrow morning" at Denver will be colder than any temperature reported to the north in Wyoming, or even Montana "this morning". This results from a snow situation which deposits a fairly heavy amount of snow in the Denver area

during the day followed by rapid clearing in the early evening. The system will forecast the correct trend in temperature under these conditions, but the combination of snow and clear skies results in a much lower temperature than is forecast. *If* the forecaster can forecast this combination of circumstances correctly a large error may be avoided.

(b) In the opposite sense, when a warning trend is forecast, a strong chinook or downslope wind may blow the entire night maintaining unusually warm temperatures. The chinook wind is a result of the development of a surface "lee" trough east of the mountains with very strong west winds aloft from immediately above the surface to 20,000 feet or higher. Whether or not these strong winds will break through the normal nighttime inversion is a very difficult forecast problem. Peculiar and very erratic temperature fluctuations can occur under such conditions [12].

(2) Incorrect Trend. There are several situations which can result in an incorrect trend indication from the variables used.

(a) Low pressure system to the west of Sheridan, when Sheridan is under the influence of a shallow surge of cold air from the north. In these cases the rising pressure trend at Sheridan sometimes results in a falling temperature forecast which fails to verify. In this situation the cold air that has pushed into the Sheridan area is generally quite shallow and the low pressure from the west takes over resulting in a falling pressure trend after the 0530 MST chart. The pressure rise is shunted eastward over the Dakotas and does not affect the Denver area.

(b) Rapidly moving surges of cold air from Canada. The assumption that Sheridan will be in the cold air 24 hours prior to Denver will not always hold. In this situation the cold air with rising pressure is sometimes just north of the Sheridan area on the 0530 MST chart and 24 hours later the surge is south of Denver. In these cases Sheridan has a falling 12-hour pressure change and the temperature trend usually falls in category I, or the warmer trend, resulting in a "bust" forecast.

(c) Well-defined storms over the North Central States. In this synoptic situation the 12-hour pressure change at Sheridan is a rising one and a high pressure area is pushing into the Sheridan area. With the rising pressure trend at Sheridan, the temperature trend from figure 3 or 5 is usually in category III or falling trend. This sometimes fails to verify, especially to the limits that the system specifies, because the main surge of the cold air is drawn eastward into the storm over the North Central States.

(d) Closed Lows aloft that stagnate west of the Divide. In these cases the temperature trend from the surface indications is generally of the category III type which calls for colder temperatures. The system assumes movement of these Lows which would bring cold air over the Denver region, but if the Low remains stationary the cold air will be delayed in reaching Denver until the Low moves eastward. A correct forecast of the movement, or stagnation, of such Lows obviously would aid in eliminating extreme errors in these cases.

(e) Rapidly falling pressure at Grand Junction and lesser falls at Sheridan. This results in the temperature trend falling in category III, calling for colder temperatures when sometimes there is actually no source of colder air coming into the area. This situation does not result in extreme errors, but may result in errors of 6° to 10° F.

CONCLUSIONS

The relatively simple method for forecasting the minimum temperature at Denver 24 hours in advance outlined in this paper has been shown to produce forecasts of comparable accuracy to those that have been issued for the past several winters. There are undoubtedly times when the experienced forecaster will recognize that the variables used are inadequate and may lead to an extremely erroneous forecast. It is hoped that with continued use of the aid and greater familiarity with its shortcomings the forecasters will be able to consistently improve upon the forecast produced by the aid and thus in the long run improve the overall skill in forecasting the minimum temperature for Denver. There is some evidence, based on the two seasons during which the aid has been in use, that this goal is being achieved, but several more seasons will be required before a definite conclusion on this point may be reached.

ACKNOWLEDGMENTS

The author wishes to thank Mr. Woodrow W. Dickey, Research Forecaster at the Denver Forecast Center, for his help and guidance throughout the development of the aid and preparation of this paper. The help given by Virginia Reynolds, Research Assistant, in the collection of data and copying of diagrams and charts is also greatly appreciated.

REFERENCES

1. A. W. Cook, The 12-Hour Pressure Change Chart, U. S. Weather Bureau, Denver, Colo. (Unpublished.)
2. Forecast Rules and Precepts, compiled by Forecast District Office, Weather Bureau Airport Station, Kansas City, Mo., revised 1948. (Unpublished.)
3. Walter T. Wilson, Washington Minimum Forecasting by Objective Relation to Upwind Index Station, U. S. Weather Bureau, Washington, D. C., 1943. (Unpublished.)
4. Glenn W. Brier, U. S. Weather Bureau, Washington, D. C. (Unpublished research results.)
5. J. E. Miller and A. E. Burgtorf, *Objective Methods of Forecasting the Daily Minimum Temperature at New York City*, New York University, 1945.
6. H. T. Mantis and W. W. Dickey, "Objective Methods of Forecasting the Daily Minimum and Maximum

UNIVERSITY OF MICHIGAN LIBRARIES

Temperature," *Report No. 4*, U. S. Army Air Force, Weather Station, New York University, 1945.

7. C. P. Mook and S. Price, "Objective Method of Forecasting Winter Minimum Temperatures at Washington, D. C.," Weather Bureau *Research Paper No. 27*, Washington, 1947, 38 pp.
8. W. W. Dickey, "Estimating the Probability of a Large Fall in Temperature at Washington, D. C.," *Monthly Weather Review*, vol. 77, No. 3, Mar. 1949, pp. 67–78.
9. W. W. Dickey, An Objective Aid in Forecasting the Minimum Temperature at Philadelphia, Pa., 1949. (Unpublished, on file U. S. Weather Bureau Library, Washington, D. C.)
10. A. V. Hardy, "An Objective Method for Forecasting Temperatures at New York City," *Weatherwise*, vol. 4, No. 2, Apr. 1951, pp. 42–45.
11. A. W. Cook, "The Prediction of Minimum Temperature for the Red River Valley," *Monthly Weather Review*, vol. 53, No. 10, Oct. 1925, pp. 443–447.
12. A. W. Cook and A. C. Topil, "Some Examples of Chinooks East of the Mountains in Colorado," *Bulletin of the American Meteorological Society*, vol. 33, No. 2, Feb. 1952, pp. 42–47.

THE WEATHER AND CIRCULATION OF AUGUST 1953[1]

Featuring an Analysis of Dynamic Anticyclogenesis Accompanying Record Heat and Drought

WILLIAM H. KLEIN
Extended Forecast Section, U. S. Weather Bureau, Washington, D. C.

WEATHER HIGHLIGHTS

The outstanding feature of the weather of August 1953 was the prolonged and widespread dry spell during the latter part of the month. The *Weekly Weather and Crop Bulletin* for the week ending August 31, 1953 reported "A large area extending from the eastern portions of South Dakota, Nebraska, and Kansas eastward over the Main Corn Belt nearly to the Atlantic Coast received less than 25 percent of the normal rainfall during the last three weeks. The major portion of this dry region did not get even 5 percent of the usual amount." No precipitation of consequence fell for 26 days in most of Indiana, 25 days in parts of New York, and 24 days in Pennsylvania before the drought was finally broken by general soaking rains on September 4 and 5.

The development of the drought during the last three weeks of August is illustrated in figure 1, which gives the total precipitation observed during each of three 5-day periods separated by one-week intervals. Note the area of no measurable rain in the Upper Mississippi Valley on the first map of the series and its expansion southward, eastward, and westward on the middle and last maps.

At the beginning of the dry spell temperatures were near to below normal as a large mass of cool polar air from Canada and the Pacific overspread the eastern two-thirds of the United States. Many new early-season low temperature records were set in the Ohio Valley and later in the Southeast. As the air mass stagnated, temperatures gradually rose to record-breaking levels, first in the Northern Plains and then progressively eastward and southward. This transition is well illustrated by the 5-day mean temperature anomalies shown in figure 2. The vast area from the Rockies to the Atlantic Coast covered by much above normal temperature in figure 2c is especially striking when it is recalled that this class normally occurs only one-eighth of the time. The heat was particularly intense between August 30 and September 3 in the heavily populated northeastern quadrant of the country, where many stations reported the hottest weather of the year and the highest temperatures on record for so late in the season. Some of the high temperatures were as follows: 107° F. in Hagerstown, Md.; 106° in Fredericksburg, Va.; 105° in Newark, N. J.; 103° in Louisville, Ky. and Huntington, W. Va.; 102° in New York, N. Y., Evansville, Ind., Cincinnati, Ohio, Pine

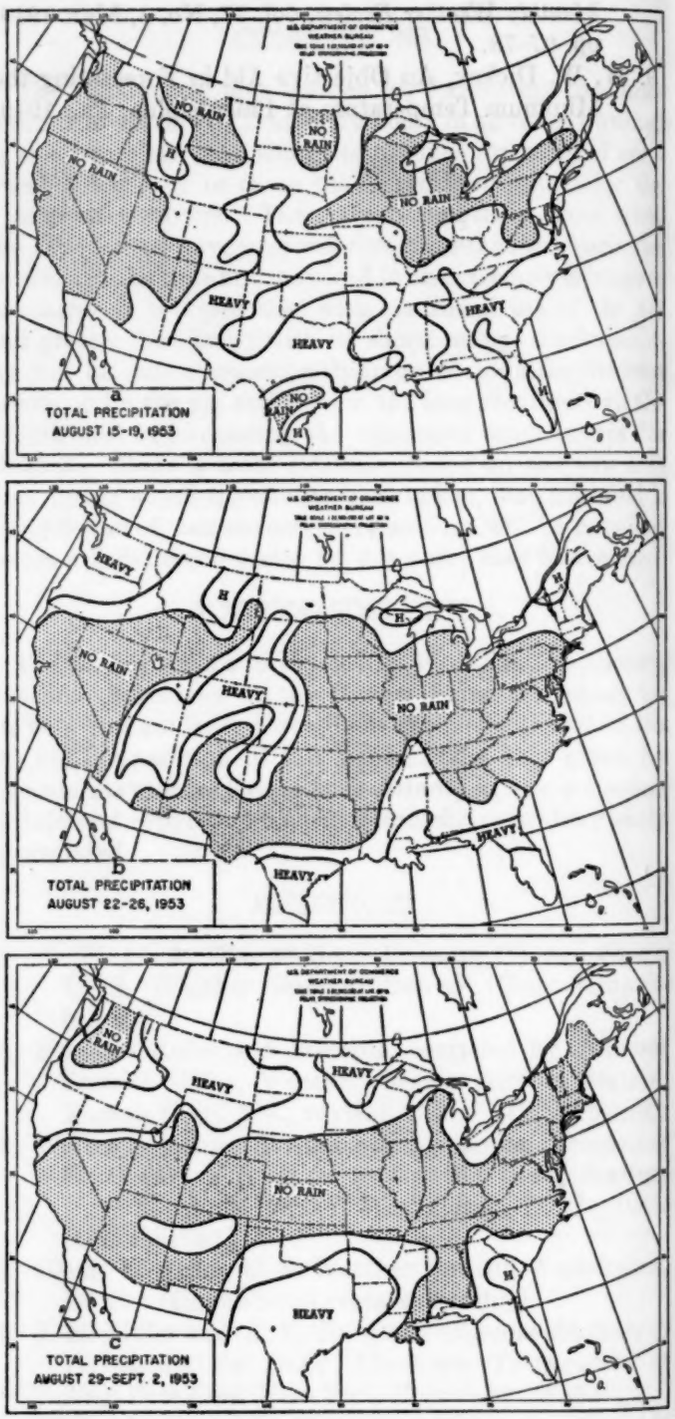

FIGURE 1.—Total precipitation during three 5-day periods a week apart from August 15 to September 2, 1953. Analysis is in terms of 3 classes; no rain, heavy (which normally occurs one-third of the time), and an intermediate class. Note the vast area without measurable rain in the eastern two-thirds of the country.

[1] See Charts I-XV following p. 265 for analyzed climatological data for the month.

UNIVERSITY OF MICHIGAN LIBRARIES

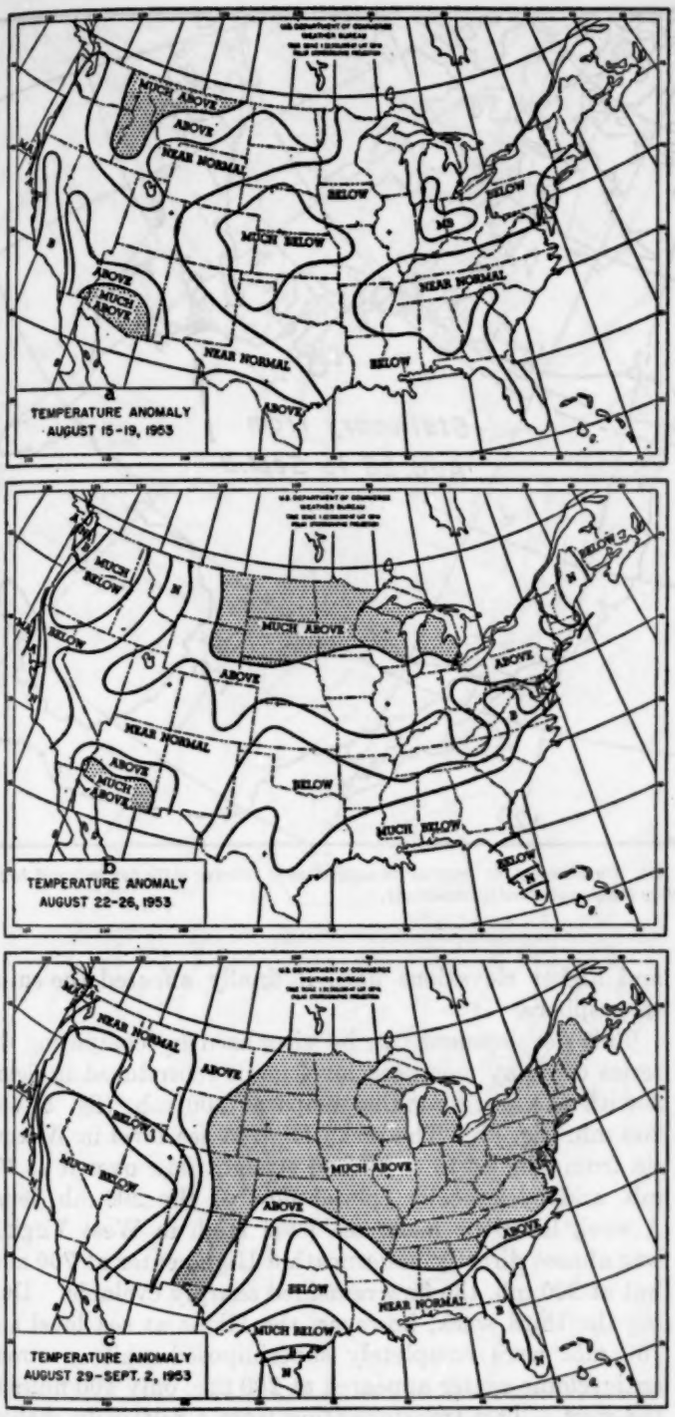

FIGURE 2.—Five-day mean surface temperature anomalies at one-week intervals from August 15 to September 2, 1953. The classes above, below, and near normal occur on the average one-fourth of the time, while much above and much below each occur normally one-eighth of the time. Note the progressive southeastward expansion of the area of much above normal.

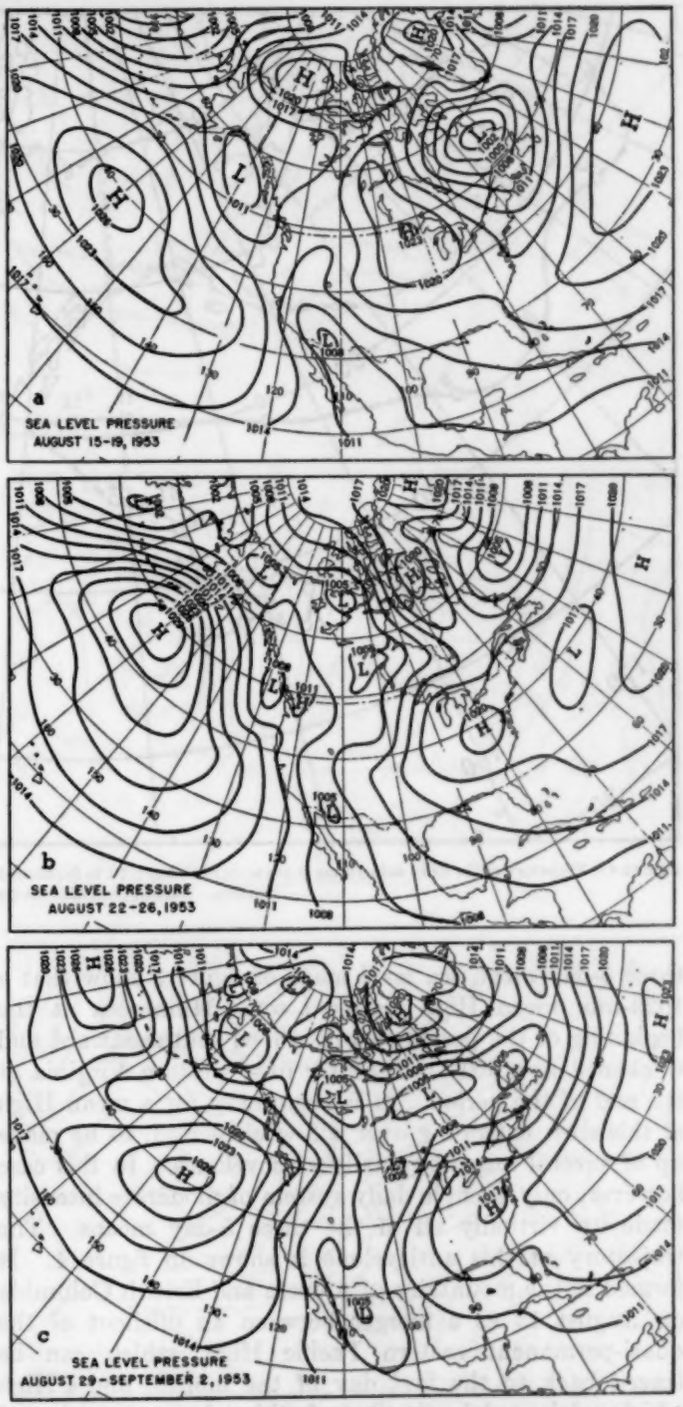

FIGURE 3.—Five-day mean sea level maps (in mb.) during the same three weeks shown in figure 1. Note the southeastward motion of the mean High from Minnesota to West Virginia, and its subsequent stagnation.

River, Wis., and Baltimore, Md.; 101° in Chicago, Ill., Cleveland, Ohio, Philadelphia, Pa., St. Louis, Mo., and Hartford, Conn. The heat wave was unusual not only for its intensity but also for its duration. For example, in Washington, D. C. there were 12 straight days of temperatures above 90° and 7 in a row above 95° between August 25 and September 5, while Richmond, Va., had 5 consecutive days with maxima of 100° or more starting August 29.

THE ANTICYCLONE

During the three weeks of dry weather described above, the eastern half of the United States was dominated by a pronounced anticyclonic circulation at sea level. The

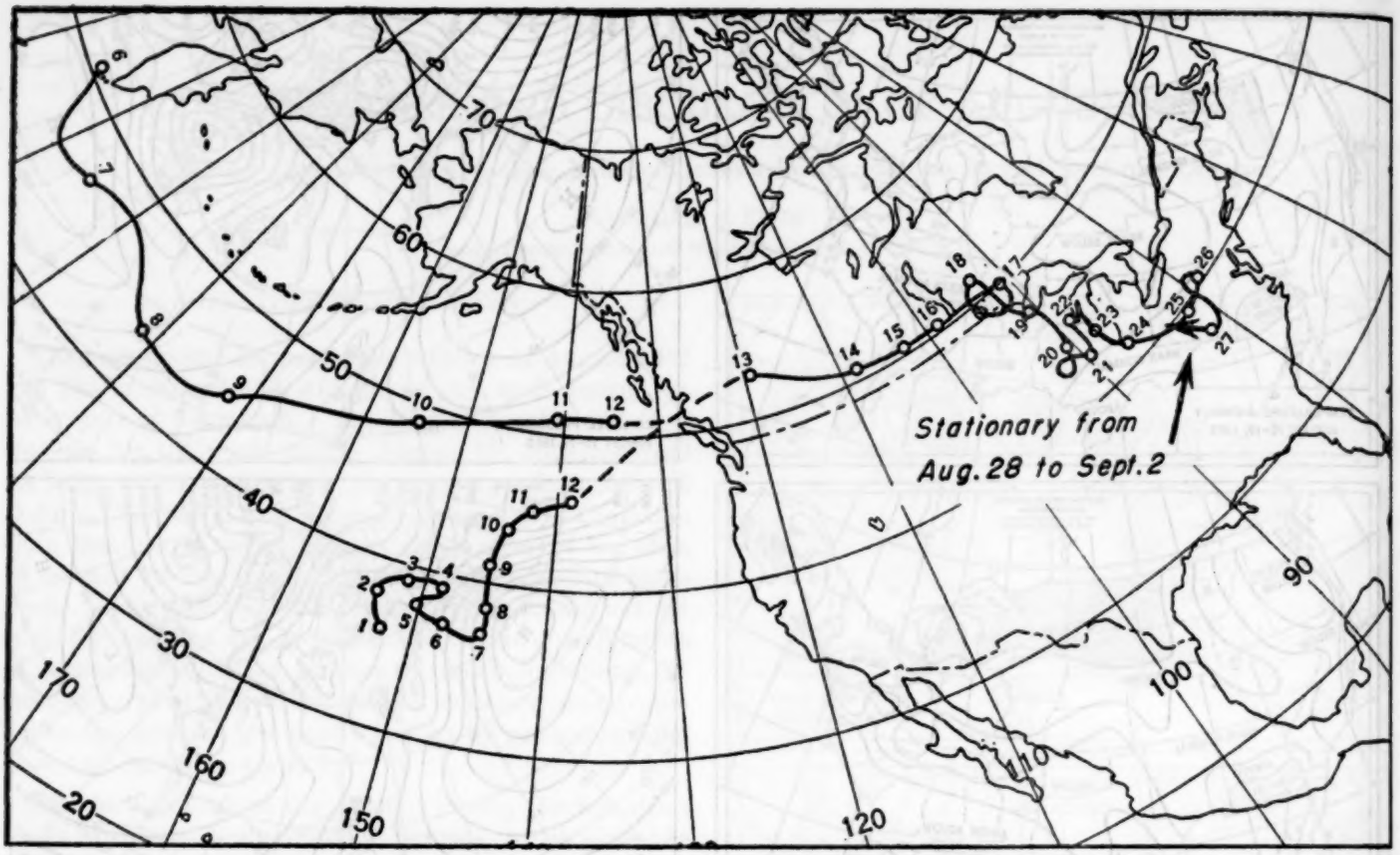

FIGURE 4.—Trajectory of the daily anticyclone at sea level from August 1 to September 2, 1953. Circles locate the center of the anticyclone at 1230 GMT of the day indicated by the number. Dashed portion of the trajectory is region of uncertain continuity.

three 5-day mean sea level maps of figure 3 show that a 1023-mb. mean High centered over Minnesota at the beginning of the period slowly moved southeastward and weakened to a 1017-mb. center over western Virginia at the end of the period. It is customary for a mean High of this sort, extending over a 3-week period, to be made up of several migratory daily anticyclones. In this case however, only a single daily system of moderate intensity made up virtually all of the three 5-day means. The trajectory of this anticyclone is shown in figure 4. It formed in the mountains of Alberta and British Columbia on August 13 as a merger between an offshoot of the quasi-permanent eastern Pacific High, which can be traced back to the first day of the month, and a High which originated in the Sea of Okhotsk on the 6th and then moved rapidly eastward across the northern Pacific. From August 14 to 18 the anticyclone skirted the northern border of the United States before definitively entering the country at the western end of Lake Superior on the 19th. After moving slowly through Wisconsin for four days the anticyclone moved rapidly southeastward through Indiana and Ohio and entered West Virginia on the 25th. Here a most remarkable stagnation occurred. For nine consecutive days, from August 25 to September 2, the High center remained in the West Virginia area. During this period the anticyclonic circulation extended to higher and higher elevations until it finally affected the entire troposphere.

This development can be visualized by comparing the series of 5-day mean sea level maps reproduced in figure 3 with the corresponding maps at 700 mb. (fig. 5) and 200 mb. (fig. 6). The mean High at sea level in Wisconsin from August 15 to 19 had straight flow over it at 700 mb. and cyclonically curved flow at the 200-mb. level. A week later the mean sea level High in West Virginia was almost directly underneath a High center at 700 mb., but at 200 mb. the flow remained sharply cyclonic. During the third week, however, the Highs at sea level and 700 mb. were completely superimposed while a strong anticyclonic center appeared at 200 mb. only 400 miles to the west. This transformation from a relatively shallow cool High to a deep warm or dynamic High was not accompanied by an increase of central pressure at sea level, as is customary in dynamic anticyclogenesis. Instead the sea-level pressure at the center of the High fluctuated slightly around the 1025-mb. level between August 13 and 27. The High then progressively weakened to a 1017 center on September 2, after which its separate identity was lost as it merged with the quasi-permanent Bermuda High. On the 5-day mean sea level charts (fig. 3) the pressure at the center of the High diminished by 6 mb. from the first to the third week of

UNIVERSITY OF MICHIGAN LIBRARIES

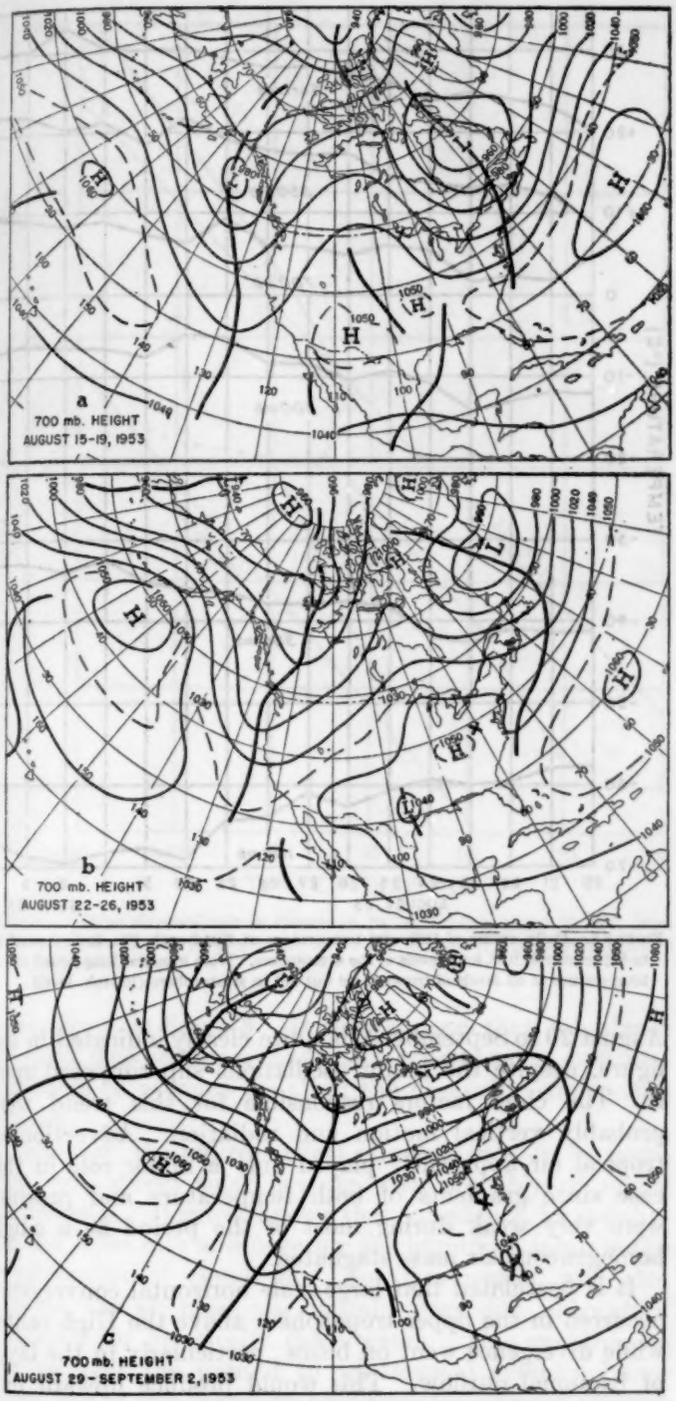

FIGURE 5.—Five-day mean charts at 700 mb. (in tens of feet) during the periods corresponding to figure 1. The center of the 5-day mean anticyclone at sea level, indicated by the crosses, gradually approached the High center at 700 mb.

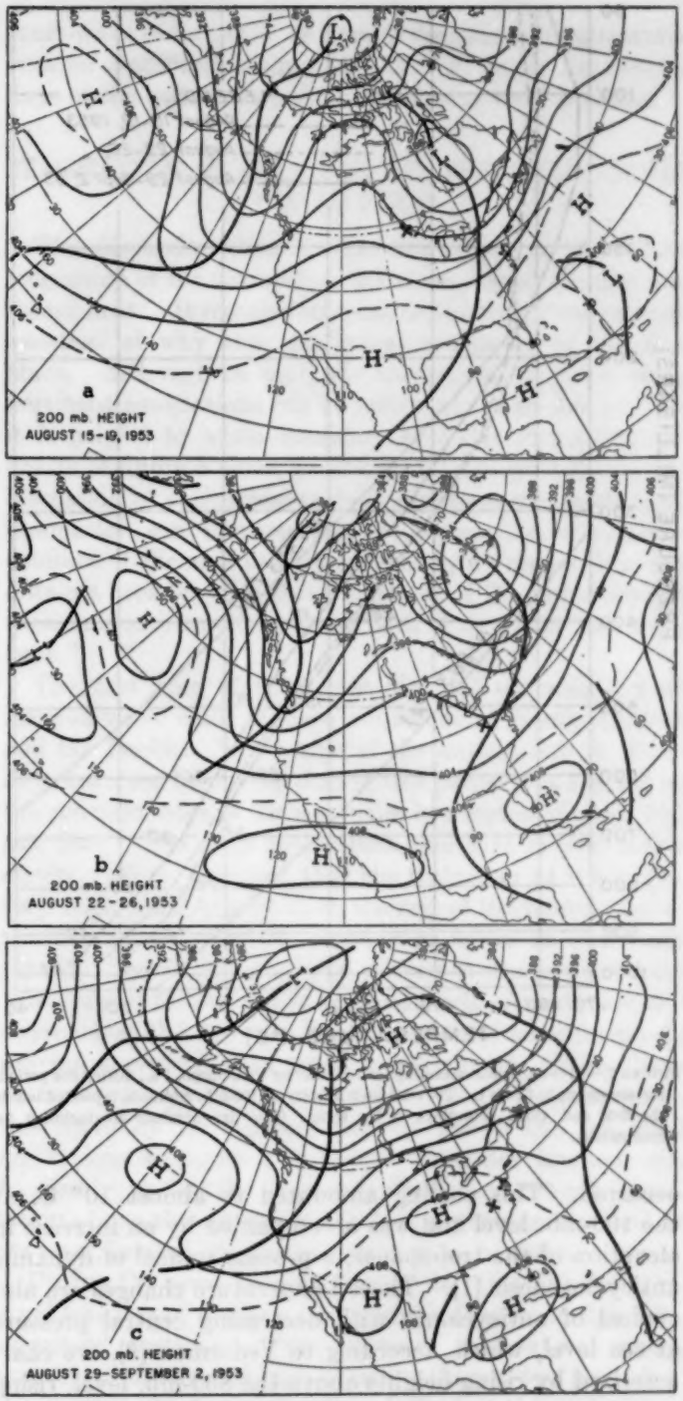

FIGURE 6.—Five-day mean charts at 200 mb. (in hundreds of feet) during the periods corresponding to figure 1. Note the development of the High center in southern Illinois, just west of the sea level anticyclone (indicated by cross) during the third week of the series.

the series. During the same period upper level heights above the center of the sea level anticyclone increased by about 180 feet at 700 mb. (fig. 5) and 1,000 feet at 200 mb. (fig. 6).

AIR MASS TRANSFORMATION

Transformation of the anticyclone is also indicated by comparing the three 5-day mean upper-air soundings at Pittsburgh, Pa., the closest RAOB station to West Virginia. Figure 7 shows that the entire troposphere up to 200 mb. underwent progressive warming from the first to the third week of the series, with the greatest change in the second half of the period. The largest heating (about 10° C.) occurred in the lower levels and also around 400 mb., with lesser warming elsewhere. In the stratosphere, on the other hand, progressive cooling

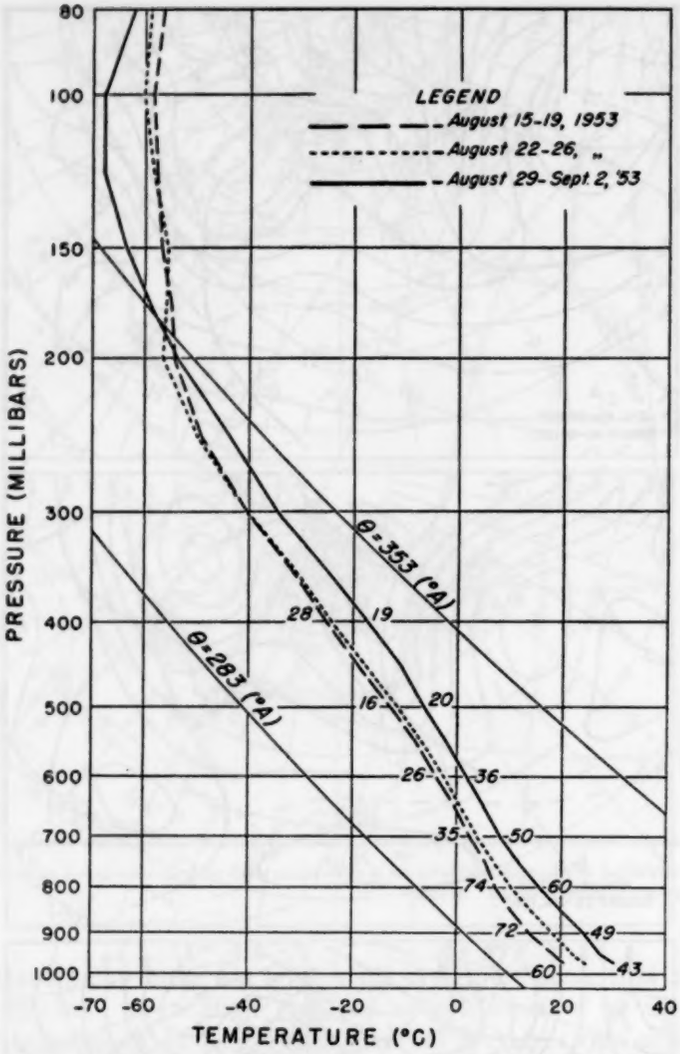

FIGURE 7.—Five-day mean soundings at 1500 GMT for Pittsburgh, Pa., during the periods corresponding to figure 1. The relative humidity, at 100-mb. intervals, is plotted beside the first and third soundings of the series. Two dry adiabats are included for comparison.

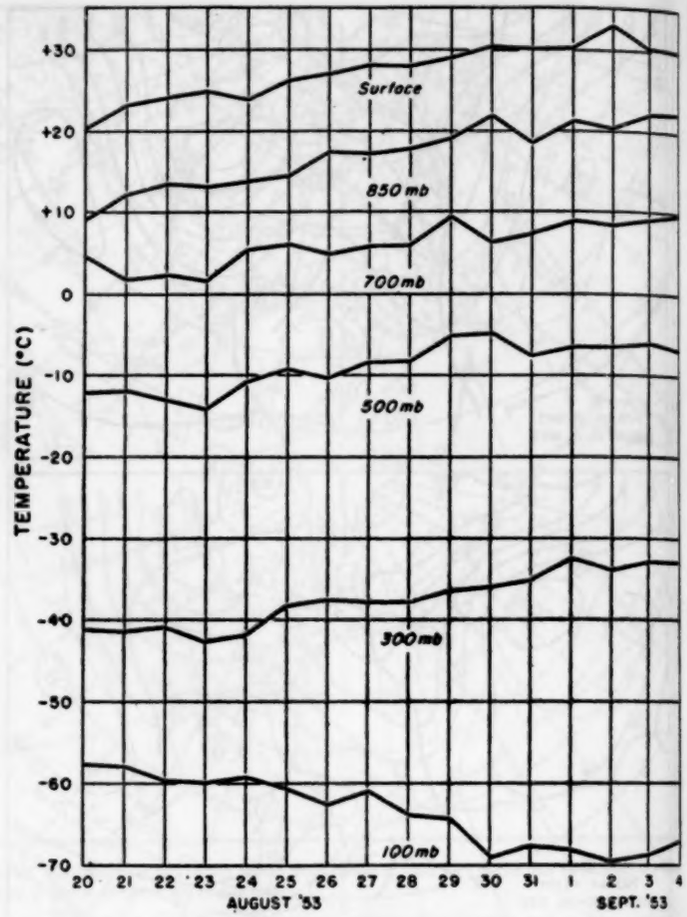

FIGURE 8.—Daily values of 1500 GMT temperature at Pittsburgh, Pa., from August 20 to September 4, 1953, for 6 levels of the atmosphere. Note irregular long-period rise of temperature at all levels of troposphere but fall in stratosphere (100-mb. level).

occurred. This cooling amounted to almost 10° C. at the 100-mb. level and was accompanied by an increase in elevation of the tropopause, a process typical of dynamic anticyclogenesis [1]. These temperature changes are also typical of anticyclones with decreasing central pressure at sea level, which, according to Vederman [2], are characterized by rising heights above the 850-mb. level, rising temperatures from 1000 to 250 mb., falling temperatures above the 250-mb. level, and a southward component of motion. The behavior of the anticyclone from August 19 to September 2, 1953 conformed quite closely to each of the four criteria listed above.

The exact mechanism responsible for the pressure and temperature changes observed in the anticyclone is difficult to determine. The complexity of the problem is indicated by the apparently irregular day-to-day fluctuations of temperature which occurred, as illustrated by the thermograms of figure 8 for six different levels of the atmosphere at Pittsburgh. The long-period trend, from August 20 to September 4, is quite clearly indicated in the figure, despite the minor oscillations superimposed upon it. The chief factors responsible for this trend were probably vertical motion and radiation. Advection of tropical air apparently played only a minor role in this case since gradients of both temperature and pressure were very weak during most of the period as a single homogeneous air mass stagnated.

It is postulated that large-scale horizontal convergence occurred in the upper troposphere above the High center while divergence went on below, particularly in the layer of frictional outflow. This would produce upward motion, cooling, and ascent of the tropopause above the 200-mb. level. Below this level downward motion or subsidence would result in increasing temperatures since the lapse rate was initially stable. The most striking daily sounding illustrating this process is shown in figure 9, where a sharp decrease in dew point at the subsidence inversion is clearly indicated. On the other hand, many daily soundings made during this period contain little if any evidence of subsidence, nor is subsidence clearly indicated in figure 7. Instead the daily soundings suggest that complicated mixing and convergence processes were responsible for irregular temperature fluctuations of the

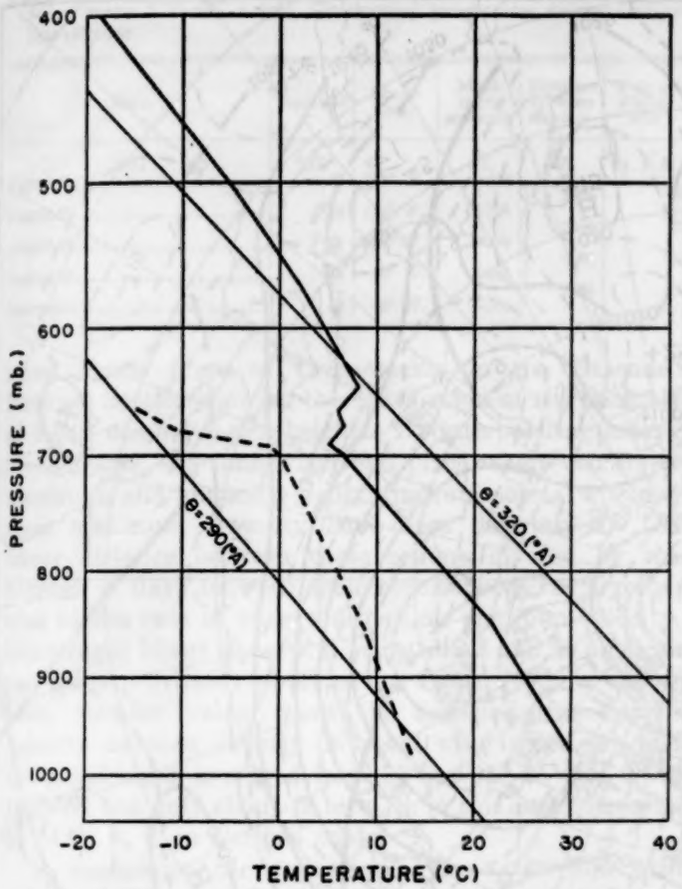

FIGURE 9.—Upper air sounding over Pittsburgh, Pa., at 1500 GMT, August 30, 1953. Note sharp decrease in dew point (dashed curve) and temperature inversion just above 700 mb.

type shown in figure 8. It thus appears that subsidence by itself was neither a continuous process nor a sufficient condition to account for all of the observed temperature change.

However, the indirect effect of subsidence, in conjunction with direct solar heating, was probably of major significance. It is well known that subsidence, by stabilizing the lapse rate and lowering the humidity, inhibits the development of clouds [3]. For this reason, and also because the air mass was initially very dry, clear skies prevailed for practically three weeks. This enabled the sun to heat the ground to an unusual extent. Large quantities of this incoming heat were transported upward through turbulent mixing. The mean soundings (fig. 7) indicate that this process was particularly important in heating the atmosphere below the 700-mb. level. In these layers the lapse rate was practically dry adiabatic, and the net temperature change was almost twice as great as it was in mid-troposphere. It is also probable that excessive surface heating was instrumental in weakening the sea level anticyclone by increasing divergent outflow above the heated layer, in accordance with the mechanism proposed by Priestley [4]. As the temperature of the air column rose the amount of heat lost by long-wave radiation increased rapidly and eventually balanced the incoming short-wave radiation. As a result maximum temperatures became stabilized around the 100° F. mark for several days at the end of the period throughout the Northeast.

STAGNATION IN RELATION TO THE BROAD-SCALE CIRCULATION

The discussion thus far has attempted to show how stagnation of the anticyclone led to prolonged drought and record heat. It remains to examine the more fundamental question of why the anticyclone stagnated in the first place. Although no complete answer can be given, some pertinent associations can be indicated. For this purpose it is helpful to again consider the 5-day mean 700-mb. charts of figure 5 since, as Wexler [1] has stated: "In any discussion of anticyclonic origin, development, movement, dissipation, etc., it is necessary to depart from the narrow confines of the area usually covered by an anticyclone and obtain a broader view of the behavior of the westerlies and their influence on anticyclones both of the polar and warm type."

The first map of the series (fig. 5a) contains a well-marked wave train of large amplitude in North America and the Pacific. The center of the anticyclone on the 5-day mean sea level map during this period was located on the southern edge of the westerlies in a region of weak 700-mb. flow. The daily anticyclone therefore moved rather slowly. Note, however, that the trajectory of the migratory High from August 14 to the end of the month (fig. 4) paralleled the 10,400-ft. contour of figure 5a extremely closely. As the surface High moved southeastward from Wisconsin it passed out of the main belt of westerlies and approached the 700-mb. High which was simultaneously moving east-northeastward from Oklahoma. When both centers subsequently stagnated in West Virginia there was virtually no steering current above the sea level anticyclone to cause it to move. This development can be seen by noting the progressively weaker 700-mb. circulation above the centers of the 5-day mean anticyclone at sea level, located by crosses in figures 5a, b, and c.

During the second week of the period (fig. 5b) the principal features of the long wave pattern shown in figure 5a advanced eastward. This eastward motion was much greater at middle and high latitudes than at low latitudes. As a result the horizontal tilt of the troughs and ridges started to change from north-south or northwest-southeast to northeast-southwest. The latter orientation favored the northward transfer of angular momentum [5], so that the 700-mb. westerlies over North America increased in intensity but in a position well north of the sea level anticyclone in the Ohio Valley.

Acceleration of the westerlies continued during the third week of the series, when an extremely fast zonal flow extended across southern Canada at both 700 mb. (fig. 5c) and 200 mb. (fig. 6c). This westerly jet stream was concentrated in a narrow belt between the warm anticyclone over West Virginia and a blocking High over

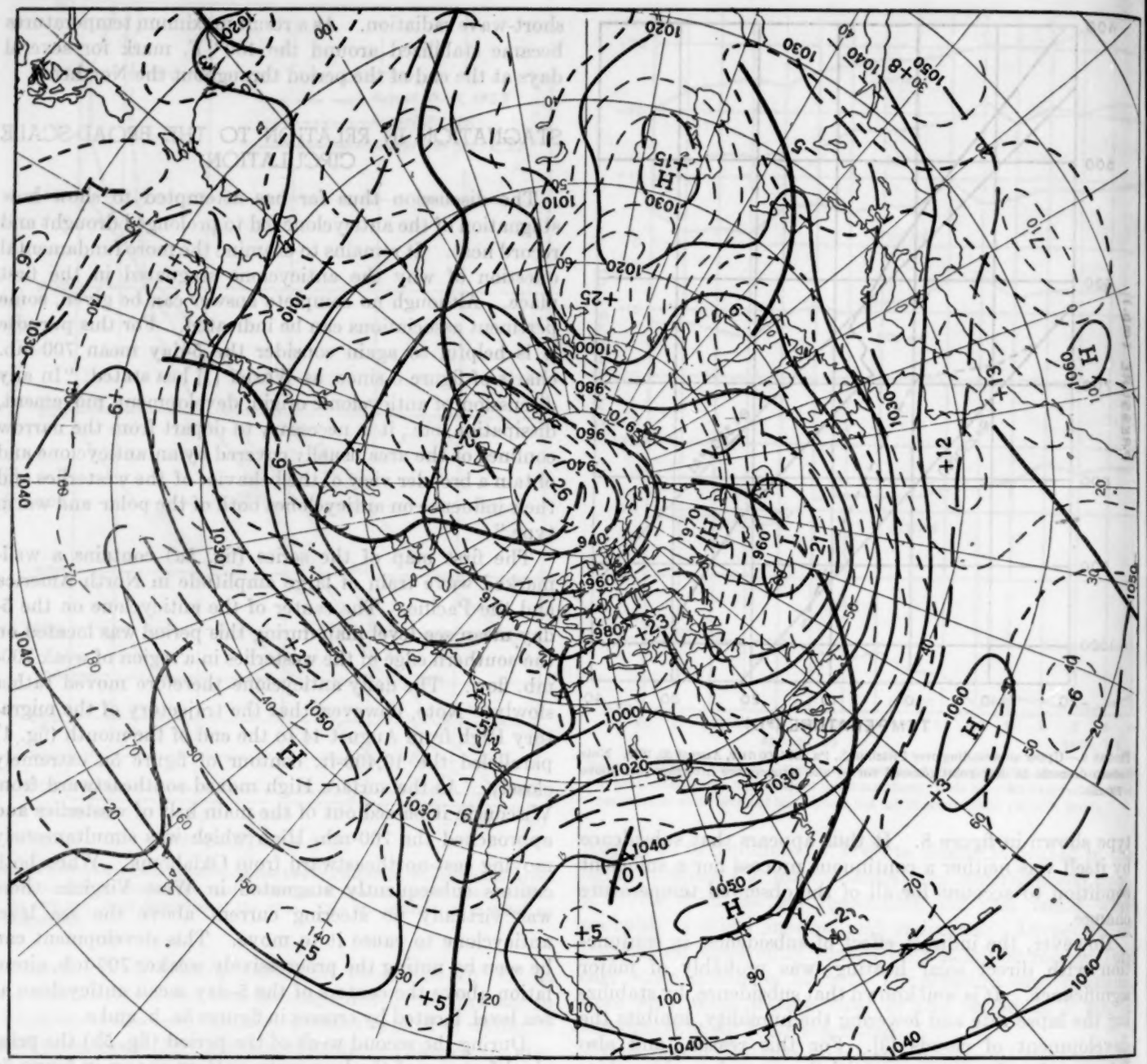

FIGURE 10.—Mean 700-mb. height contours and departures from normal (both in tens of feet) for August 1-30, 1953. Heights were above normal in all portions of the United State except Florida and the Pacific Coast.

Baffin Bay. The latter can be traced back to a blocking surge which originated in northern Asia and crossed Greenland earlier in the period (fig. 5a and b). Banking to the right of the westerly jet probably contributed to the continued development of the stagnant High over West Virginia, by means of the process described by Rossby in 1938 [6]. The great expansion of the area covered by the 10,500-ft. contour around this High, shown by comparison of figures 5b and c, was directly related to the stagnation of the sea level anticyclone and the accompanying heat wave and drought.

Intensification of the upper level High in the eastern United States may also be attributed to barotropic energy dispersion from the Pacific. From August 15 to 19 marked deepening of a 700-mb. trough in the western Pacific took place. A few days later the ridge in the central Pacific increased greatly in amplitude. Note the northward motion and expansion of the 10,600-ft. contour from figure 5a to figure 5b. Deepening of the west coast trough occurred next in this chain of events, as indicated by the progressive southward displacement of the 10,200-ft. contour from the first to the third 700-mb. maps of the series. Finally the ridge in the eastern United States intensified, attaining its highest heights in figure 5c. Table 1 portrays these events in a more quantitative fashion. It is based upon the series of overlapping 5-day

TABLE 1.—*Time, place, and intensity of maximum anomalies of 5-day mean 700-mb. height, illustrating progressive intensification downstream*

Date	Latitude	Longitude	Maximum anomaly	Distance between centers	Rate of dispersion
1953	° *N.*		*Ft.*	*Mi.*	*m. p. h.*
August 18	48	153° E.	−450	1660	17
August 22	50	170° W.	+720	2040	21
August 26	45	124° W.	−270	2140	22
August 30	43	80° W.	+240	1830	19
September 3	53	42° W.	−500		

mean charts prepared twice-weekly in the Extended Forecast Section showing the distribution of the anomaly of 5-day mean 700-mb. height. By interpolating among these charts, the time when and place where centers of maximum and minimum departure from normal attained their maximum intensity have been determined. The linear distance between these centers divided by the number of days between their occurrence gives a rough idea of the rate of energy dispersion or group velocity. It averaged about 20 m. p. h., only about half as much as the value previously obtained by Carlin [7] in a winter case. Smaller values would be expected since group velocity depends directly on zonal wind speed [8], and the zonal index averaged from 35° to 55° N. and 0° to 180° W. was only about 18 m. p. h. in this case compared to 26 m. p. h. in Carlin's study.

To summarize, the stagnation of the anticyclone with accompanying drought and heat has been attributed primarily to intensification of the long-wave ridge in the eastern United States. This intensification has been ascribed to dispersion of energy from the Pacific and banking to the right of fast westerly flow in southern Canada. It is pertinent to note that the three features of the general circulation previously related to the development of warm Highs in summer in the eastern half of the United States [9, 10] were again present in this situation. These factors, strong ridge in the east-central Pacific, deep trough along the west coast, and fast flat westerlies in southern Canada south of a blocking High, are all evident in figures 5b and c.

THE MONTH AS A WHOLE

The circulation pattern for the entire month of August 1953 strongly reflected the influence of the last two to three weeks described above. Thus the monthly mean charts at sea level (Chart XI), 700 mb. (fig. 10) and 200 mb. (fig. 11) all show a deeper than normal trough off the east coast of Asia, an abnormally strong ridge in the east-central Pacific with a closed High around 40° N, 155° W., an unusually deep trough along the west coast of North America, and a stronger than normal ridge in eastern and central sections of the United States. The monthly mean High associated with the latter ridge had a large vertical tilt, since the sea level center in Ohio was displaced to Mississippi at 700 mb. and to west Texas at

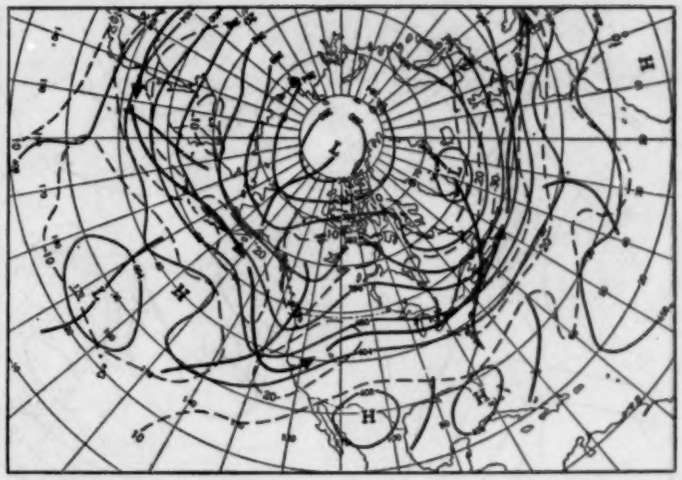

FIGURE 11.—Mean 200-mb. contours (in hundreds of feet) and isotachs (in meters per second) for August 1-30, 1953. Solid arrows indicate the average position of the jet stream, which was north of the normal August position in the Pacific and stronger than normal in the Atlantic.

200 mb. The meandering jet stream at 200 mb. is clearly delineated in figure 11 as a continuous axis stretching from Manchuria across the Pacific, United States, and Atlantic into the Mediterranean. Its maximum speed was almost one-third of the peak value observed on monthly mean 200-mb. charts during the winter of 1953.

The temperature anomalies for the month as a whole were also dominated by the weather of the last two weeks. Chart I shows that temperatures generally averaged above normal in the eastern half of the United States, the Northern Plains, and the Rocky Mountain States, all of which were regions of anticyclonic curvature and above normal heights at 700 mb. (fig. 10). Cool Pacific air flowing around the deep west coast trough produced below normal temperatures throughout the Far West, except for the northern coastal regions where the normal sea breeze was weakened by unusually cool air inland. Below normal temperature also prevailed along the Gulf and South Atlantic Coasts, where sea level and 700-mb. winds were more northeasterly than normal, and in the Southern Plains, where a weak trough in the field of 700-mb. height departure from normal was located.

Total rainfall during the month was subnormal in most of the eastern half of the United States (Chart III). As little as 10 percent of normal precipitation was recorded in southern Indiana, while less than ¼ of the normal amount fell in most of Missouri and parts of adjoining States. This deficiency was accompanied by persistent anticyclonic activity (Chart IX). A virtually complete absence of cyclones between the Appalachians and the Mississippi River is one of the most notable features of Chart X. Not only were cyclones absent but even fronts were unusually scarce. Figure 12 shows that only ⅓ of the days of the month had any surface fronts in the Ohio Valley and Great Lakes Region. The minimum number of days with fronts in this area contrasts sharply with the

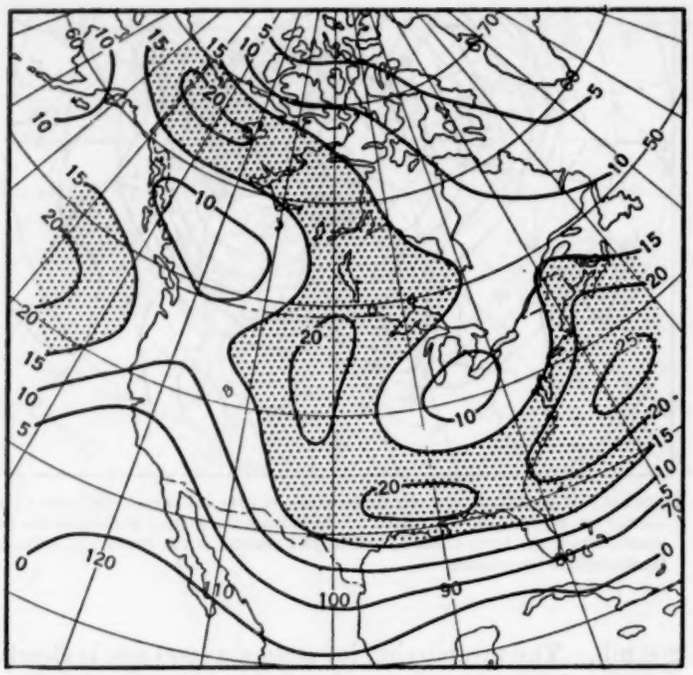

FIGURE 12.—Number of days with surface fronts (of any type) located within square areas with sides approximately 430 nautical miles during the month of August 1953. Frontal positions were those appearing on printed *Daily Weather Map* for 1830 GMT. Areas where fronts were present on 15 or more days are shaded. Rainfall (see Chart III) was generally above normal in shaded areas and below normal elsewhere, except in the Far West.

normal summer condition, when the axis of maximum frequency of fronts is located between the Great Lakes and the Ohio Valley [11].

On the other hand, figure 12 shows that surface fronts were present on about ⅔ of the days of the month along the Gulf and South Atlantic coasts, where fronts are normally infrequent in summer. As a result, rainfall was generally above average in this region (Chart III). This rain was particularly welcome in drought-stricken Texas, where this month's Statewide precipitation average of 159 percent of normal was the highest for any month since November 1952 and the first above normal average since May 1953. Rainfall in southern Texas was 4 to 6 times the monthly average and greater than the combined totals for all previous months since the beginning of the year. Sinton, just northwest of Corpus Christi, reported 8.33 inches in a 24-hour period during the last week of the month. During this period strong southeasterly flow around the stagnant High in West Virginia transported large quantities of moisture from the Gulf of Mexico (figs. 3c and 5c).

This month's precipitation was also unusually heavy in all of the Pacific Coast States (except extreme southern California), an area which normally experiences very little rain during summer. The 0.76 inch of rainfall at the Sacramento Weather Bureau City Office was the greatest for August in 105 years of record and almost four times as great as the previous record set in 1896. Statewide precipitation in Oregon averaged 361 percent of normal. Most of the moisture for this rainfall was of Pacific origin and was carried by stronger than normal southwesterly flow at all levels of the troposphere. Note the southwesterly jet stream crossing the San Francisco Bay area in figure 11. Release of this moisture through upward vertical motion was effected by an unusual concentration of cyclones (Chart X) and fronts (fig. 12) along the west coast, a region where cyclones and fronts are normally rare in summer. Also indicative of large-scale convergence in this area was the presence of a deep mean trough at 200 mb. (fig. 11) and a trough with below normal heights at 700 mb. (fig. 10). Excessive cloudiness (Charts VI and VII) accompanying the rains contributed to abnormally cool weather in this area (Chart I).

REFERENCES

1. H. Wexler, "Anticyclones," *Compendium of Meteorology*, American Meteorological Society, Boston, 1951, pp. 621-629.
2. J. Vederman, "The Growth and Decline of Anticyclones," *Bulletin of the American Meteorological Society*, vol. 33, No. 8, Oct. 1952, pp. 315–321.
3. J. Namias, "Subsidence within the Atmosphere," *Harvard Meteorological Studies*, No. 2, Cambridge, Mass., 1934.
4. C. H. B. Priestley, "Atmospheric Pressure Changes: The Importance of Deviations from the Balanced (Gradient) Wind," *Australian Journal of Scientific Research* (A), vol. 1, No. 1, Mar. 1948, pp. 41–57.
5. V. P. Starr, "An Essay on the General Circulation of the Earth's Atmosphere," *Journal of Meteorology*, vol. 5, No. 2, Apr. 1948, pp. 39–43.
6. C.-G. Rossby, "On the Mutual Adjustment of Pressure and Velocity Distributions in Certain Simple Current Systems," *Journal of Marine Research*, vol. 1, No. 1, Nov. 1937, pp. 15–28.
7. A. V. Carlin, "A Case Study of the Dispersion of Energy in Planetary Waves," *Bulletin of the American Meteorological Society*, vol. 34, No. 7, Sept. 1953, pp. 311–318.
8. C.-G. Rossby, "Dispersion of Planetary Waves in a Barotropic Atmosphere," *Tellus*, vol. 1, No. 1, Feb. 1949, pp. 54–58.
9. W. H. Klein, "The Weather and Circulation of June 1952—A Month with a Record Heat Wave," *Monthly Weather Review*, vol. 80, No. 6, June 1952, pp. 99–104.
10. J. S. Winston, "The Weather and Circulation of June 1953—The Second Successive June with Record-Breaking Drought and Heat," *Monthly Weather Review*, vol. 81, No. 6, June 1953, pp. 163–168.
11. T. E. W. Shumann and M. P. von Rooy, "Frequency of Fronts in the Northern Hemisphere," *Archiv für Meteorologie, Geophysik, und Bioklimatologie*, Serie A, Band IV, 1951, pp. 87–97.

HURRICANE BARBARA, 1953

R. P. JAMES AND C. F. THOMAS

WBAN Analysis Center, U. S. Weather Bureau, Washington, D. C.

INTRODUCTION

The second hurricane of the 1953 season, "Barbara", developed during the night of August 11 a short distance northeast of the Bahama Islands from an easterly wave that had been under observation by the Miami Hurricane Forecast Office for several days. On the morning of the 12th, aerial reconnaissance located the center still in the formative stage near 29° N., 76° W. The storm moved on a northerly course until it crossed the North Carolina coastline the night of August 13. Then it began to curve slowly to the north-northeast, re-entering the Atlantic the morning of the 14th. It passed south of New England and Nova Scotia, and thence into Laborador (fig. 1). In comparison to earlier tropical storm tracks, as reproduced by Tannehill [1], Barbara's track was almost identical to that of the storm of September 10–16, 1933; both had their eastward movement blocked near Newfoundland and were deflected northward. Although Hurricane Barbara was not an outstandingly destructive storm, it presents good material for the study of several ideas on steering.

DEVELOPMENT

The wave in the easterlies from which Barbara developed was weak on the surface as it moved across the West Indies toward Cuba, although some squally weather did accompany it. The charts at 700 and 500 mb. show good continuity of the wave which crossed San Juan, Puerto Rico about 1500 GMT, August 8. The 700-mb. chart for 1500 GMT, August 10 (fig. 2) showed the first definite indication of a closed circulation over eastern Cuba. The pilot balloon report 12 hours earlier from Guantanamo Bay, Cuba showed light west-northwesterly winds to the termination of the run at 6,000 feet which suggested a closed circulation at that time. This Low aloft deepened slightly and moved northward to a position just east of Eleuthera Island in the Bahamas at 1500 GMT, August 11 with the closed circulation extending to the 500-mb. level. It wasn't until the afternoon of the 11th that a definite Low could be noted on the surface chart. On the morning of the 12th the first reconnaissance into the suspicious area estimated winds near 75 m. p. h. on the northeast side of the center and observed that the southwest side was undeveloped—fewer clouds, less wind, and no complete wall of clouds around the "eye". As it moved northward on the 12th and 13th the storm increased slowly in intensity. A central sea level pressure of 29.15 inches and winds slightly above 100 m. p. h. were reported a short time before the storm passed inland.

STEERING

As noted earlier, the Low at 700 mb. was moving northward on the 10th and 11th. Because of the poorly defined circulation aloft at this time it was difficult to determine the steering level until about 0300 GMT of the 12th. According to information supplied by the Miami Forecast Office, 30,000 ft. seemed to be the best level from which to compute steering at that time. By 1500 GMT of the 13th, winds at 40,000 ft. (the 200-mb. level) were steering the storm (fig. 3). The contours at that time very closely paralleled the track for the succeeding 24 hours, crossing the coast east of Cherry Point, N. C. and continuing out into the Atlantic again near the Virginia-North Carolina border. Figure 4, the 200-mb. chart for 0300 GMT, August 15, again shows close similarity between the track of the storm and the contours, allowing for some eastward movement of the ridge at 65° W. This ridge, over eastern Hudson Bay in figure 3, intensified and moved eastward to merge with the High already off the east coast. Movement continued to a position east of Newfoundland where the ridge contributed toward blocking the eastward movement of Barbara. The trough which developed southeast of the Hudson Bay Low and extended into the Maritime Provinces on the 16th (fig. 5) changed the direction of flow at the steering level from southwest through south to southeast over the storm. This was another factor accounting for the movement of the storm northward into Laborador.

Investigation of the warm-tongue steering suggested by Simpson [2] gives good results for this storm. Simpson says that the analysis of temperature fields in the intermediate layer between 700 and 500 mb. reveals that a tongue of warmer, lighter air is associated with the moving tropical cyclone and that the major axis of this tongue of warm air is parallel to the instantaneous direction of storm movement. Further, that a good lag correlation exists between the present orientation of the warm tongue and the future path of the storm.

The thickness charts of the 700- to 500-mb. layer for

August 13–16 were analyzed for every 50 feet, and some of the results are given in figures 6, 7, and 8. With the storm about 150 miles south of Cape Hatteras at 1500 GMT, August 13 (fig. 6), a line paralleling the warm tongue, but through the storm center, would give an expected track crossing Cape Hatteras then curving northeastward and passing about 60 miles south of Nantucket. Reference to the actual track of the storm which is reproduced on the chart shows a close similarity between the two tracks for 40 hours in advance. Figure 7, 24 hours later, shows the same relationship maintained between the two tracks, although they are now closer together. The thickness chart for 0300 GMT of the 16th (fig. 8) shows a sharp warm tongue across Sable Island and into the Davis Straits—a very good indication of the northward track taken by the storm after this time.

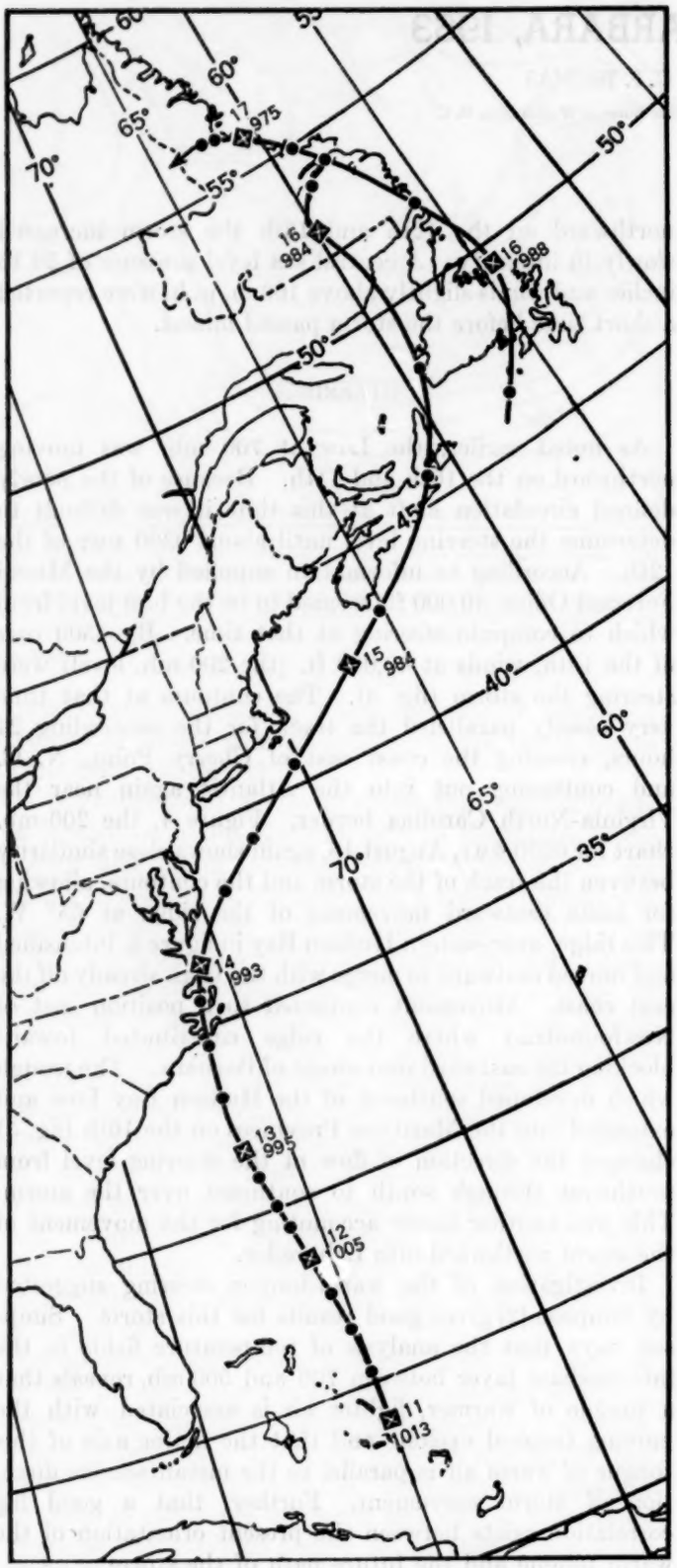

FIGURE 1.—Track of Hurricane Barbara and associated cyclogenesis near Newfoundland. The 1230 GMT positions are indicated by an "X". Circles indicate intermediate 6-hour positions. Plotted number groups are date and sea level pressure.

EXTRATROPICAL CYCLOGENESIS

Under the influence of the steering at 200 mb. and the north-south orientation of the warm tongue in the 700-500-mb. layer, the storm turned northward over eastern Nova Scotia, passing just to the west of Newfoundland. It was at this time, 0630 GMT, August 16, that cyclogenesis took place to the southeast of Barbara. Hourly surface maps were plotted for the Nova Scotia-Newfoundland area to follow the formation of this new center, and a

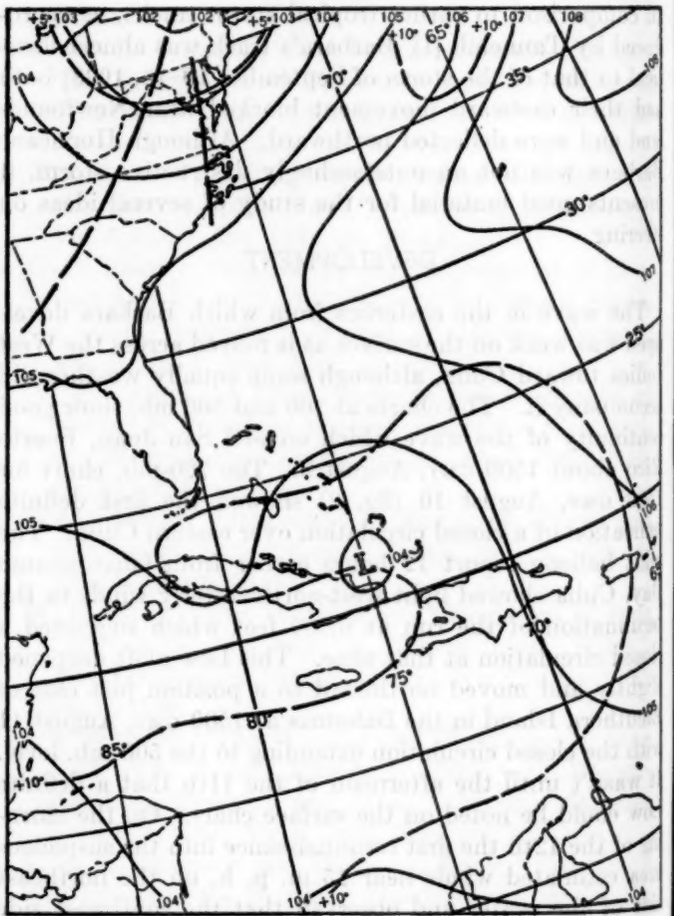

FIGURE 2.—700-mb. chart for 1500 GMT, August 10, 1953. Solid lines are contours labeled in hundreds of geopotential feet. Dashed lines are isotherms drawn for every 5° C. The Low near eastern Cuba is the first closed circulation noted in connection with Hurricane Barbara at any level.

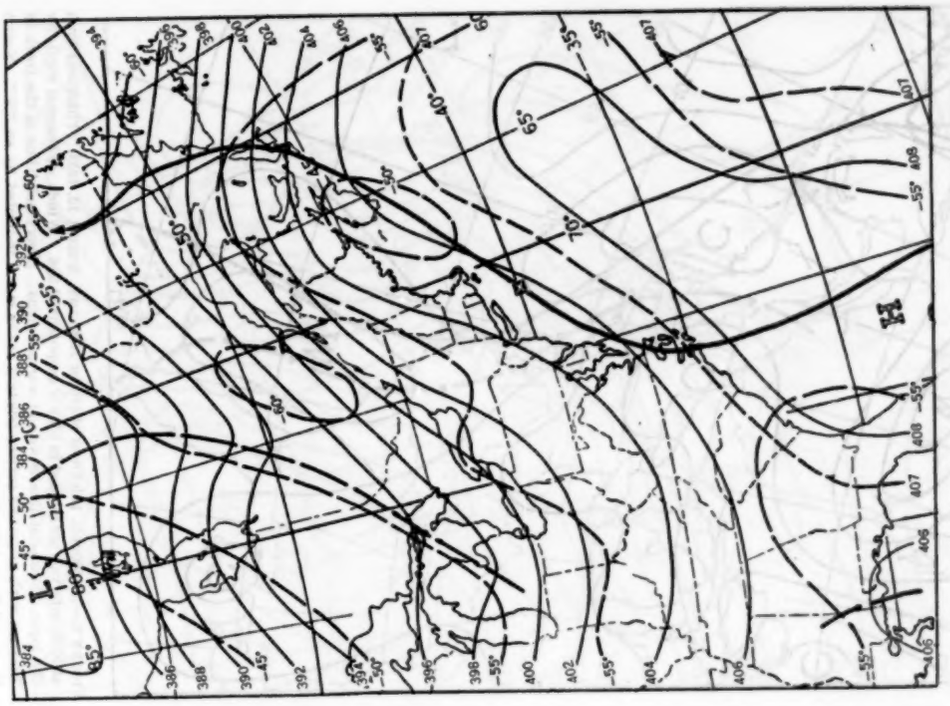

FIGURE 4.—200-mb. chart for 0300 GMT, August 15, 1953.

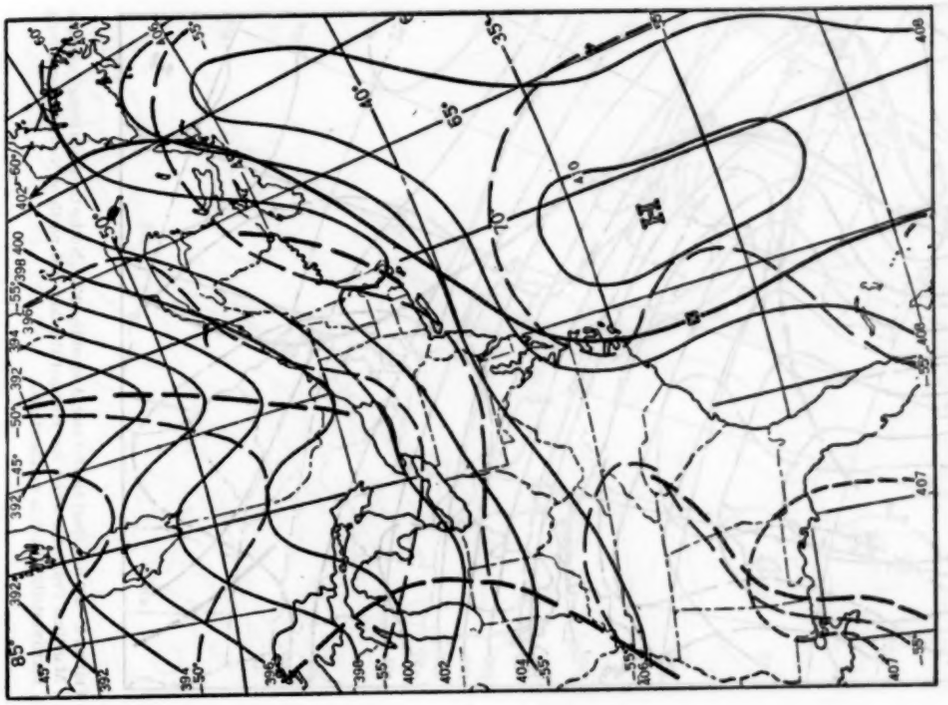

FIGURE 3.—200-mb. chart for 1500 GMT, August 13, 1953. Solid lines are contours labeled in hundreds of geopotential feet. Light dashed lines are isotherms drawn for every 5° C. Heavy dashed lines are troughs. Heavy solid line is the track of Barbara with map-time surface position of the storm indicated by an "X".

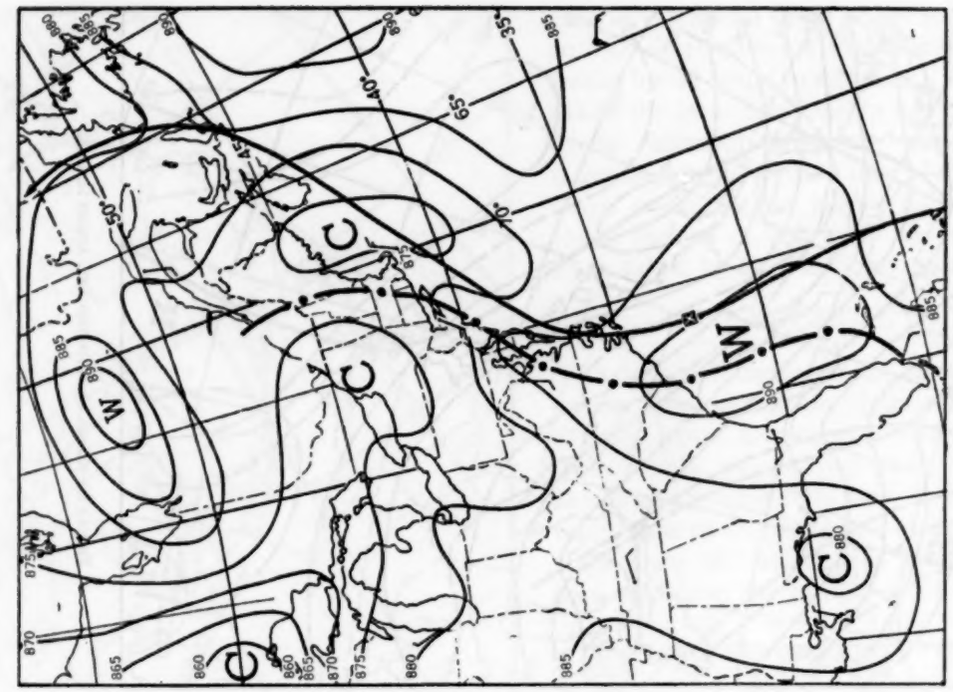

FIGURE 6.—700-500-mb. thickness chart for 1500 GMT, August 13, 1953. Thickness lines at 50-ft. intervals are labeled in tens of geopotential feet. Winds are thermal winds for the layer. Dash-dot line is axis of warm tongue. Heavy solid line is the track of Barbara with map-time surface position of the storm indicated by an "X". Notice the parallelism of the warm tongue and the surface track.

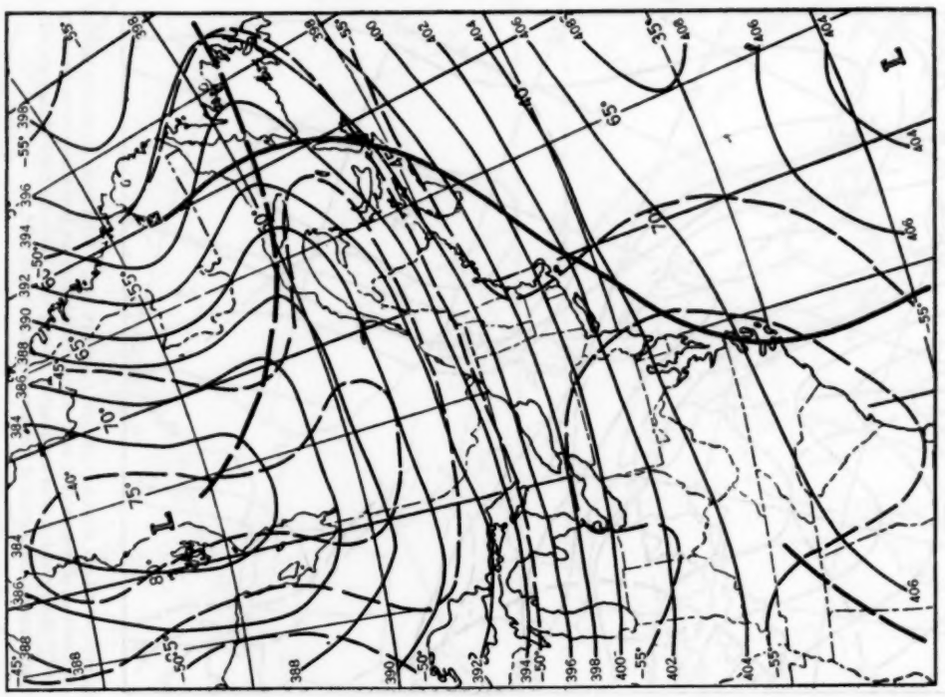

FIGURE 5.—300-mb. chart for 1500 GMT, August 16, 1953. Notice the sharp trough over the Maritime Provinces which has changed the flow just north of Newfoundland from northwesterly (fig. 4) to southeasterly.

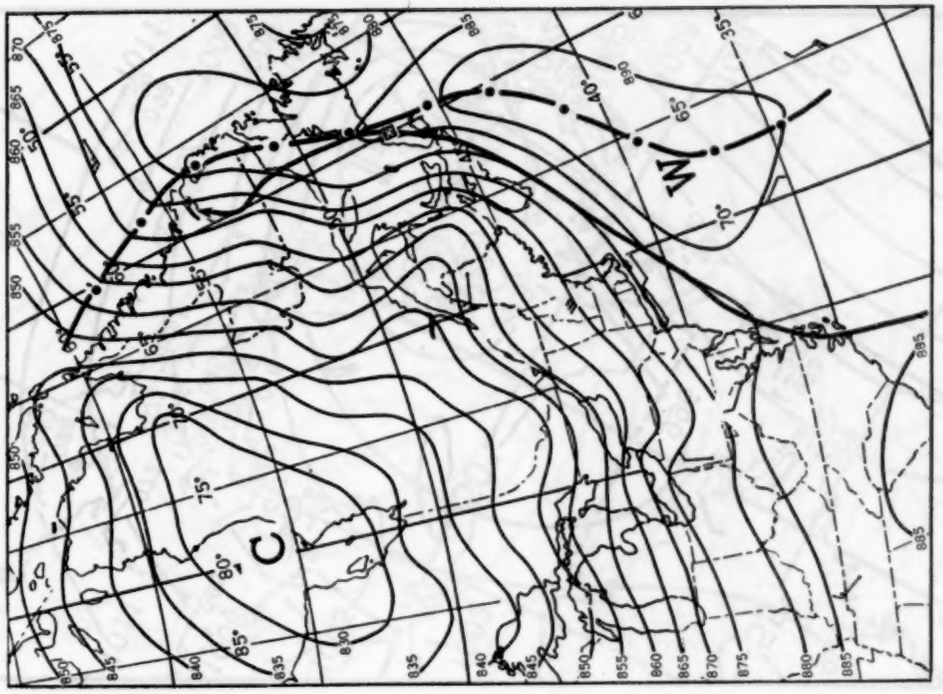

FIGURE 8.—700-500-mb. thickness chart for 0300 GMT, August 16, 1953. Notice sharp north-south warm tongue across Newfoundland.

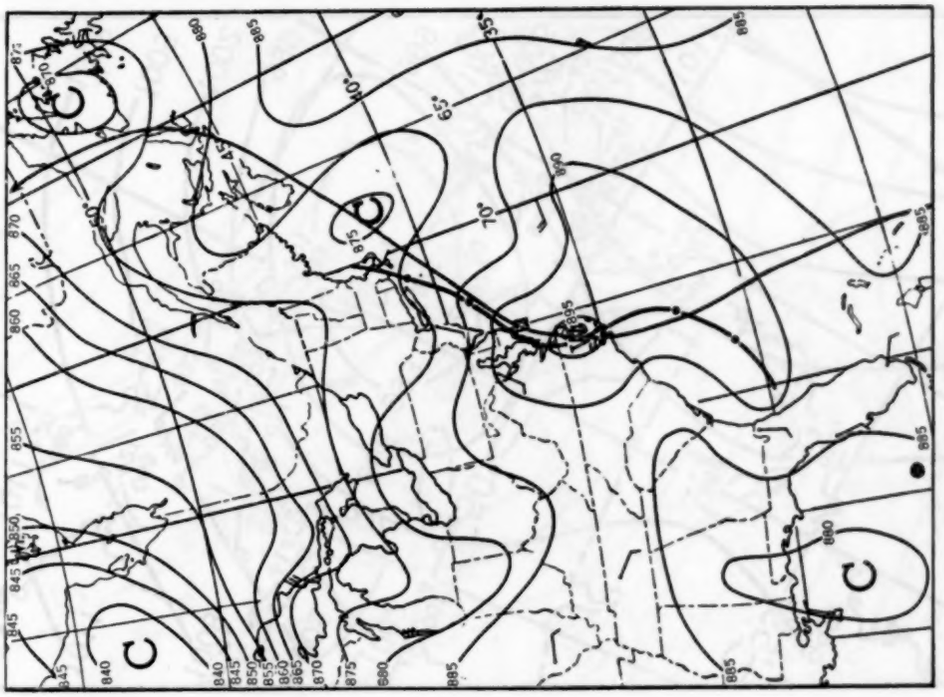

FIGURE 7.—700-500-mb. thickness chart for 1500 GMT, August 14, 1953.

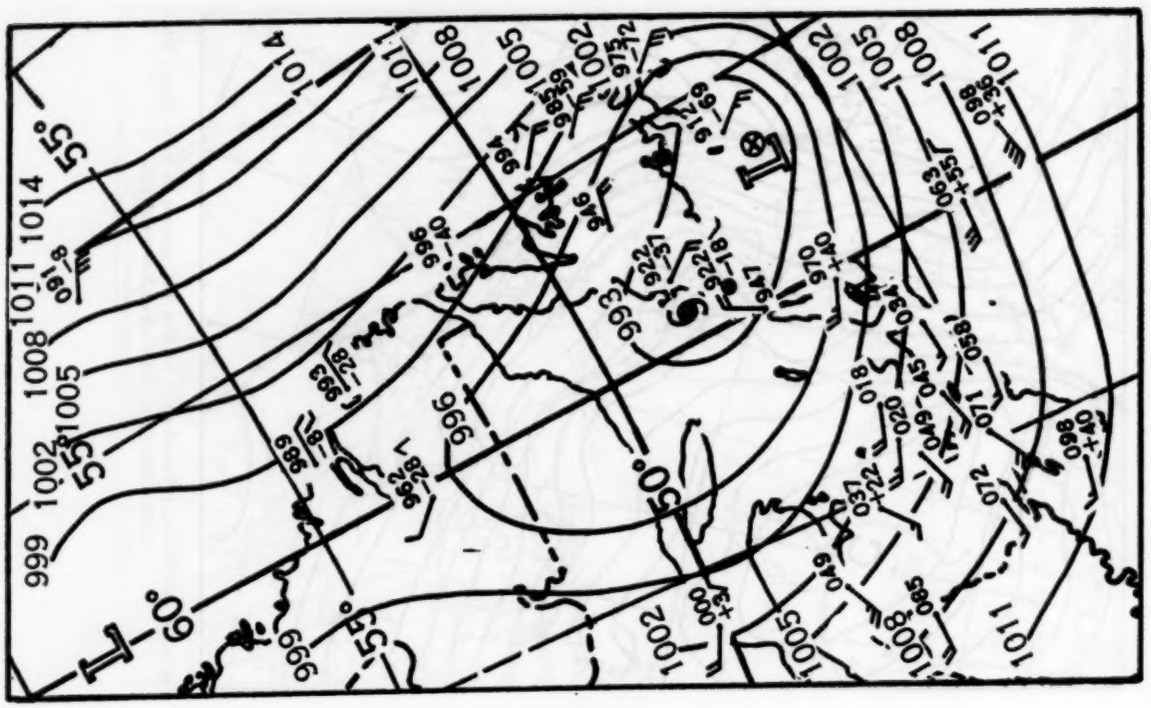

FIGURE 10.—Surface weather map for 0630 GMT, August 16, 1953. The time of the first appearance of the new Low on the southern coast of Newfoundland.

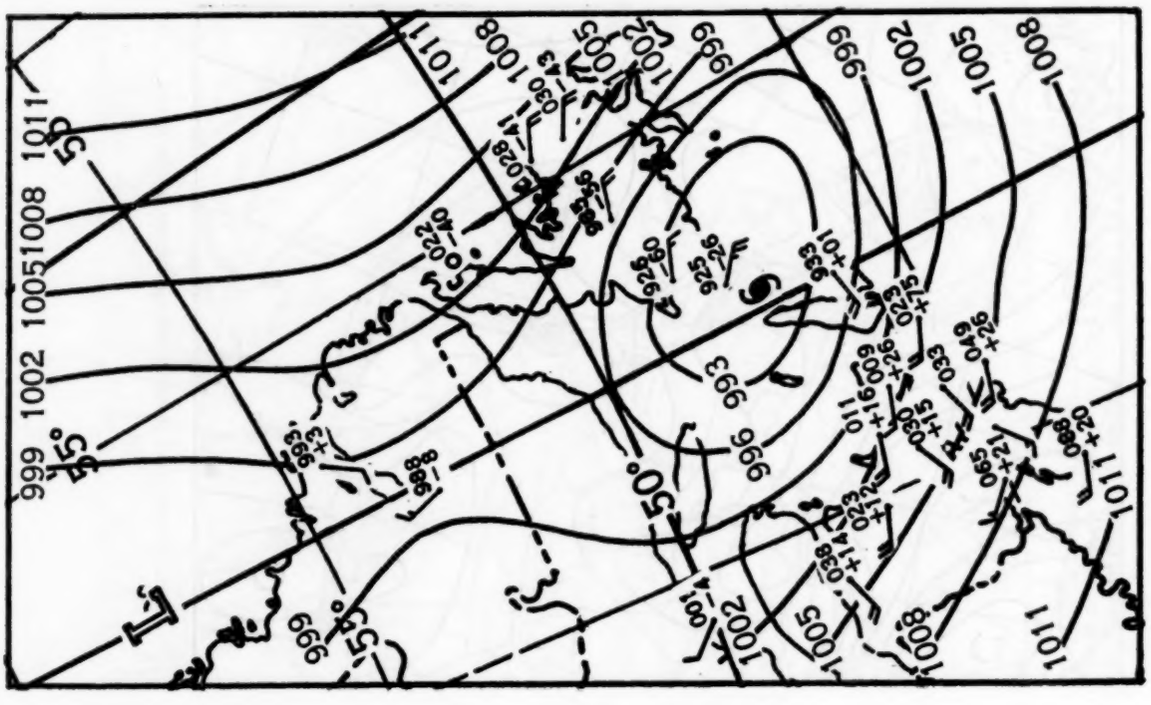

FIGURE 9.—Surface weather map for 0430 GMT, August 16, 1953. Isobars are labeled in whole millibars. Fronts and precipitation are not indicated. A trough has developed southeast of Barbara.

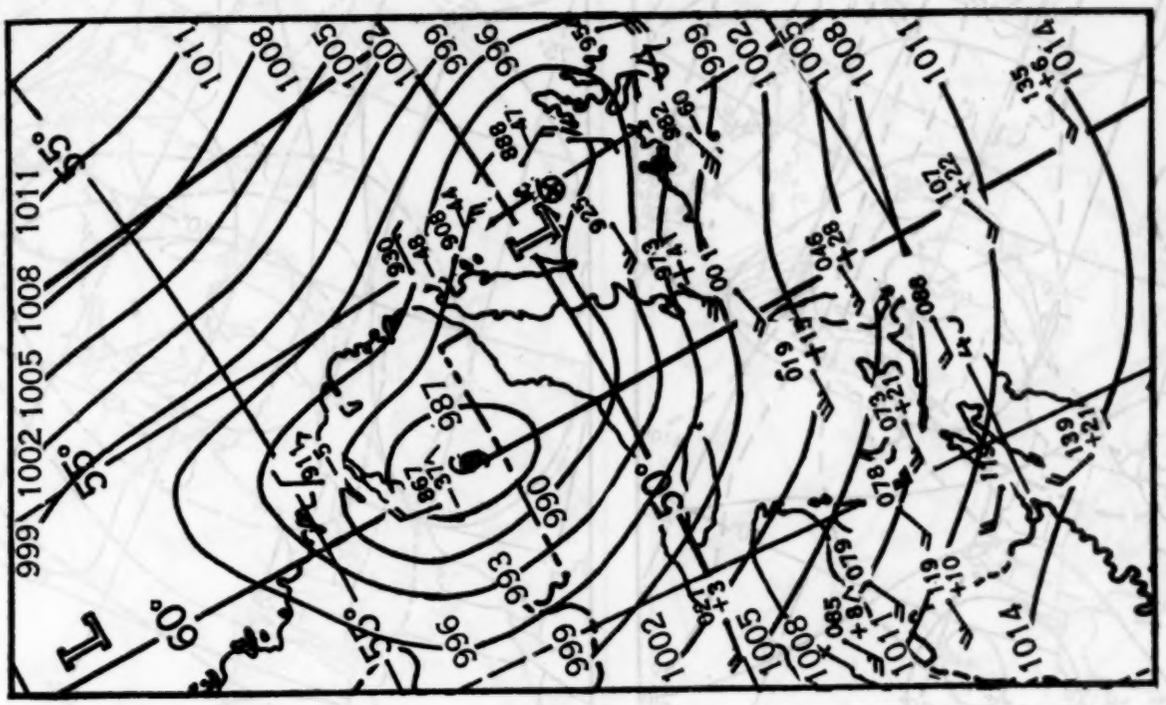

FIGURE 12.—Surface weather map for 1230 GMT, August 16, 1953. Both Lows continue moving northward.

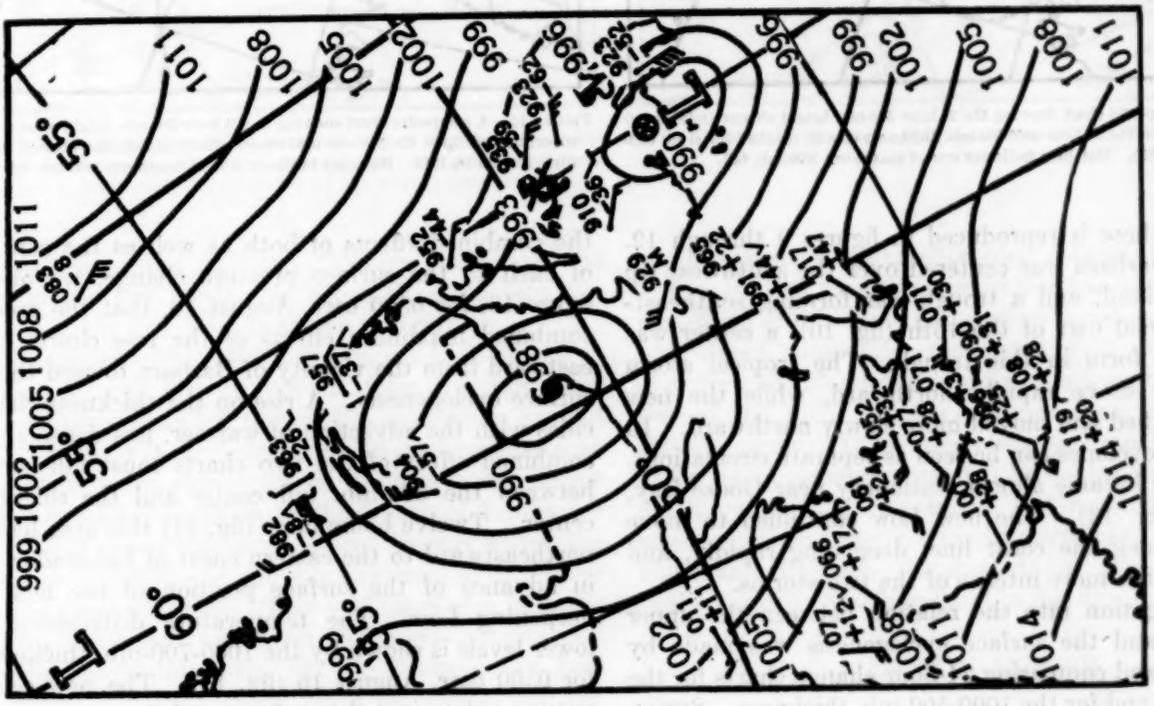

FIGURE 11.—Surface weather map for 0030 GMT, August 16, 1953. The two distinct circulations can be seen on this chart.

FIGURE 13.—A composite chart showing the 24-hour 500-mb. height change (solid lines) superimposed upon the 24-hour 1000-500-mb. thickness change (dashed lines) for 0300 GMT, August 16, 1953. Hatching indicates area of maximum 1000-mb. fall.

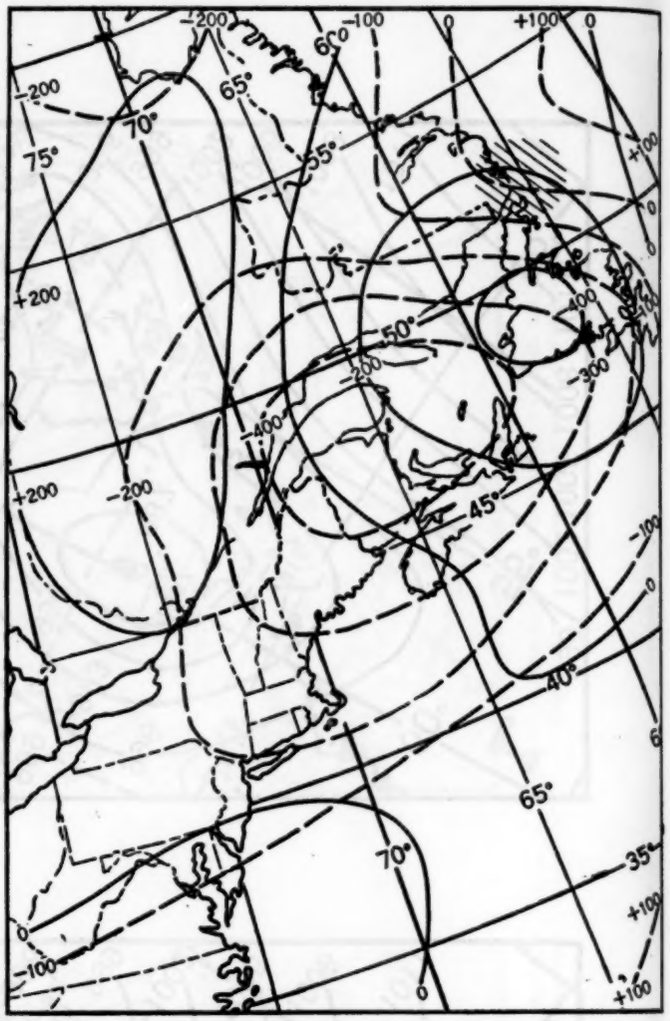

FIGURE 14.—A composite chart showing the 24-hour 500-mb. height change (solid lines) superimposed upon the 24-hour 1000-500-mb. thickness change (dashed lines) for 1500 GMT, August 16, 1953. Hatching indicates area of maximum 1000-mb. fall.

selection of these is reproduced in figures 9 through 12. In figure 9 Barbara was centered over the southwest tip of Newfoundland, and a trough was forming southeastward. By 0630 GMT of the 16th (fig. 10), a center was beginning to form in this trough. The tropical storm continued to move rapidly northward, while the new center intensified and moved more slowly northward. In figure 11 the cyclones can be seen as separate circulations. Barbara then became almost stationary near Goose Bay, Laborador (fig. 12). The new Low continued to move northward along the coast line, deepening rapidly, and soon became the more intense of the two storms.

An investigation into the relation between the upper level charts and the surface cyclogenesis was made by constructing and comparing 24-hour change charts for the 500-mb. level and for the 1000-500-mb. thickness. Superimposing the 24-hour change of the thickness on the 24-hour 500-mb. height change so as to be able to estimate the combined effects of both as well as the contribution of each to the surface pressure change, we observe in figure 13, for 0300 GMT, August 16, that the area of the combined maximum effects of the two charts extended eastward from the vicinity of Barbara toward the area of surface cyclogenesis. A rise on the thickness chart coincides with the advection of warmer, less dense air, so the combined effect of the two charts must fall somewhere between the 500-mb. fall center and the thickness rise center. Twelve hours later (fig. 14) this area had moved northeastward to the eastern coast of Laborador, slightly in advance of the surface position of the new rapidly deepening Low. The temperature distribution in the lower levels is shown by the 1000-700-mb. thickness chart for 0300 GMT, August 16 (fig. 15). The new center was not in evidence on the surface until three hours later, but it will be noted that cold air was being advected into the cyclogenetical area from the vicinity of Sable Island by

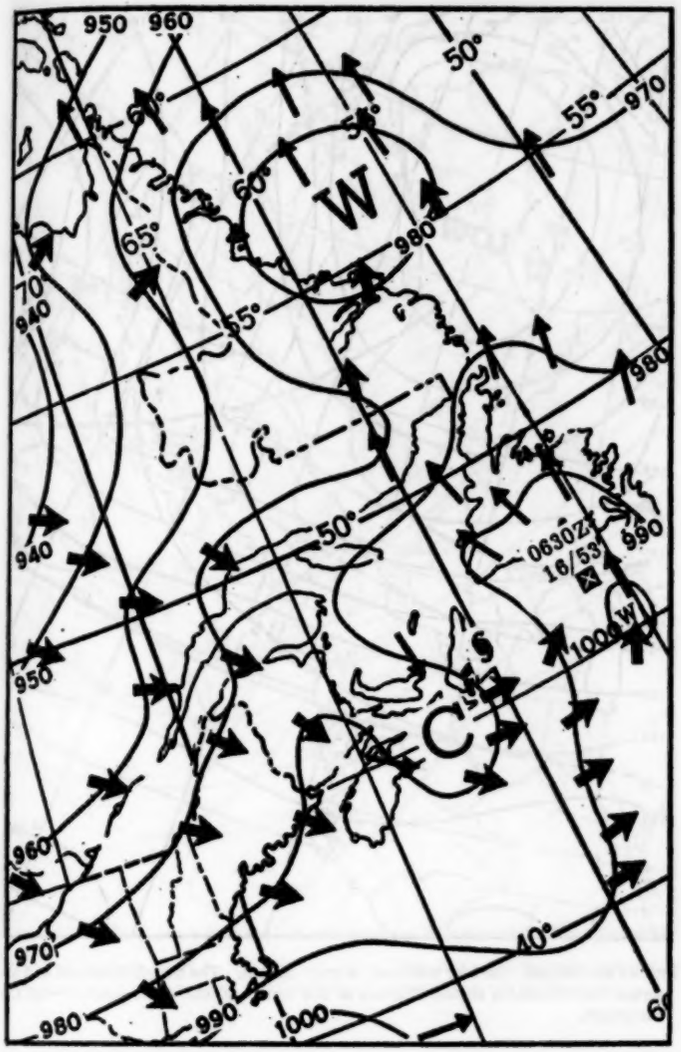

FIGURE 15.—1000-700-mb. thickness chart for 0300 GMT, August 16, 1953. Thin arrows indicate warm advection, and thick arrows cold advection. Hurricane symbol shows surface position of Barbara and "X" the surface position of the cyclogenesis.

FIGURE 16.—1000-700-mb. thickness chart for 1500 GMT, August 16, 1953.

the circulation around Barbara. Twelve hours later the cold air in the low levels was being advected into the circulation of the new Low as shown in figure 16.

The 500-mb. chart for 0300 GMT, August 15 is shown in figure 17. A weak trough extends from the Low east of Hudson Bay southward toward the circulation around Barbara. Note that the temperature in the hurricane area is higher than in the surroundings. This is in agreement with Palmén's findings [3] in the hurricane of September 11–20, 1947 in which the temperatures directly above the hurricane at 500, 400 and 300 mb. averaged 4° C. higher than in the areas adjacent. The −10° isotherm in figure 17 outlines the warm tongue in the Nova Scotia area. Twenty-four hours later (fig. 18) the Hudson Bay Low had deepened slightly without much movement and the circulation around Barbara at 500 mb. had become absorbed in the deepening trough which was oriented northwest-southeast by 0300 GMT, August 16. The warm tongue by this time had moved northeastward over Newfoundland and become quite pronounced.

A closed circulation, associated with the cyclogenesis over Newfoundland developed in the trough, and by 1500 GMT of the 17th (fig. 19) this new Low dominated the 500-mb. chart. It is interesting to note that this Low had a warm center surrounded by colder air except in the north quadrant. This is the last remnant of the pronounced warm tongue brought northward in advance of Hurricane Barbara (illustrated by the mean virtual isotherms over Newfoundland in fig. 8).

EFFECTS ASHORE

Barbara crossed the North Carolina coastline between Morehead City and Ocracoke about 2200 EST, August 13

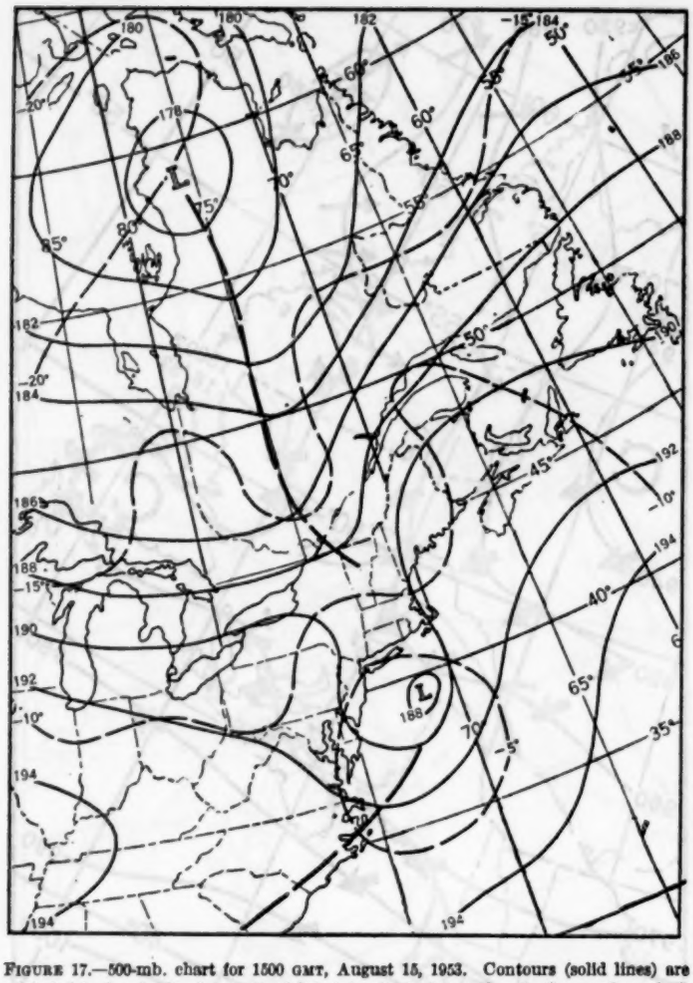

FIGURE 17.—500-mb. chart for 1500 GMT, August 15, 1953. Contours (solid lines) are labeled in hundreds of geopotential feet for 200-ft. intervals. Isotherms (long dash lines) are drawn for 5° C. intervals. Trough lines are heavy dash lines. Note the small closed "188" contour surrounded by the warmest air in the region (−5° C.) off the New Jersey coast; also, the north-south cold trough preceded by a warm ridge (−10° C.).

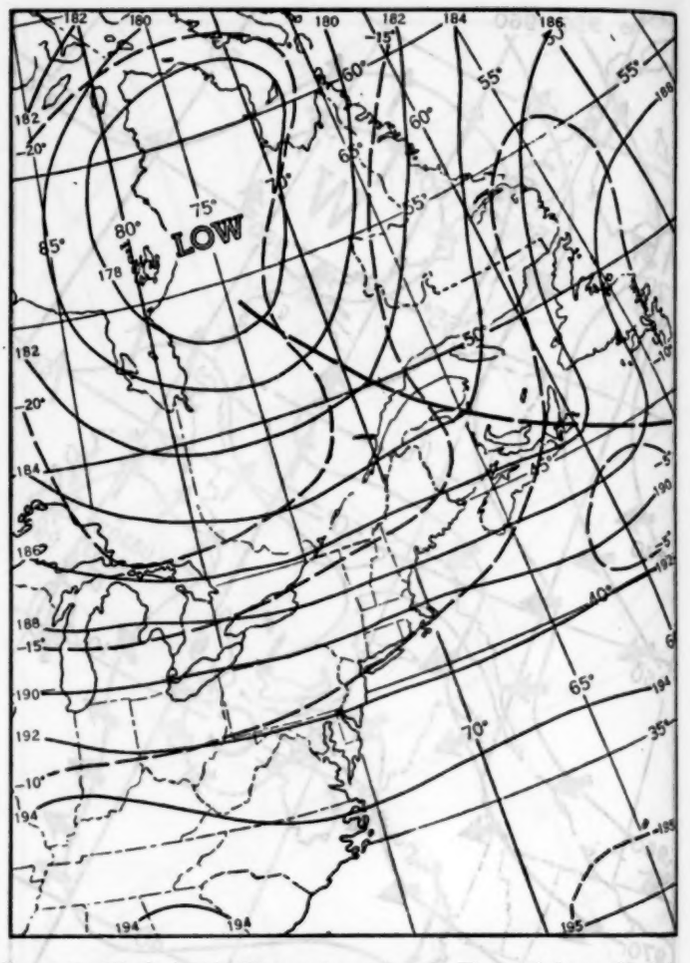

FIGURE 18.—500-mb. chart for 0300 GMT, August 16, 1953. The trough deepened and absorbed the circulation around Barbara at this level, and the warm tongue (−10° C.) sharpened.

(fig. 20), and after sweeping the entire Capes section of North Carolina passed out to sea again about 0600 EST, August 14. The lowest pressure reported on land was 29.19 inches at Coinjock, N. C. near where the storm re-entered the Atlantic; both Morehead City and Belhaven reported 29.20 inches. The strongest winds reported from land stations were gusts of 90 m. p. h. at Hatteras and Nags Head, N. C. Gusts to 78 m. p. h. were reported from Cherry Point before a power failure rendered some instruments useless. Radar fixed the center of the storm 23 miles east of Cherry Point at 2130 EST, August 13; an amateur radio operator at Ocracoke reported being in the eye one hour later; and at about 0300 EST, August 14 the eye passed about 10 miles west of Nags Head. Some unofficial rainfall amounts associated with Barbara are given in table 1.

The only known casualty of the storm occurred at Wrightsville Beach near Wilmington, N. C. where a man was swept from a pier and drowned. Two marines were injured at the Cherry Point base.

TABLE 1.—*Rainfall amounts (unofficial) for August 12–14, 1953 during passage of Barbara*

Station	Amount (inches)	Station	Amount (inches)
Wilmington, N. C.	1.29	New Holland, N. C.	5.70
Morehead City, N. C.	5.92	Cape Hatteras, N. C.	3.66
Cherry Point, N. C.	5.58	Elizabeth City, N. C.	6.09
New Bern, N. C.	5.11	Nags Head, N. C.	9.67
Oriental, N. C.	3.28	Portsmouth, Va.	6.55

Damage from the storm was light to moderate in the North Carolina-Virginia Capes area. Preliminary press reports indicated around a million dollars in damage to crops and property, crop damage in some areas reaching as high as 25 percent. Elizabeth City, Nags Head, New Bern, Kitty Hawk, and Cherry Point suffered some damage to buildings. A report from Nags Head mentioned that numerous trees were uprooted, some being large ones that survived the great September 14, 1944 hurricane unharmed.

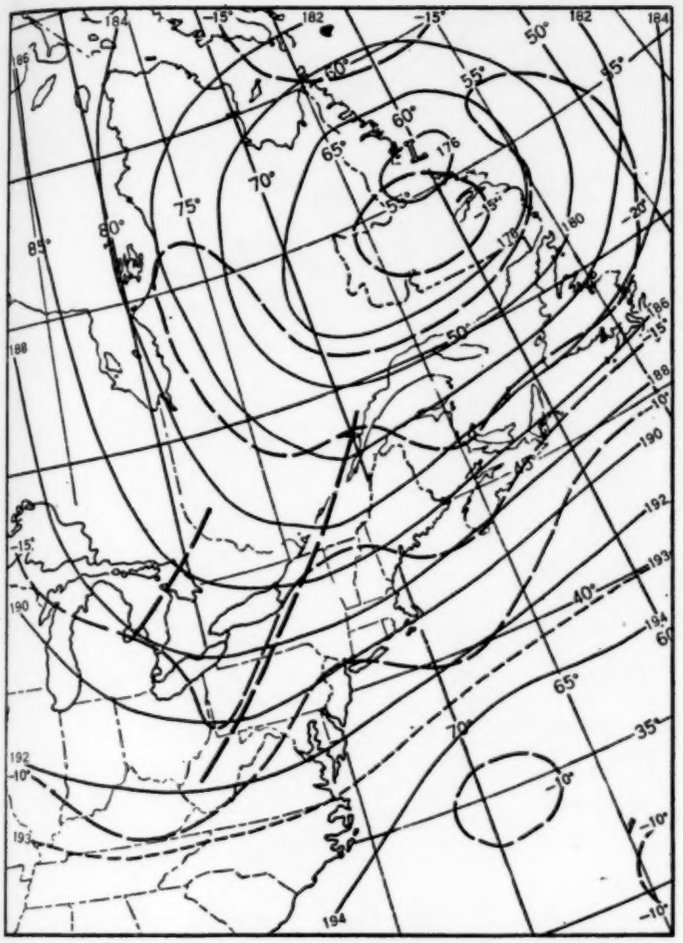

FIGURE 19.—500-mb. chart for 1500 GMT, August 17, 1953. Note that the −15° C. isotherm indicated a warm Low, while cold air surrounded it except to the north.

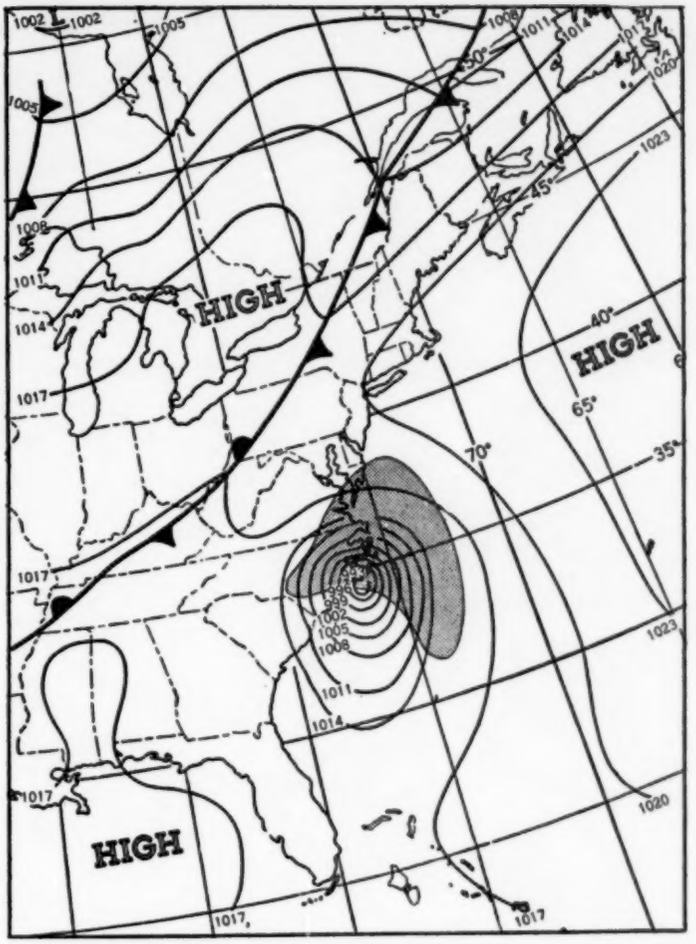

FIGURE 20.—Surface weather map for 0030 GMT, August 14, 1953. Contours are in millibars, and shaded area represents active precipitation.

After re-entering the Atlantic, Barbara continued on a northeasterly course, deepening slightly and passing a short distance southeast of Nantucket. The strongest winds in New England were only about 60 m. p. h. There were no casualties there, and damage was minor.

ACKNOWLEDGMENTS

The authors wish to thank Mr. Grady Norton, Mr. R. C. Schmidt, Mr. Oscar Tennenbaum, and Mr. Frank B. Denwiddie for material used in this article; Mr. Roger Watkins and Mr. Earl Robinson for assistance in constructing charts; and Mr. A. K. Showalter, Mr. G. Norton, Mr. C. M. Lennahan and Mr. J. Vederman for their suggestions and reviewing of this article.

REFERENCES

1. I. R. Tannehill, *Hurricanes*, Princeton University Press, Princeton, N. J., 1950, pp. 163–238.
2. R. H. Simpson, "On the Movement of Tropical Cyclones," *Transactions*, American Geophysical Union, vol. 27, No. 5, Oct. 1946, pp. 650–655.
3. E. Palmén, "On the Formations and Structure of Tropical Hurricanes," *Geophysica*, Helsinki, vol. 3, 1948, pp. 26–38. (See pp. 34–35.)

U. S. GOVERNMENT PRINTING OFFICE: 1953

Chart I. A. Average Temperature (°F.) at Surface, August 1953.

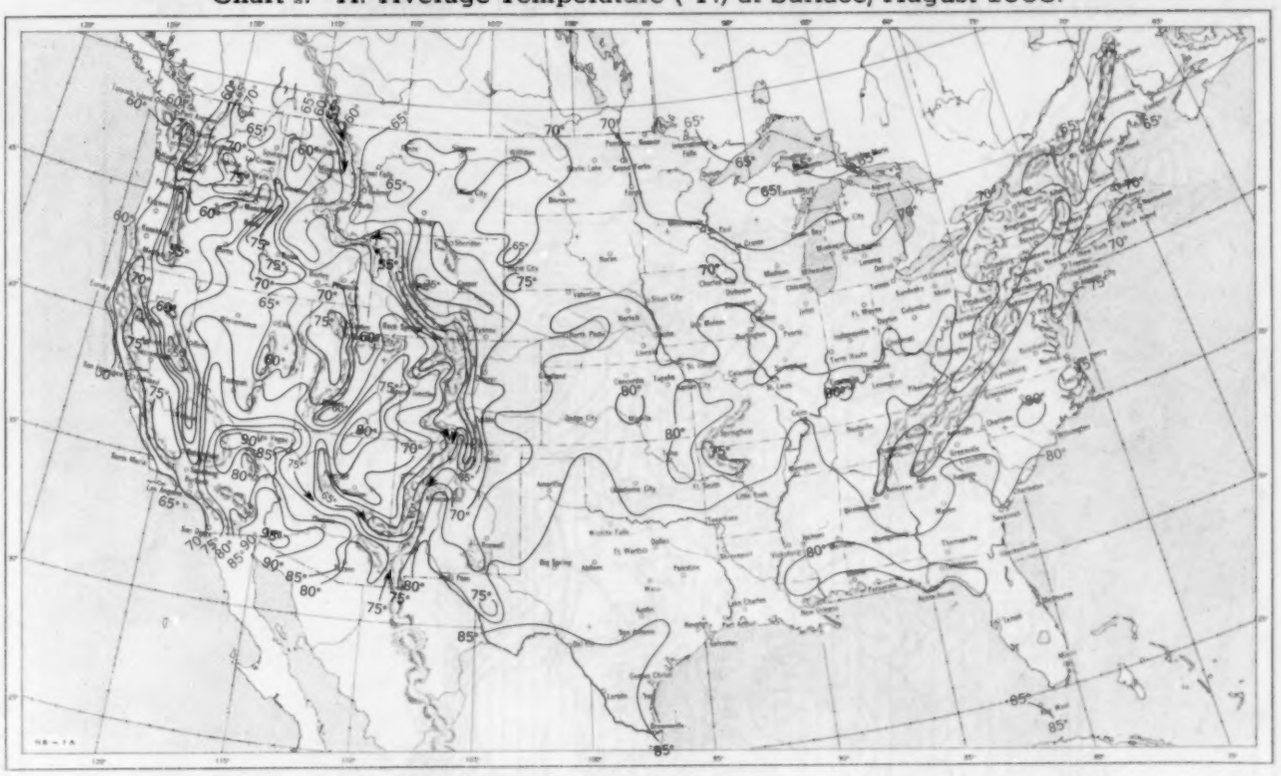

B. Departure of Average Temperature from Normal (°F.), August 1953.

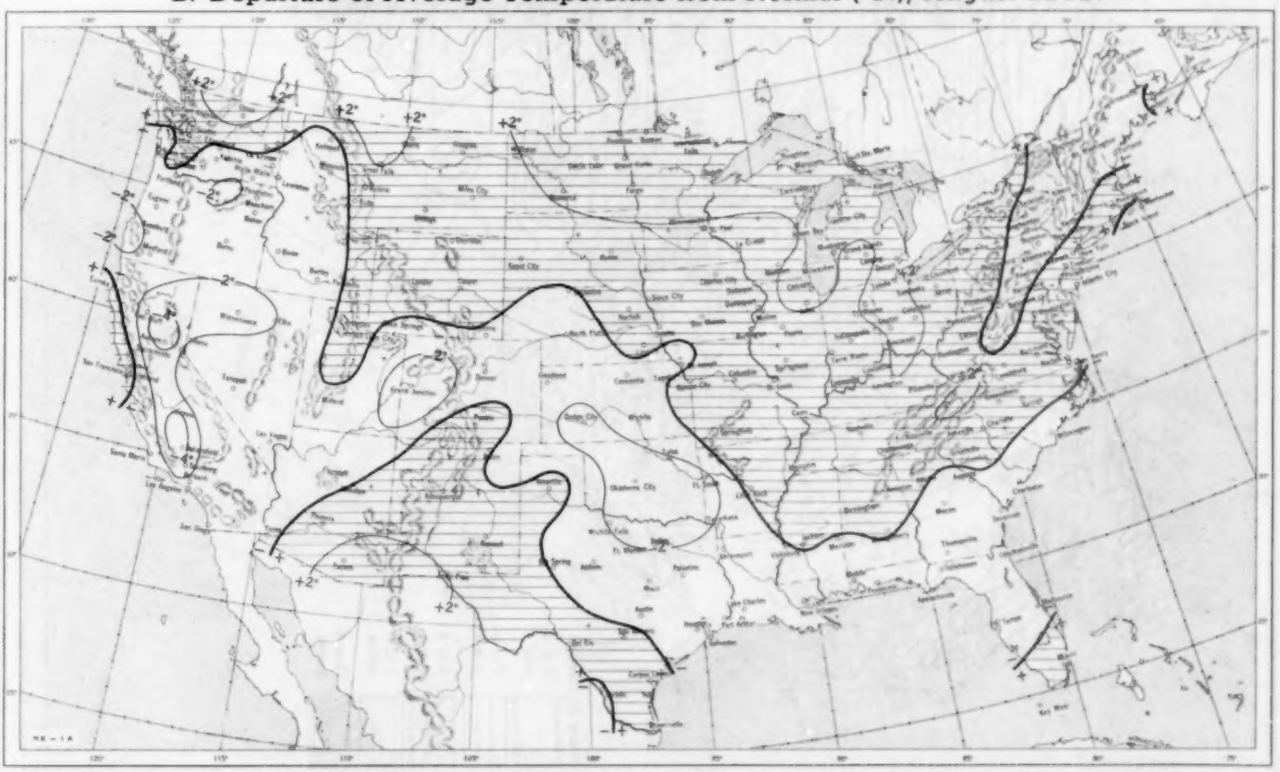

A. Based on reports from 800 Weather Bureau and cooperative stations. The monthly average is half the sum of the monthly average maximum and monthly average minimum, which are the average of the daily maxima and daily minima, respectively.
B. Normal average monthly temperatures are computed for Weather Bureau stations having at least 10 years of record.

Chart II. Total Precipitation (Inches), August 1953.

Based on daily precipitation records at 800 Weather Bureau and cooperative stations.

Chart III. A. Departure of Precipitation from Normal (Inches), August 1953.

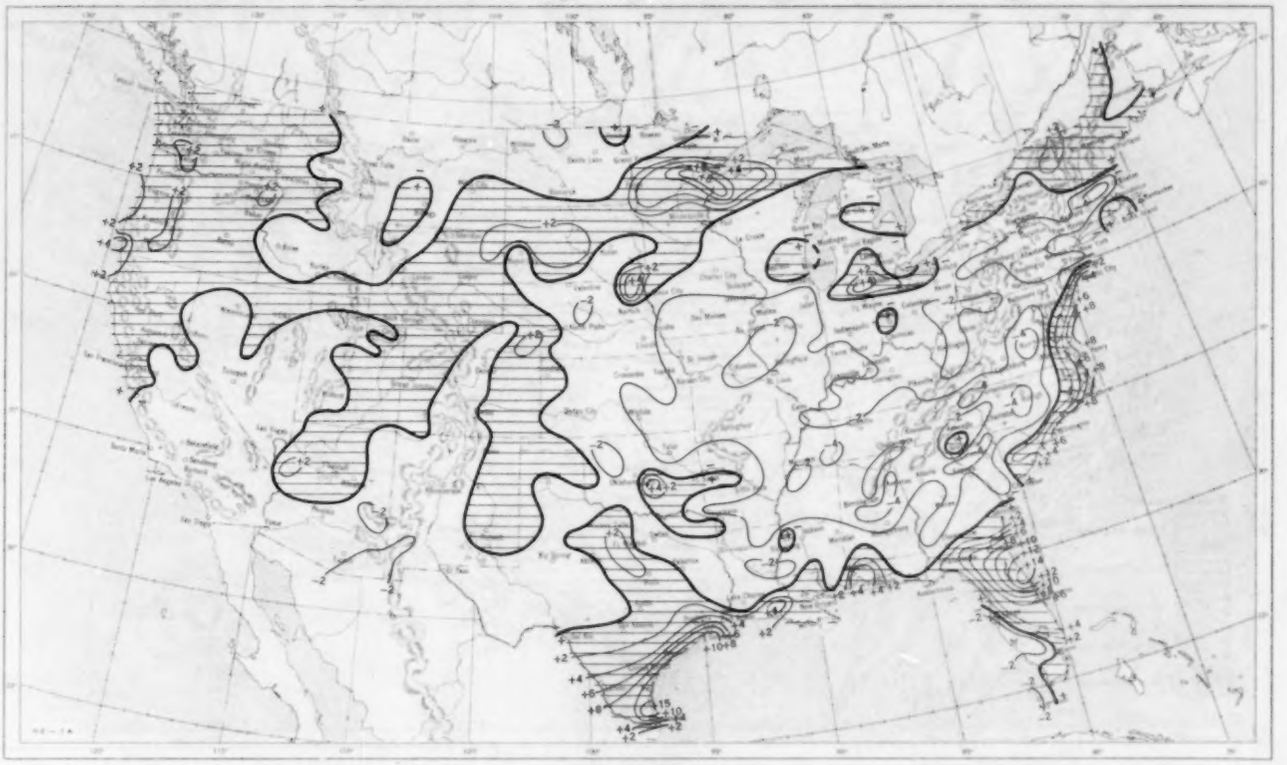

B. Percentage of Normal Precipitation, August 1953.

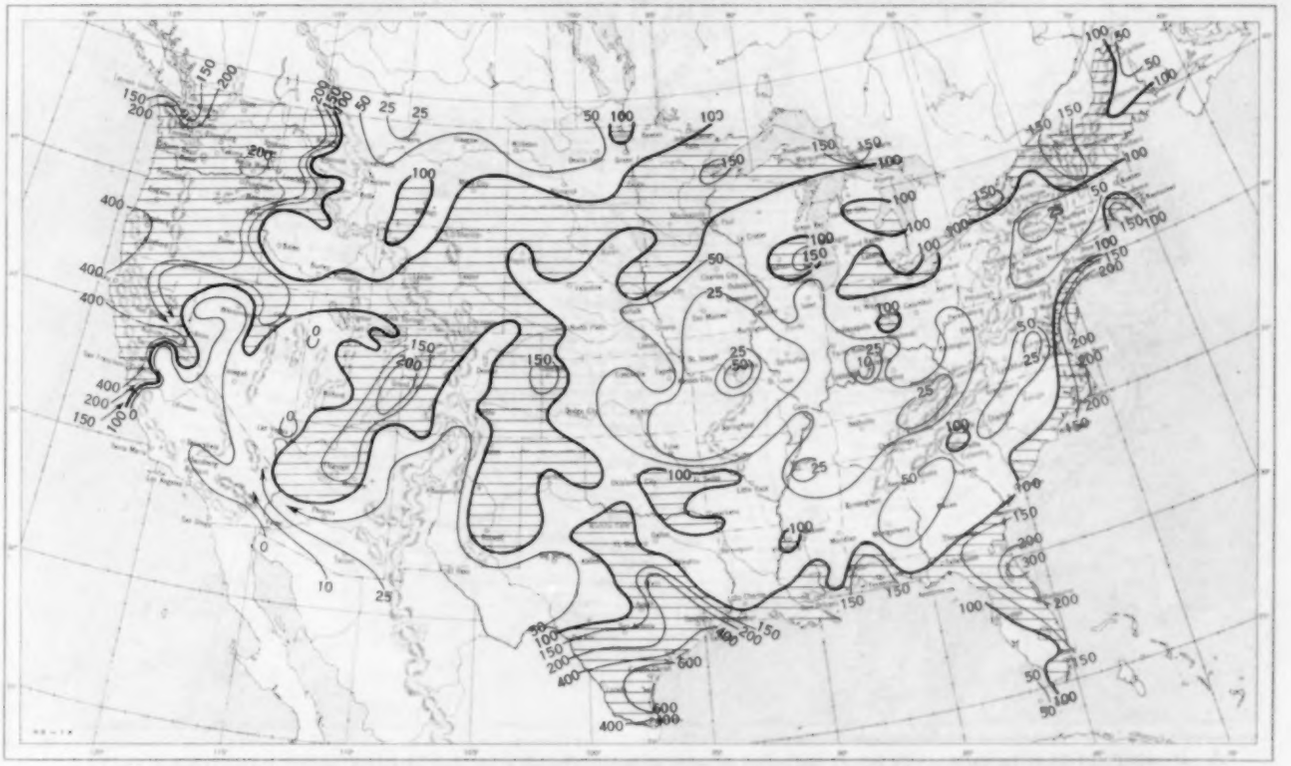

Normal monthly precipitation amounts are computed for stations having at least 10 years of record.

Chart VI. A. Percentage of Sky Cover Between Sunrise and Sunset, August 1953.

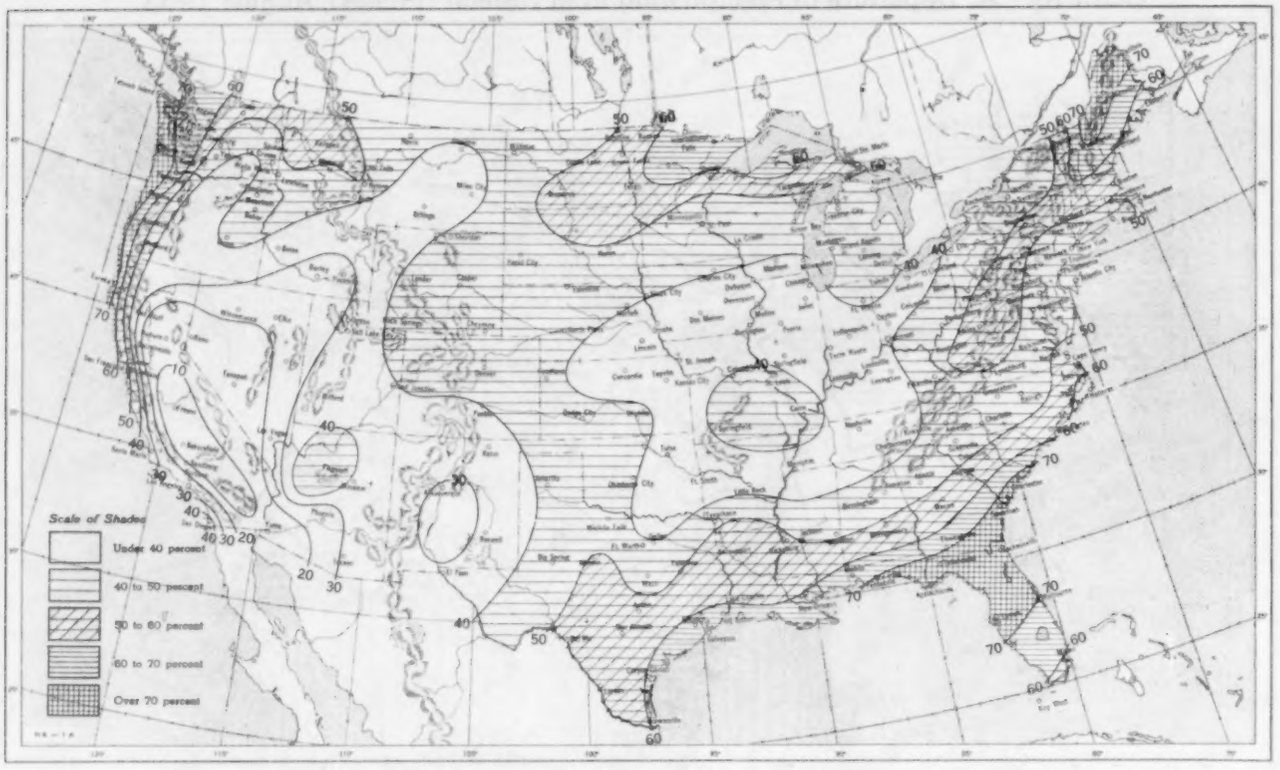

B. Percentage of Normal Sky Cover Between Sunrise and Sunset, August 1953.

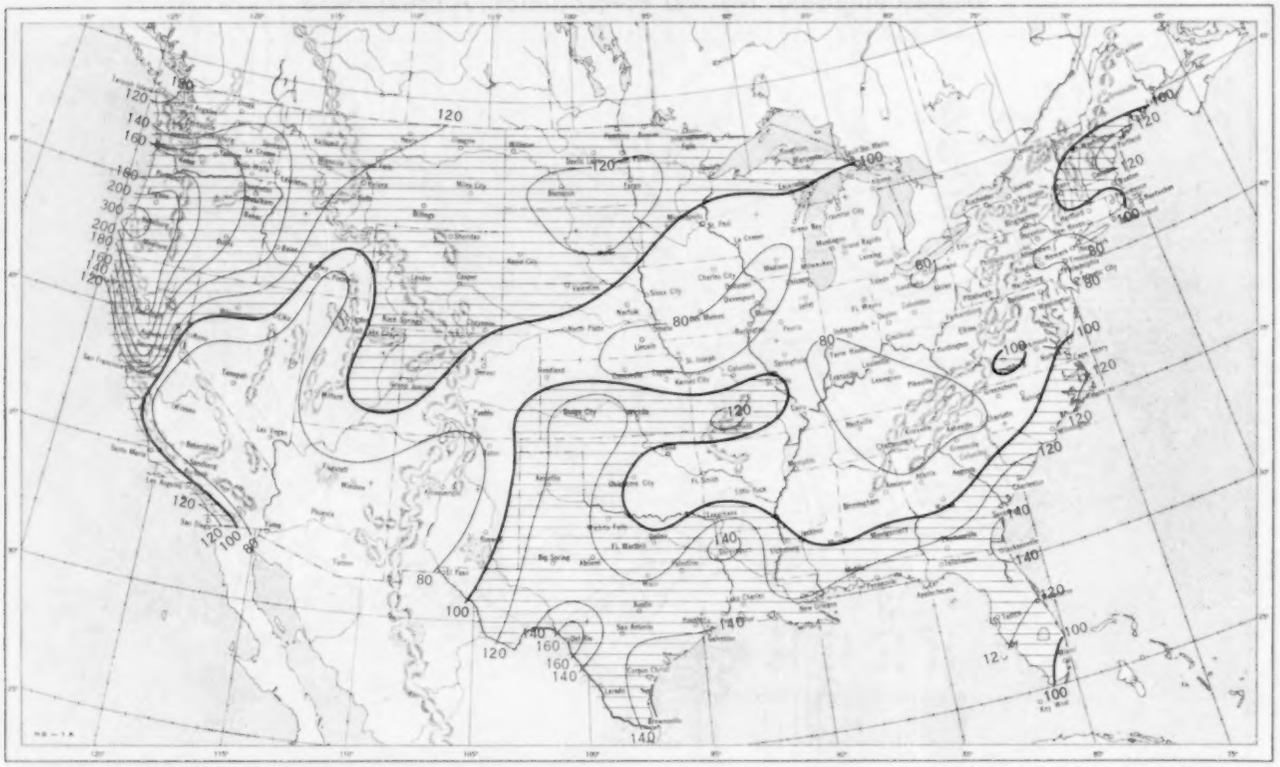

A. In addition to cloudiness, sky cover includes obscuration of the sky by fog, smoke, snow, etc. Chart based on visual observations made hourly at Weather Bureau stations and averaged over the month. B. Computations of normal amount of sky cover are made for stations having at least 10 years of record.

Chart VII. A. Percentage of Possible Sunshine, August 1953.

B. Percentage of Normal Sunshine, August 1953.

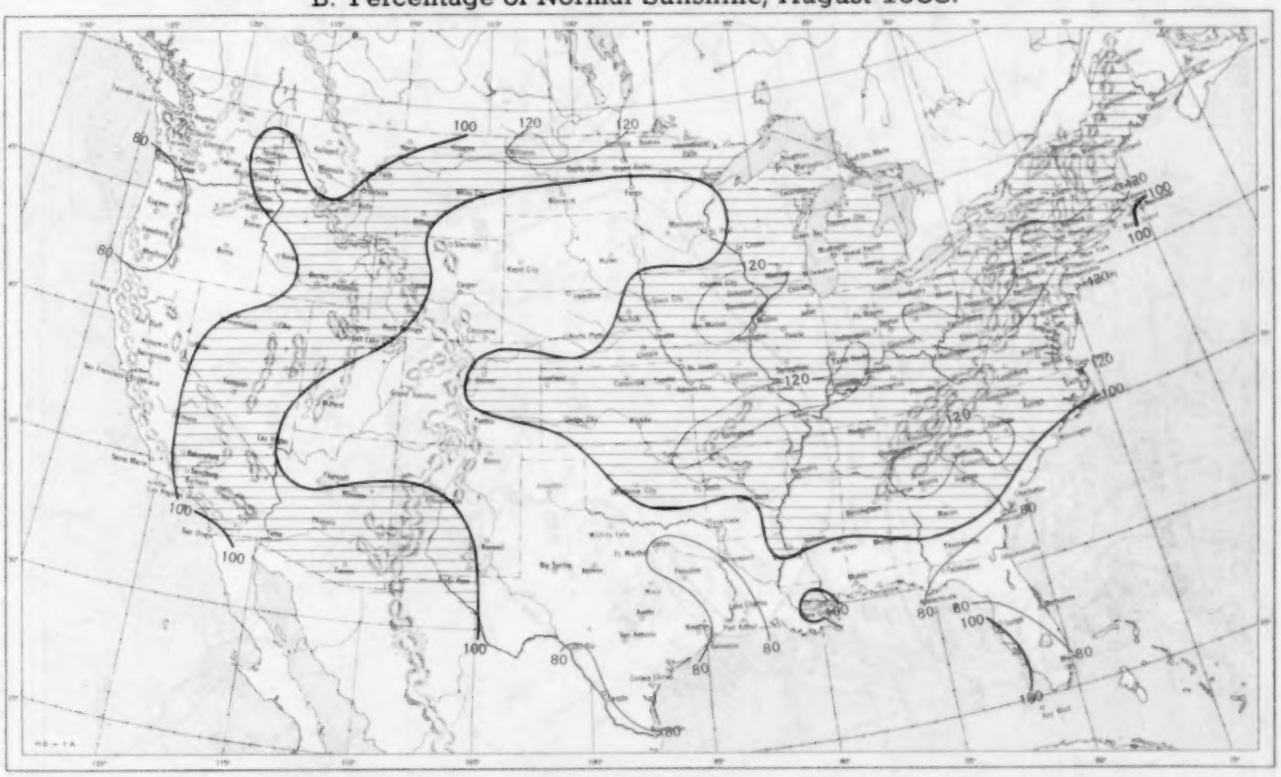

A. Computed from total number of hours of observed sunshine in relation to total number of possible hours of sunshine during month. B. Normals are computed for stations having at least 10 years of record.

Chart VIII. Average Daily Values of Solar Radiation, Direct + Diffuse, August 1953. Inset: Percentage of Normal Average Daily Solar Radiation, August 1953.

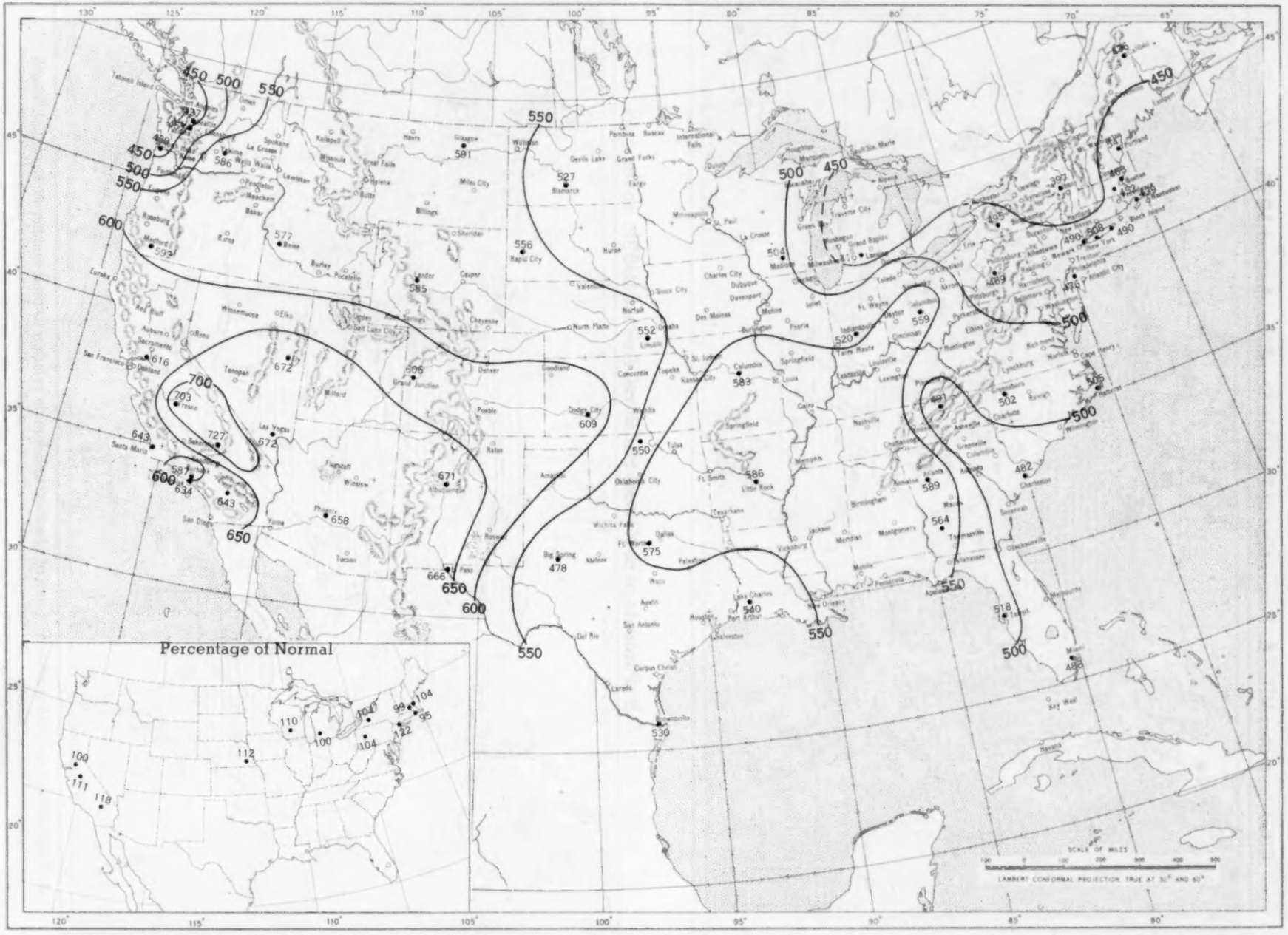

Chart shows mean daily solar radiation, direct + diffuse, received on a horizontal surface in langleys (1 langley = 1 gm. cal. cm. $^{-2}$). Basic data for isolines are shown on chart. Further estimates are obtained from supplementary data for which limits of accuracy are wider than for those data shown. Normals are computed for stations having at least 9 years of record.

are computed for stations having at least 5 years of record.

Chart IX. Tracks of Centers of Anticyclones at Sea Level, August 1953.

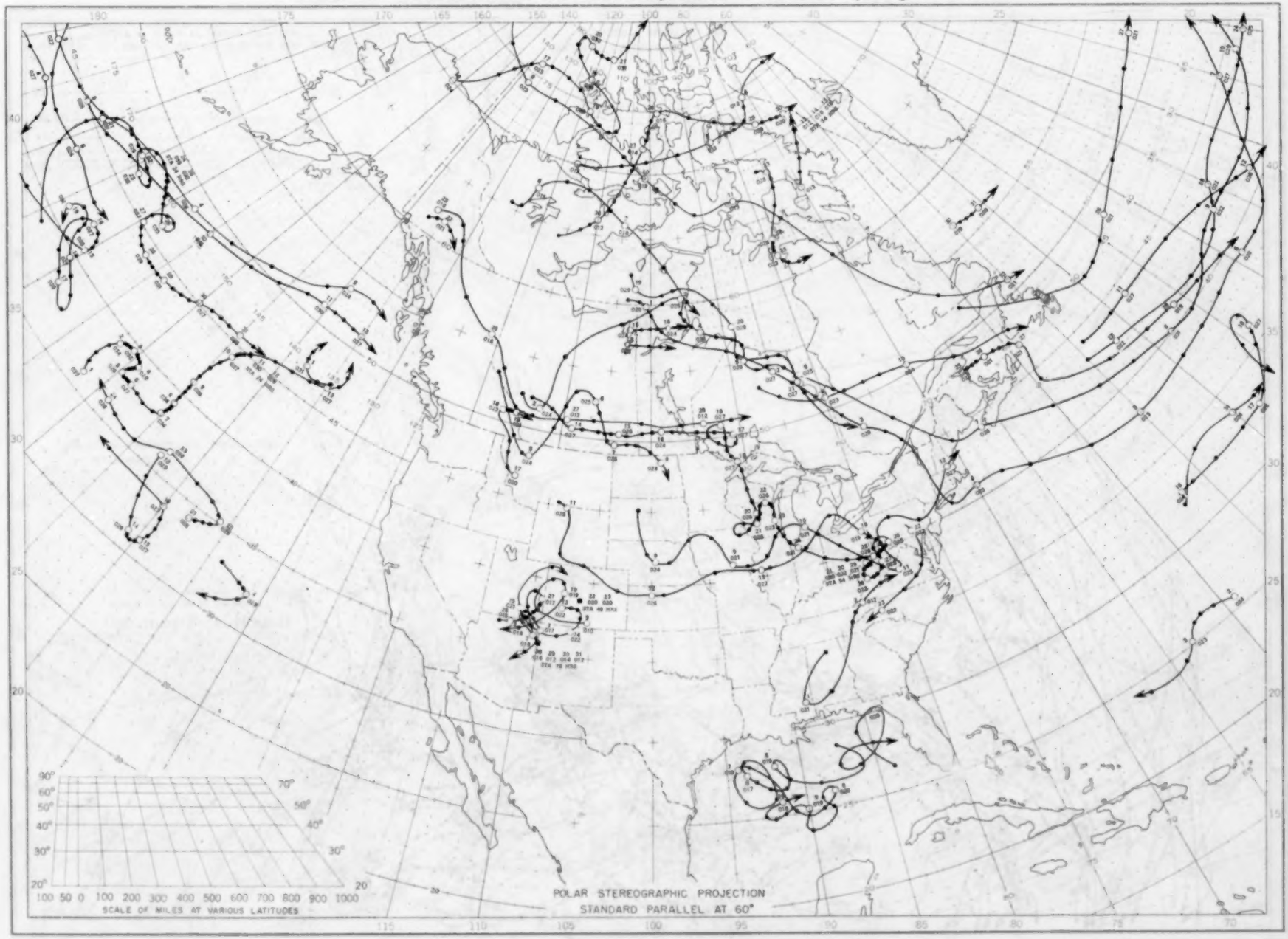
POLAR STEREOGRAPHIC PROJECTION
STANDARD PARALLEL AT 60°
SCALE OF MILES AT VARIOUS LATITUDES
100 50 0 100 200 300 400 500 600 700 800 900 1000

Circle indicates position of center at 7:30 a. m. E. S. T. Figure above circle indicates date, figure below, pressure to nearest millibar. Dots indicate intervening 6-hourly positions. Squares indicate position of stationary center for period shown. Dashed line in track indicates reformation at new position. Only those centers which could be identified for 24 hours or more are included.

Chart X. Tracks of Centers of Cyclones at Sea Level, August 1953.

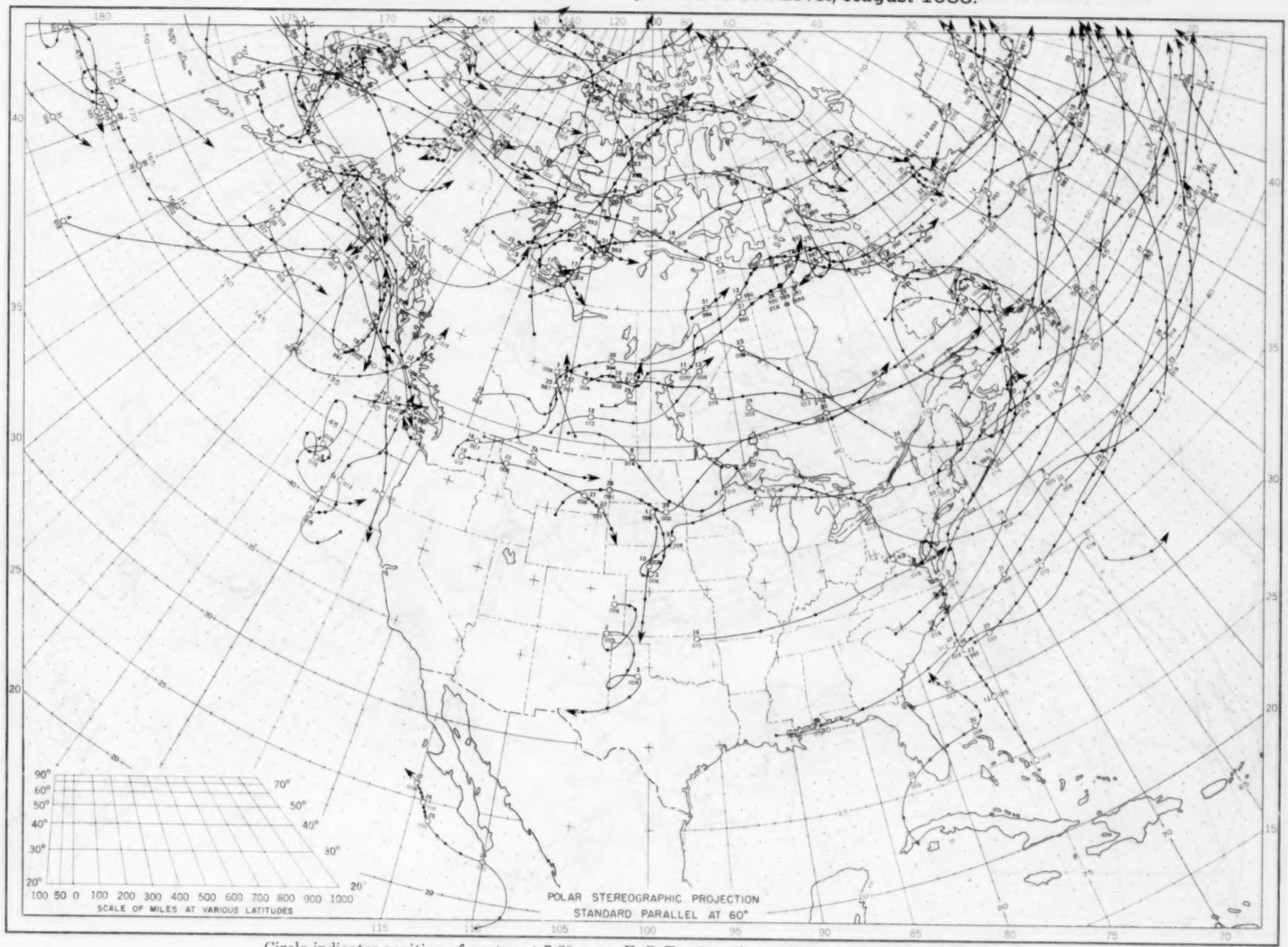

Circle indicates position of center at 7:30 a. m. E. S. T. See Chart IX for explanation of symbols.

Chart XI. Average Sea Level Pressure (mb.) and Surface Windroses, August 1953. Inset: Departure of Average Pressure (mb.) from Normal, August 1953.

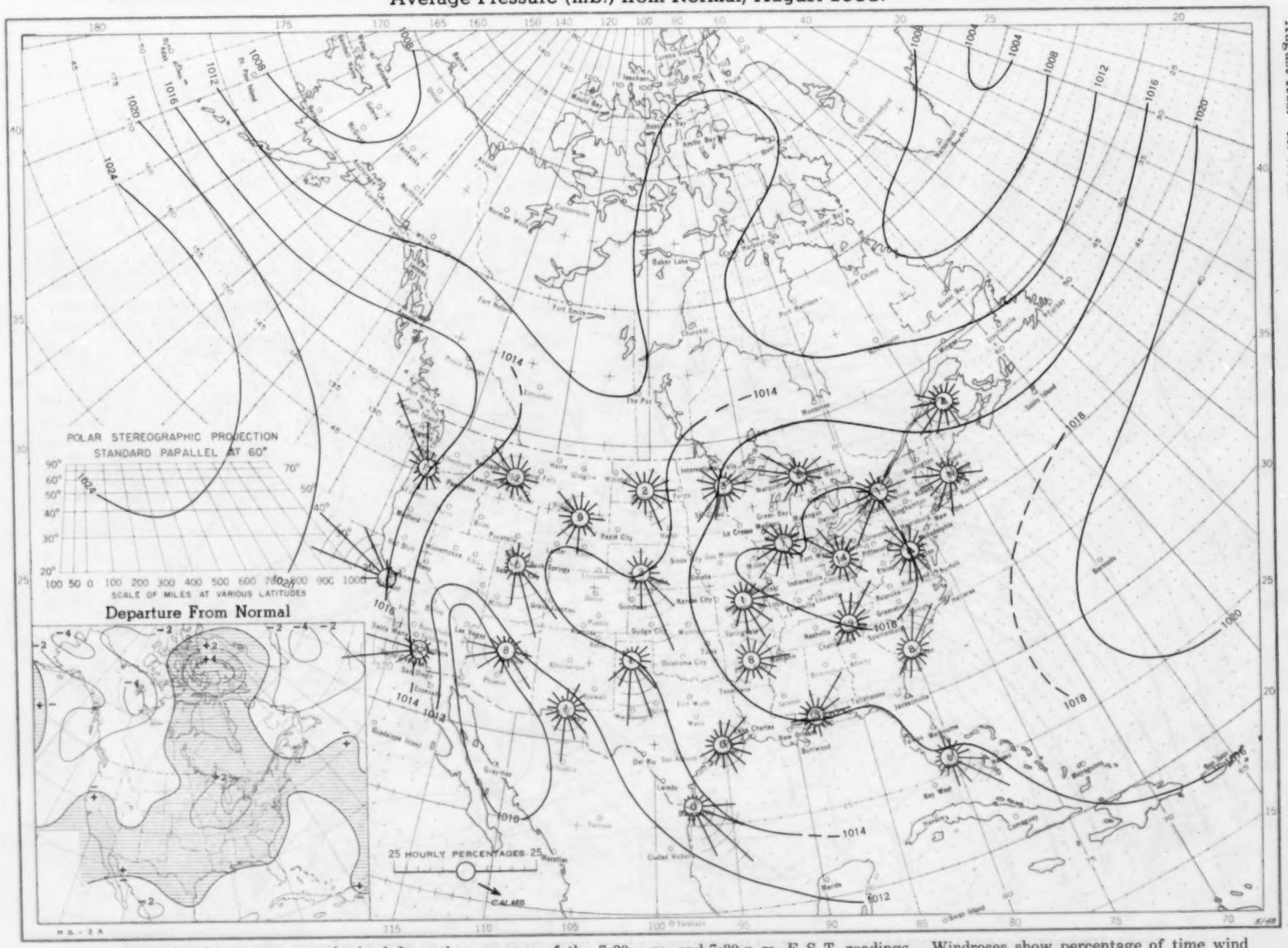

Average sea level pressures are obtained from the averages of the 7:30 a. m. and 7:30 p. m. E. S. T. readings. Windroses show percentage of time wind blew from 16 compass points or was calm during the month. Pressure normals are computed for stations having at least 10 years of record and for 10° intersections in a diamond grid based on readings from the Historical Weather Maps (1899-1939) for the 20 years of most complete data coverage prior to 1940.

Chart XII. Average Dynamic Height in Geopotential Meters (1 g.p.m. = 0.98 dynamic meters) of the 850-mb. Pressure Surface, Average Temperature in °C. at 850 mb., and Resultant Winds at 1500 Meters (m.s.l.), August 1953.

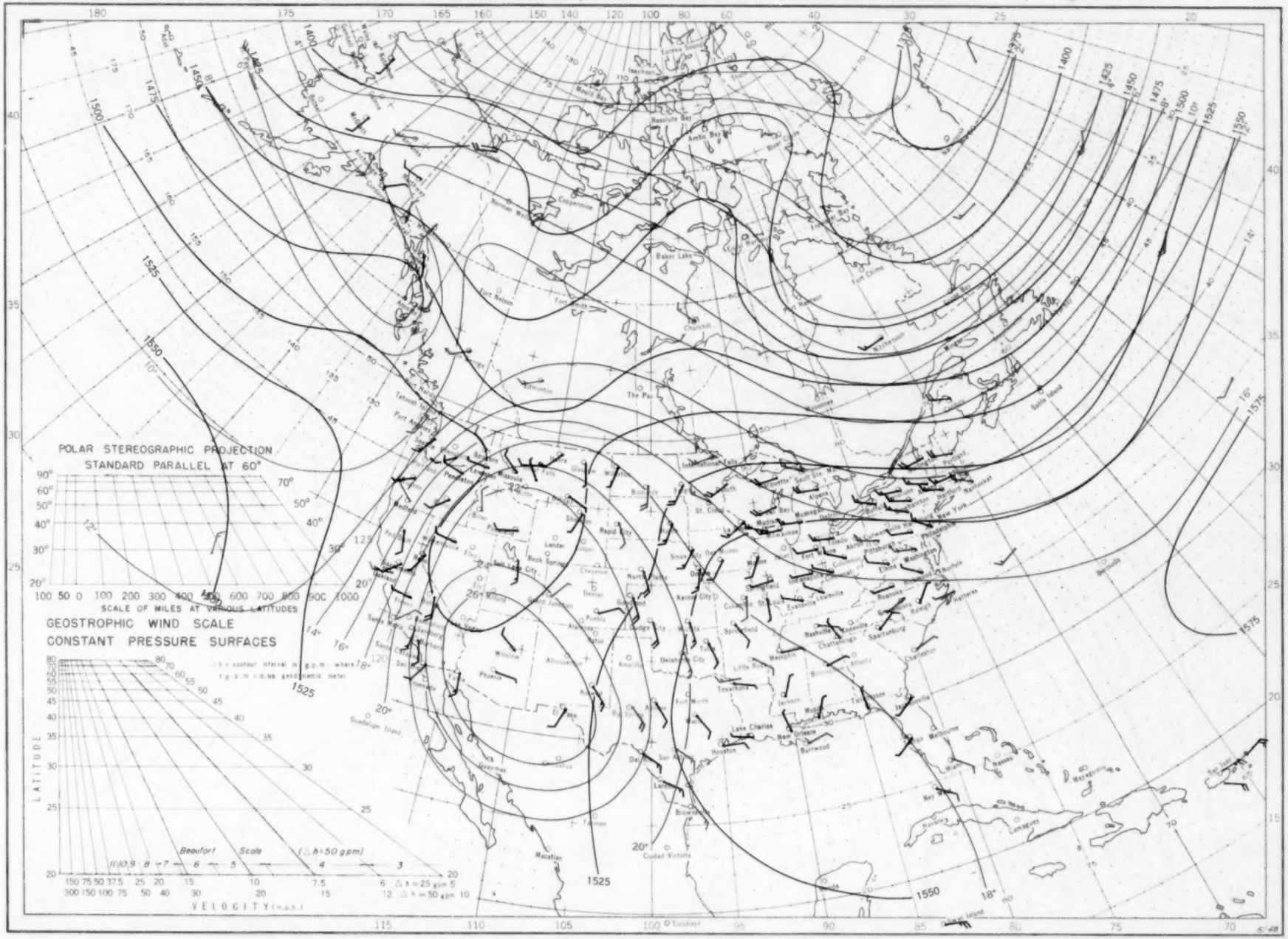

Contour lines and isotherms based on radiosonde observations at 0300 G. M. T. Winds shown in black are based on pilot balloon observations at 2100 G. M. T.; those shown in red are based on rawins taken at 0300 G. M. T.

Chart XIII. Average Dynamic Height in Geopotential Meters (1 g.p.m.. = 0.98 dynamic meters) of the 700-mb. Pressure Surface, Average Temperature in °C. at 700 mb., and Resultant Winds at 3000 Meters (m.s.l.), August 1953.

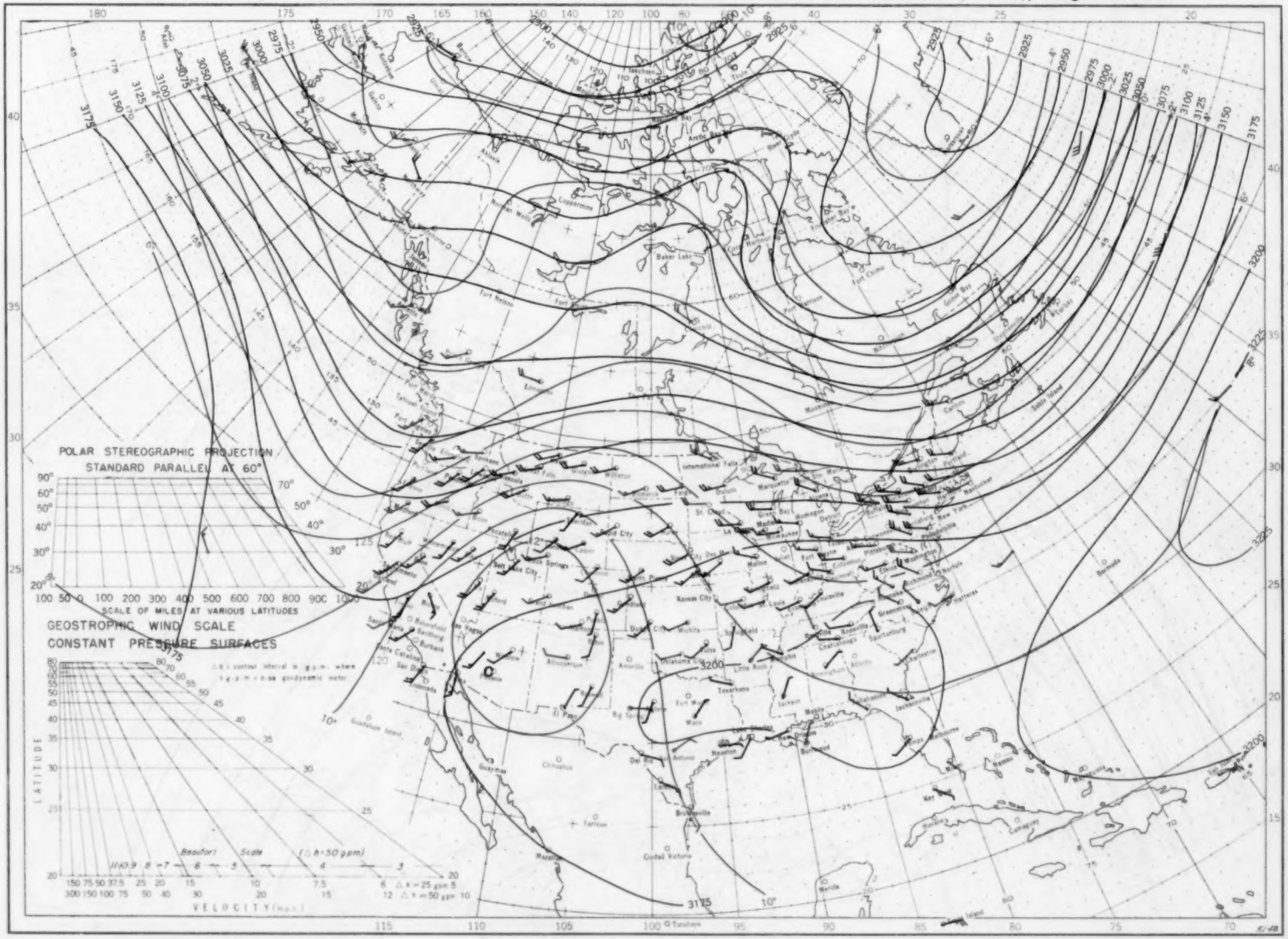

Contour lines and isotherms based on radiosonde observations at 0300 G. M. T. Winds shown in black are based on pilot balloon observations at 2100 G. M. T.; those shown in red are based on rawins taken at 0300 G. M. T.

Chart XIV. Average Dynamic Height in Geopotential Meters (1 g.p.m. = 0.98 dynamic meters) of the 500-mb. Pressure Surface, Average Temperature in °C. at 500 mb., and Resultant Winds at 5000 Meters (m.s.l.), August 1953.

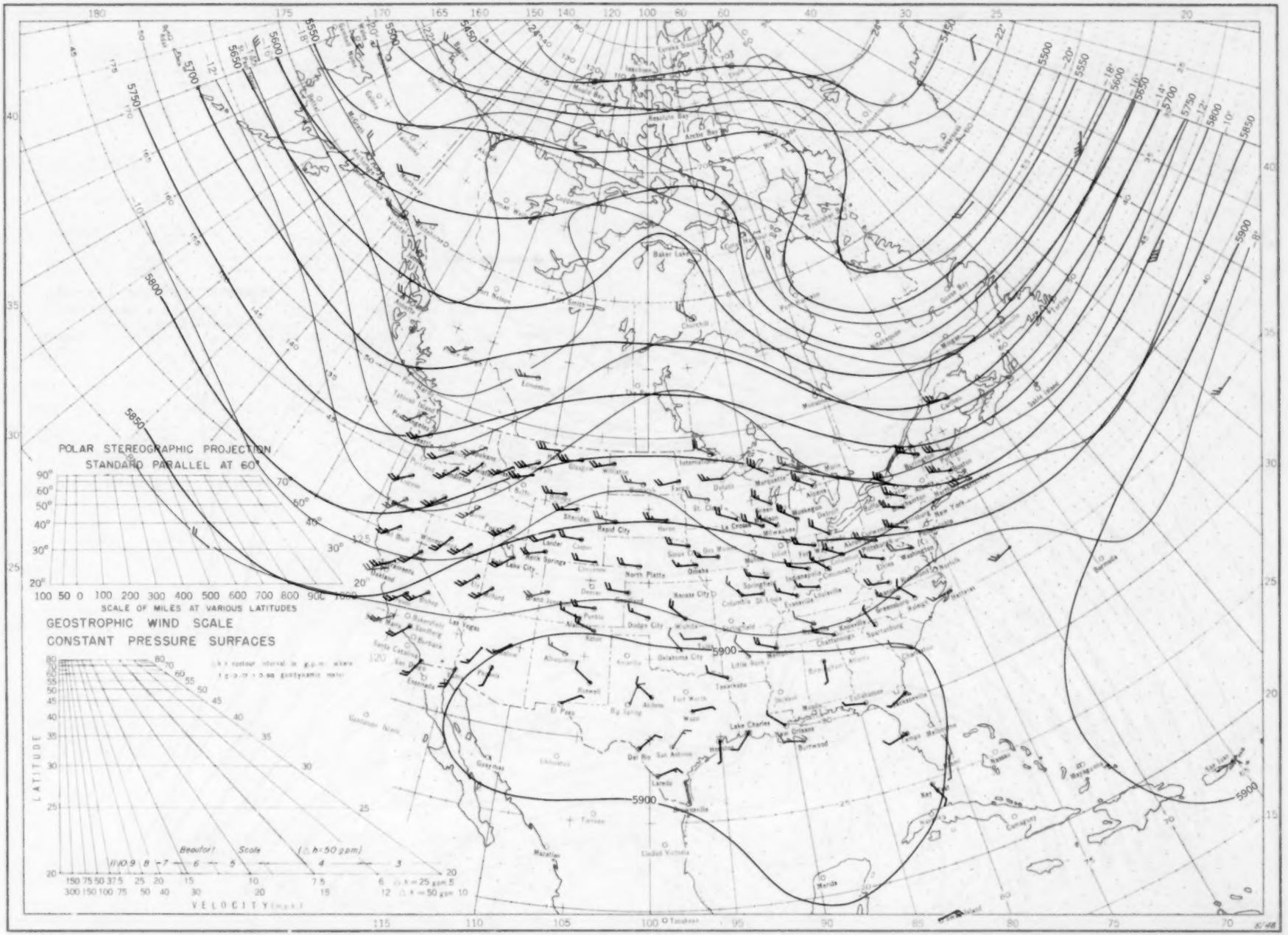

Contour lines and isotherms based on radiosonde observations at 0300 G. M. T. Winds shown in black are based on pilot balloon observations at 2100 G. M. T.; those shown in red are based on rawins at 0300 G. M. T.

Chart XV. Average Dynamic Height in Geopotential Meters (1 g.p.m. = 0.98 dynamic meters) of the 300-mb. Pressure Surface, Average Temperature in °C. at 300 mb., and Resultant Winds at 10,000 Meters (m.s.l.), August 1953.

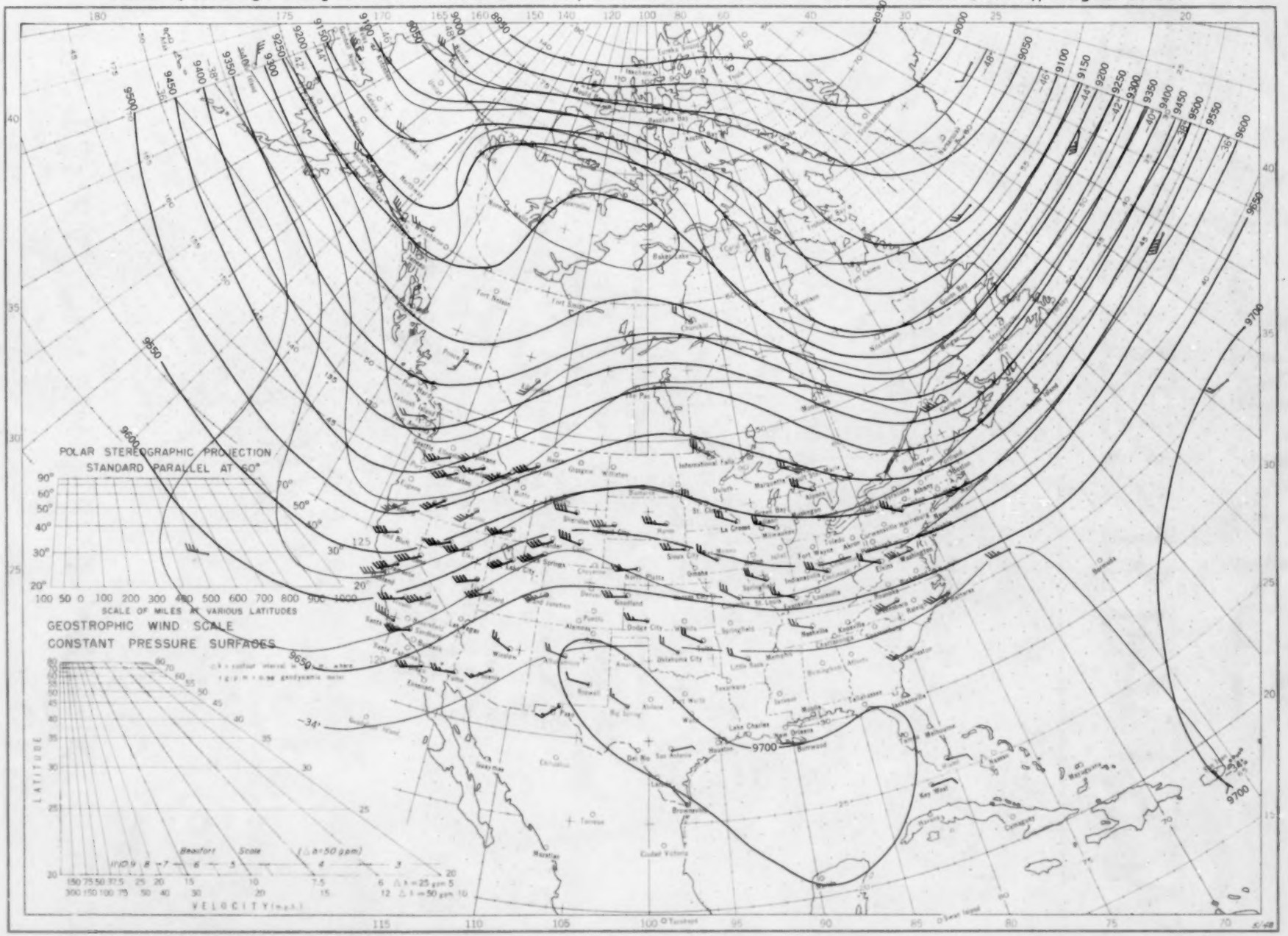

Contour lines and isotherms based on radiosonde observations at 0300 G. M. T. Winds shown in black are based on pilot balloon observations at 2100 G. M. T.; those shown in red are based on rawins at 0300 G. M. T.